Fakultät für Medizin

Institut für Virologie

Anti-HBs conjugated Superparamagnetic iron oxide nanoparticles (SPION) to visualize and target HBV infection *in vitro* and *in vivo*

Lili Zhao

Vollständiger Abdruck der von der Fakultät für Medizin der Technischen Universität München zur Erlangung des akademischen Grades eines

Doktors der Naturwissenschaften (Dr. rer. nat.)

genehmigten Dissertation.

Vorsitzende: Prof. Dr. Gabriele Multhoff

Prüfer der Dissertation:

1. Prof. Dr. Ulrike Protzer
2. Prof. Dr. Franz Pfeiffer

Die Dissertation wurde am 23.03.2021 bei der Fakultät für Medizin der Technischen Universität München eingereicht und durch die Fakultät für Medizin am 13.07.2021 angenommen.

List of abbreviations

ALT	Alanine aminotransferase
aa	Amino acid
Ab	Antibody
bp	Base pair
BSA	Bovine serum albumin
CAR	Chimeric antigen receptor
cccDNA	Covalently closed circular DNA form of HBV
cDNA	Complementary DNA
CHB	Chronic hepatitis B
CT	Computed tomography
Ctrl	Control
d	Day
ddH2O	Double distilled water
DMSO	Dimethylsulfoxid
dsDNA	double-stranded DNA
ELISA	Enzyme linked immunoabsorbent assay
ER	Endoplasmic reticulum
EtBr	Ethidiumbromide
FACS	Fluorescence-activated cell sorting
FCS	Fetal calf serum
h	Hour
HBcAg	HBV core protein
HBeAg	HBV e-antigen
HBsAg	HBV surface antigen
HBV	Hepatitis B virus
HCV	Hepatitis C virus
HBVtg	Hepatitis B virus transgenic
HRP	Horse radish peroxidase
HPLC	High performance liquid chromatography
IFN	Interferon
Ig	Immunoglobulin

i.v.	intravenously
IU	International units
IL	Interleukin
kb	Kilo base
kDa	Kilo Dalton
µg	Microgram
µl	Microliter
µM	Micromolar
mg	Milligram
MHC	Major histocompatibility complex
Min	Minute
MRI	Magnetic resonance imaging
µl	Microliter
ml	Milliliter
MOI	Multiplicity of infection
mM	Mill molar
mRNA	Messenger RNA
ng	Nanogram
NK cell	Natural killer cell
N-terminal	Amino-terminal
NTCP	Na+-taurocholate cotransporting polypeptide
OD	Optical density
ORF	Open reading frame
P	P-value
PAGE	Polyacrylamide gel electrophoresis
PBS	Phosphate buffered saline
PBMC	Peripheral blood mononuclear cell
PCR	Polymerase chain reaction
PEG	Polyethyleneglycol
Pen/Strep	Penicillin / Streptamycin
pgRNA	Pregenomic RNA template of HBV
PHH	Primary human hepatocytes

preS1	C-terminal domain of HBV L-protein
preS2	C-terminal domain of HBV M-protein
qPCR	Quantitative real-time PCR
rcDNA	Relaxed circular DNA: partial double-stranded HBV-genome
RIG-I	Retinoic acid inducible gene I
RNA	Ribonucleic acid
RT	Room temperature
RT-PCR	Reverse transcription PCR
scFv	single chain variable fragment
SD	Standard deviation
SDS	Sodium dodecylsulfate
SVP	Subviral particle
SPIONs	Superparamagnetic iron oxide nanoparticles
s.c.	subcutaneous
TAE	Tris-acetate-EDTA buffer
TCR	T cell receptor
TNF-α	Tumor necrosis factor α
TBS	Tris buffered saline
TEM	Transmission electron microscopy
TLR	Toll-like receptor
VP	Virus particle
WHO	World Health Organization
WT	Wild type
w/o	Without

Abstract

The hepatitis B virus (HBV) infects hepatocytes in human livers, which can result in severe liver diseases including cirrhosis and hepatocellular carcinoma. Despite the availability of a safe and effective vaccine, HBV is a leading cause of infection-related mortality, causing approximately 887,000 deaths per year. Current available antivirals can efficiently suppress viral replication but are not curative and need long-term therapy due to the persistence of covalently closed circular DNA (cccDNA). Even though antivirals efficiently suppress viral replication, their application has only limited impact on HBV related morbidity and mortality. Innovative methods to specifically identify HBV infected hepatocytes could aid the development of therapies which specifically target infected cells.

HBV constitutes three isoforms of its envelope protein, also called the hepatitis B surface antigens (HBsAg). The different isoforms are N-terminally truncated variants of the largest envelope protein and, hence, are termed the small (SHBs), middle (MHBs), and large (LHBs) surface proteins. In non-permeabilized HBV-replicating hepatoma cells, which were labeled with different anti-HBs antibodies, HBsAg co-localized with the plasma membrane. Using a conformation-specific anti-HBsAg antibody (MoMab), we showed that MoMab recognizes HBsAg expressed on hepatocytes of transgenic mice *in vivo*, indicating that the membrane-associated HBsAg is correctly folded. Thus, our experiments revealed that the SHBs protein is embedded in the membrane of HBV positive hepatocytes in liver sections of HBV-transgenic mice and HBV-infected chimpanzee hepatocytes, as well as on the membrane of HBV-induced carcinomas that express HBsAg from integrated HBV DNA.

Superparamagnetic iron oxide nanoparticles (SPIONs), coated with MoMab, were applied to identify HBsAg in the supernatant of HBV replicating cells by NMR relaxometry, and to directly detect membrane-associated HBsAg *in vitro* by electron microscopy on the surface of HBV-infected cells. Subsequently, we showed that intravenously administrated MoMab-SPIONs target HBsAg-expressing hepatocytes in HBV transgenic mice, and in immunodeficient mice with HepG2.2.15-cell xenografts. First experiments using standard T2-weighted magnetic resonance imaging indicated that MoMab-SPIONs accumulate in HBsAg-positive livers and allow visualization of an HBV positive tumor.

Last not least, we demonstrated that T cells engrafted with chimeric antigen receptor using the same single-chain antibody binding HBsAg as the MoMab specifically recognize and kill HBsAg expressing cells. Similarly, bispecific antibodies employing this binder could redirect T cells to specifically kill HBsAg expressing cells. Our results indicate that membrane-associated HBV envelope proteins can be used to target HBV replicating cells.

Thus, our results indicate that MoMab-SPIONs can be applied to develop new detection and monitoring approaches for HBV infected patients.

Table of Contents

1. Introduction

1.1 Hepatitis B virus

1.1.1 Taxonomic classification, genotypes, and epidemiology

1.1.1.1 Classification

The human hepatitis B virus (HBV) is a partially double-stranded DNA virus and as such belongs to the hepadnaviridae, encompassing the mammalian Orthohepadnaviruses and the avian hepadnaviruses[1]. HBV shows narrow species specificity and almost exclusively infects hepatocytes. It is classified as a member of genera Orthohepadnavirus, which also contains the Ground squirrel hepatitis virus, Woodchuck hepatitis virus, and the Woolly monkey hepatitis B virus[2]. HBV replication is facilitated by reverse transcription that requires a viral RNA intermediate. Therefore, HBV is also classified as a pararetrovirus[3].

1.1.1.2 Genotypes

HBV has been divided phylogenetically into 10 genotypes, A to J, based on at least 8 % sequence diversity[4-5]. HBV genotypes show distinct geographic distribution. Genotype A is prevalent mainly in Africa, North America, and Europe, whereas genotypes B and C are mainly found in Southeast Asia. Genotype E is confined to Western Africa while HBV genotypes in other regions are correlating with the migration patterns of humans within Africa. In Central and South America genotypes F and H are found. On the other hand, genotypes D and G occur worldwide. Their sub-genotypes, however, are geographically restricted[6]. Serologically, HBV can be divided into 9 serotypes, named ayw1, ayw2, ayw3, ayw4, ayr, adw2, adw4q-, adrq+, and adrq- [4, 7].

1.1.1.3 Epidemiology

Hepatitis B virus infection is a global health threat with 257 million chronic carriers at high risk to develop hepatocellular carcinoma (HCC) and cirrhosis[8]. Its consequences account for 887,000 deaths per year **(WHO 2017)**[9]. In HBV highly infected risk areas, like Asia and Africa, HBV is

commonly spread by perinatal transmission (mother to child at birth), horizontal transmission (by exposure to infected blood or various body fluids) and sexual transmission[10-11]. In acute hepatitis B, the virus can be cleared within 30 to 60 days after infection[12-13]. However, if the virus can not be eliminated by the adaptive immune system, the infection develops into chronic hepatitis B (CHB). Depending on the age at which infection occurs, up to 90 % of HBV infected infants will develop a chronic infection. In contrast, only 5-10% of the people infected as adults develop chronic infection[14]. An estimated 20–30 % of chronically infected patients will develop cirrhosis and/or liver cancer[8, 15].

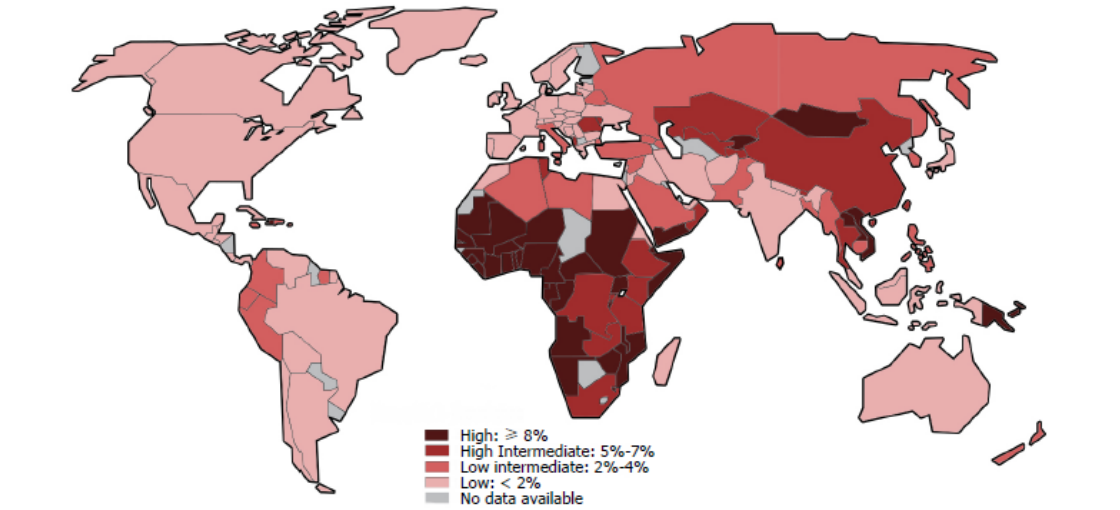

Fig. 1.1 Global prevalence of hepatitis B virus infection. HBsAg prevalence was estimated as a marker for HBV chronic infection. According to the limited data, the figure might only present the chronic HBsAg carriers (**WHO 2017)[16-17].**

The global prevalence of HBV infection varies dramatically worldwide[16] **(Fig.1.1)**. The highest prevalence has been reported in sub-Saharan Africa and East Asia (5-10 %). Besides, the Amazon, the Southeast, and Central Europe have all demonstrated a high rate of chronic infections. An intermediate prevalence rate is found in the Middle East and the Indian sub-

continent, amounting to 2-5 %. In Western Europe and North America, less than 1 % of the population is suffering from chronic HBV infection. The prevalence is decreasing in several highly endemic regions due to improvements in the socioeconomic status, universal vaccination programs, and effective antiviral treatment[18]. However, population movement and migration are currently shaping the prevalence and incidence in several low endemic countries in Europe, such as Italy and Germany, since these countries received migrants and refugees with high HBsAg prevalence rates[19-20].

1.1.2 HBV genome, proteins and structure

1.1.2.1 Genome

The infectious HBV particles have a 3.2 kb circular, partially double-strand DNA genome. In these so-called Dane particles, the full-length minus-strand of the viral DNA carries the complete genetic information of HBV. It also contains two small redundancies of 8-9 nucleotides on both sides, which are essential for viral replication[21]. On the other hand, the plus-strand spans around 2/3 of the genome.

The HBV genome consists of four overlapping open reading frames (ORFs), which are all transcribed from the minus-strand DNA **(Fig. 1.2)**. Four promoters (Cp, PS1p, Sp, and Xp) drive transcriptional initiation at a different position to generate the 3.5, 2.4, 2.1, and 0.7 kb polydenylated RNA, respectively. The pregenomic RNA, is reverse transcribed to the viral DNA, and at the same time serves as a template for the translation of the viral polymerase and core proteins. The slightly longer precore mRNA encodes the precore proteinswhich can cleave to HBV e antigen (HBeAg). From the 2.1 and 2.4 kb mRNA's, the viral envelope proteins (S, M, and L protein) are translated, while the X mRNA encodes the viral X protein. The transcription of these RNAs is augmented by two transcription-enhancing elements (Enh1 and Enh2). In addition, the genome contains cis-regulating elements (CRE), which act as binding sites for transcription factors to regulate (m)RNA transcription.

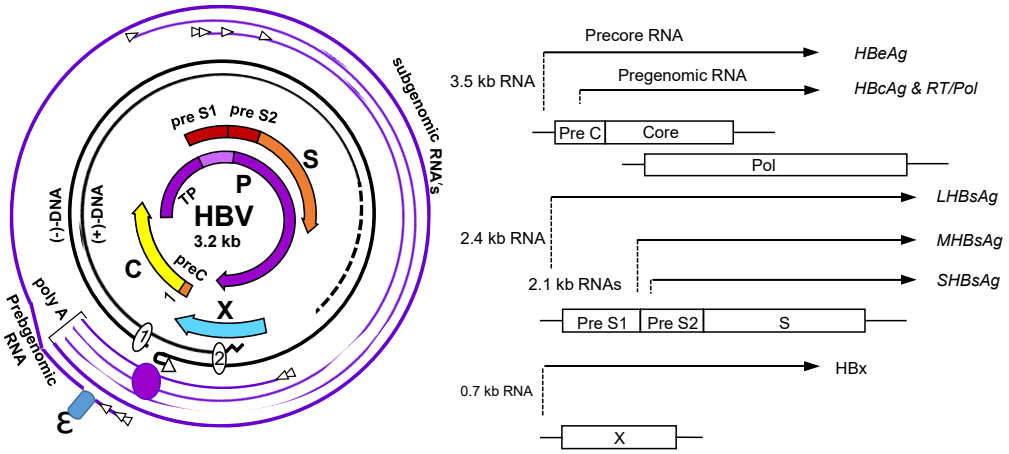

Fig. 1.2 The HBV genome. The outer thin lines represent the viral transcripts with several key regulatory elements. The hairpin structure ξ RNA is located on the terminally redundant pgRNA. The thick lines represent the RC-DNA form of genome in infectious virions. The inner arrows indicate the open reading frames of viral proteins. The transcription starts sites of various HBV transcripts and the proteins they encode (see text for details). Modified from[21-22].

1.1.2.2 HBV proteins

The HBV genome encodes structural proteins such as the core protein, envelope proteins, and polymerase, as well as the non-structural proteins, including the HBeAg and HBx protein.

Envelope proteins: The viral envelope proteins are collectively known as the surface antigens (HBsAg). These three proteins, consisting of small (SHBs), middle (MHBs), and large proteins (LHBs), are expressed from ORF preS1/preS2/S by means of three different start codons. Therefore, the sequence of the 226 amino acids-long SHBs is repeated in MHBs and LHBs. In addition to SHBs, MHBs carry the additional preS2 domain (55 amino acids), which is further extended in LHBs by preS1 comprising 108 amino acids (or 119, depending on genotypes)[23]. Furthermore, the HBV envelope proteins are N and O-glycosylated. Increasing in size, there are non-glycosylated SHBs (25kDa), glycosylated SHBs (28kDa), once-glycosylated MHBs (33kDa), twice-glycosylated MHBs (36kDa), non-glycosylated LHBs (39kDa) and glycosylated LHBs (42 kDa), respectively[24].

All three proteins are incorporated into the membrane of the endoplasmic reticulum (ER), where they form disulfide-linked dimers or heterodimers, bud into the ER lumen, and are secreted out of the cell mainly as subviral particles that can be detected as HBsAg, but also within the viral envelope[25]. In the HBV life cycle, LHBs and SHBs both play an important role in virus formation while MHBs are less essential[26]. The functional nature of these proteins is related to their unique structures or topology **(Fig. 1.3)**. SHBs contain four transmembrane TM domains (TM1, TM2, TM3, and TM4, the latter two being predicted)[27-28]. Due to the exist of TM segments, the N and C terminus are oriented to the lumen of ER, thereby generating two cytosolic and one luminal loop[28-30]. This luminal loop with the N-glycosylation site (Asn-146) and the major conformational HBsAg epitope is exposed on the surface of the viral envelope, while the first cytosolic loop might contribute to interaction with nucleocapsids[31]. The topology of MHBs is highly similar to that of SHB. Yet, it is N-glycosylated at Asn-4[32] and O-glycosylated at Thr-37 (depending on genotype)[33-34]. The preS2-linked N-glycans are required for the secretion of HBV by interaction with calnexin[35]. However, MHBs are dispensable for viral particle formation[36-37]. By contrast, LHB is a multifunctional viral protein, because it mediates the attachment of HBV to hepatocytes, the envelopment of viral capsids, the release of subviral particles (SVPs), the regulation of cccDNA amplification. LHBs (preS1, preS2 and S domain) display a dual topology (i-preS1 and e-preS2), resulting from the interaction between the C-terminal region (70-90 aa) of preS1 and the Hsc70 chaperone[38-41]. After translation, the preS domain of i-preS stays in the cytosol with TM1, whereas in e-preS, preS translocates into the ER lumen[42-45]. The preS1 domain is essential for hepatocyte binding and intracellular uptake. The myristoylated motif (2-48 aa) of the preS1 domain has been characterized to bind to the HBV receptor sodium taurocholate cotransporting polypeptide (NTCP)[46-47]. The myristic acid can protect virions against recognition by neutralizing antibodies and may contribute to the viral immune evasion[48]. In the late stages of infection, the i-preS form is important for virus assembly. A short linear sequence in the C-terminal of preS1 was identified as a matrix domain for the interaction with the nucleocapsids[49].

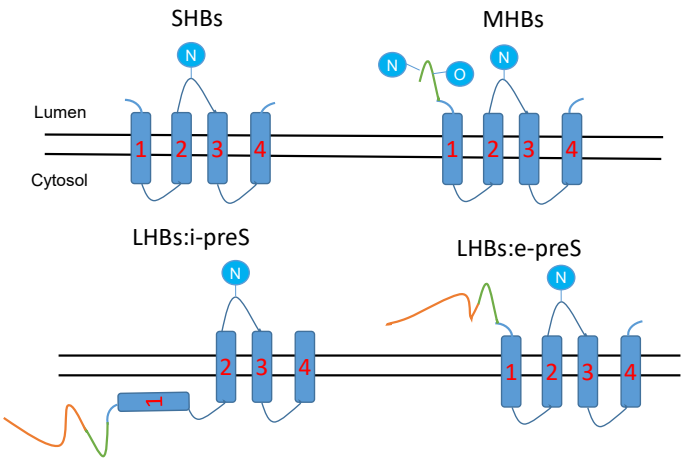

Fig.1.3 The topology of HBV envelope proteins. The four TM segments of the SHBs project their N- and C-terminus into the ER lumen, thereby generating two cytosolic and one luminal loop. The MHBs show a similar topology to SHBs, with N-terminal extended preS2 domain into the ER lumen. The LHBs display a mixed topology (i-preS and e-preS). In i-preS, preS1 remains in the cytosol, whereas in e-preS, preS1 is translocated through the membrane into the ER lumen. N and O represent N-glycosylation and O-glycosylation, respectively. The figure is modified from[41, 44].

Core protein: The full-length core protein (about 21 kDa) contains a 140 amino acids-long structure domain and a 34-36 amino acid-long C-terminal domain (CTD) separated by a spacer of nine amino acids. The phosphorylation of the CTD by cellular protein kinases results in the conformational change of the core proteins, which correlates with pgRNA packing during the process of nucleocapsid assembly and the maturation[50-51]. Apart from this, the CTD harbors a nuclear localization signal (NLS), as well as the nuclear export signals (NES) which are necessary for nucleocytoplasmic shuttling of the core protein or capsid[52-53]. The N-terminal part is important for the dimerization and assembly process[54].

Polymerase: Polymerase contains 832 aa with four domains (terminal protein domain (TP), the spacer domain, reverse transcriptase domain, and RNase H domain). This enzyme is required for HBV replication cycle, including viral RNA binding RNA binding, RNA packaging, protein priming, template switching, DNA synthesis and RNA degradation[55-57]. In addition, HBV polymerase must interact with host proteins in order to complete a successful replication cycle.

HBeAg: HBeAg is a secreted HBV polypeptide that originates from the precore protein. After cleavage of the N-and C-terminal domains of the precore protein by cellular proteases, the HBeAg is secreted as a monomeric protein[58]. HBeAg is viewed as an important marker for active viral replication. It is therefore widely used in diagnostics[59].

HBx protein: ORF X encodes the 16.5 kDa X protein (HBx), that is composed of 154 amino acids. HBx is HBV's only accessory protein and is essential to initiate and maintain HBV RNA transcription[60-62].

1.1.2.3 HBV structure

The HBV Dane particles are 42-44 nm spheres. The inner shell of the virus consists of a 30-32 nm icosahedral nucleocapsid, which self-assembles from 120 dimers of the core protein and contains a 3.2kb relaxed circular DNA (rcDNA). Based on the core protein expression, nucleocapsids have been reported to form two types; 240 subunits with the triangulation number (T) 4 and 180 subunits with the triangulation number T=3[63]. The former (T=4) has been characterized to form the virion-derived capsids[64]. The nucleocapsid is enveloped by host cellular lipids[38] and HBV's three envelope proteins in which the stoichiometric ratio of LHBs, MHBs, and SHBs is approximately 1: 1: 4[23, 46] **(Fig. 1.4A).** In addition to Dane particles, there is an excessive production and secretion of non-infectious subviral particles (SVPs) which are known to have either a spherical or filamentous form[65]. The spherical structures measure around 22 nm in diameter, while the filaments are of similar width, but of variable length[66] **(Fig. 1.4B)**. SVPs are predominantly containing SHBs, but only filaments contain LHBs.

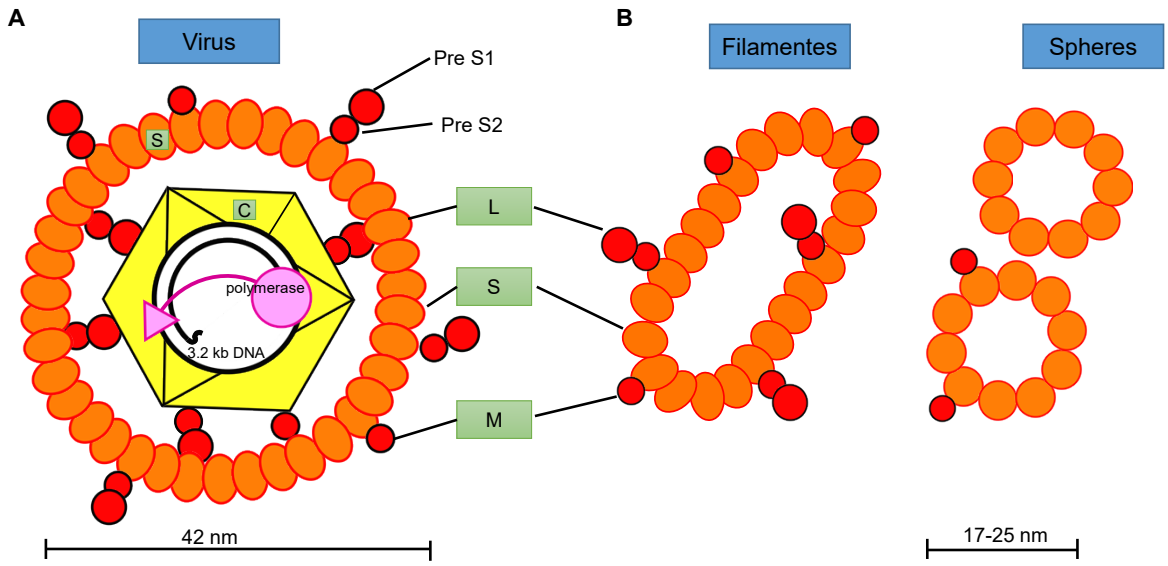

Fig. 1.4 Structures of hepatitis B virus particles. A) Structure of a Dane particle. The viral envelope is composed of the host-derived lipid membrane and the three viral envelope proteins (L, M and S). The inner shell consists of the core proteins and harbors the rcDNA genome which is associated with the viral polymerase. B) Structure of the SVPs. SVPs do not contain viral nucleic acids. Based on the different structure, size, and the distribution and composition of HBsAg, SVPs are divided into filaments (Left) and spheres (Right). The figure is modified from[46, 67].

1.1.3 HBV life cycle

The HBV life cycle starts with the viral particles' entry into the hepatocytes and ends with the secretion of the newly produced virus out of the infected hepatocytes. An overview of this process is depicted in **Fig. 1.5**.

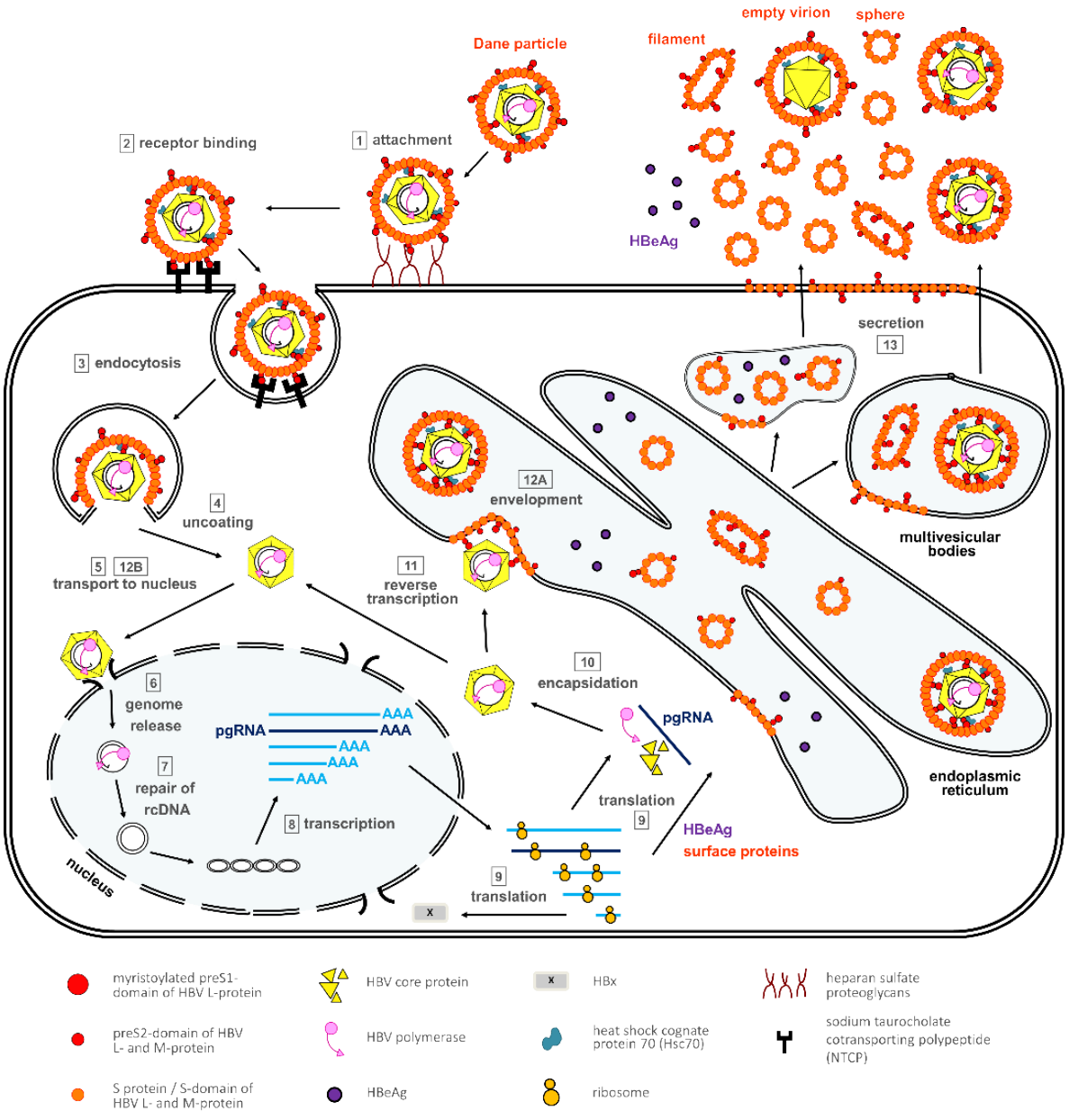

Fig. 1.5 Hepatitis B virus life cycle. HBV infectious Dane particles attach to the surface of hepatocytes via HSPGs and specifically bind to NTCP receptor, followed by viral particle endocytosis and the removal of the envelope protein. The nucleocapsid is released into the cytoplasm, then the rcDNA is imported into the nucleus and repaired to form cccDNA which serves as the template for the transcription of viral mRNAs and subgenomic RNA. The viral mRNAs are translated into viral proteins in the cytoplasm. pgRNA with core proteins and polymerase self-assemble to RNA containing nucleocapsid. After reverse transcription of RNA, the nucleocapsid is either re-imported into the nucleus or buds into the ER to envelope the surface proteins. Finally the virions and subviral particles are secreted out of hepatocytes[67].

1.1.3.1 HBV entry

The entry of HBV is thought to begin with the reversible attachment of HBV virions to the cell surface via Heparan sulfate proteoglycans (HSPGs)[68], leading to the exposure of the myristoylated N-terminus of pre-S1. This enables it to specifically recognize and bind the sodium taurocholate cotransporting polypeptide (NTCP), also known as SLC10A[69], which is mainly responsible for strictly hepatotropic infection and the species tropism[70-71]. Silencing NTCP inhibits the HBV infection, while exogenous NTCP expression increases the susceptibility of non-susceptible hepatoma cells[72]. Based on these findings, a synthetic myristoylated peptide (Myrcludex B), containing the same amino acids sequence (2-48 aa) as the preS1, was found to block HBV infection by binding HBV-specific NTCP *in vitro*, and *in vivo*[47, 73]. However, it is still poorly understood whether other receptors contribute to the virus entry process.

Upon binding to the cell membrane, the viral particles enter the endosome by two potential uptake pathways. On one hand, HBV particles are taken up by endocytosis with the help of host factors, such as caveolin-1[74], clathrin, and the clathrin adaptor protein AP-2[75-76]. However, this mechanism is still not fully comprehended. Another hypothesis is that HBV may enter the hepatocytes following the fusion of the viral envelope at the plasma membrane. In recent studies, the N-terminal part of the S region (amino acid residues from 164 to 186) and the whole region of preS1 and PreS2-TLM (amino acid residues from 149 to 160) have been identified as fusogenic domains[77-79]. Both pathways lead to the removal of the viral envelope proteins and the release of viral capsids.

1.1.3.2 Viral nucleocapsid transports towards the nucleus and genome release

After the release of HBV nucleocapsids, nucleocapsids are transported to the nucleus where they release the genome. Several studies have supported the notion that nucleocapsids are able to interact with motor proteins to activate the microtubule transport system towards the nucleus[80-81]. Upon interaction with nuclear pore complexes by the exposed nuclear localization signal (NLS),

mature capsids dissociate and release genome to the karyoplasm with the help of the HBV polymerase[82-84]. Empty or immature capsids are also transported through the nuclear pore. They are, however, arrested by Nup153 and do not indicate a release of any immature genome[53]. Another hypothesis, supported by the finding of *Cao et al.* and *Yao et al.* states that the disassembly of capsids and the release of the HBV genome first happens in the cytoplasm since they showed that polymerase of HBV and DHBV both exist in the cytosol[85-86]. In conclusion, it is currently uncertain where mature capsids dissemble and whether the NPC is the general environment triggering genome release[83].

1.1.3.3 cccDNA formation and HBV RNA transcription

The HBV covalently closed circular DNA (cccDNA) is an essential feature for HBV replication because it determines the chronicity of the HBV infection. Once the HBV genome is imported into the nucleus, the relaxed circular DNA (rcDNA) is converted into the cccDNA as follows. Firstly, the viral polymerase and RNA primer are removed from the minus-strand of the rcDNA. Thereby, it forms deproteinized rcDNA (DP-rcDNA) or protein-free rcDNA (PF-rcDNA)[87-88]. Secondly, the plus-strand DNA is completed via the cellular replicative machinery, following the removal of the short RNA oligomer from 5' end[88-89]. After that, both DNA strands undergo DNA-repair reactions to ligate together based on the host DNA-repair machinery[90]. Another hypothesis suggests that rcDNA may first be converted into a double–stranded linear (DSL) DNA which is subsequently formed into cccDNA with the help of the non-homologous end joining DNA repair apparatus NHEJ and host ligases (LIG1, 3, and 4)[91-93]. Finally, the cccDNA associates with host proteins, such as histones (H1, H2A, H3, and H4) and core proteins, to further form the cccDNA minichromosome[94-95].

The cccDNA minichromosome persists in the nucleus of infected cells and serves as a template for transcription of pre-genomic RNA (pgRNA) and subgenomic mRNAs. This process is performed by cellular RNA polymerase II which is responsible for cellular mRNA synthesis in the

host body[92]. In this step, the HBV transcription is regulated by both cellular and viral factors. Various transcription factors, like liver-specific hepatocyte nuclear factors (HNF)3 and 4[96-97] and certain histone deacetylases (HDACs) , play a role in HBV transcription[98]. On the other hand, recent studies have shown that HBx is capable of recruiting cccDNA minichromosomes and histone modification (acetylation and methylation)[99]. In addition, HBV core proteins can regulate the HBV transcription and replication by binding to CpG island 2 of cccDNA[100-102].

1.1.3.4 Capsid formation and maturation

Once synthesized and exported to the cytoplasm, pgRNA is recognized by the viral polymerase to form a viral pgRNA/polymerase complex. Spontaneously, core proteins are translated and utilize the N-terminal 149 aa (assemble domain Cp149) for dimerization and self-assembly. According to dynamic distribution and phosphorylation sites, core proteins can adopt multiple conformations and undergo transient unfolding or refolding transitions[103-104]. The C-terminal domain (150 to 183 aa) of core proteins is responsible for binding to the pgRNA/polymerase complex for pgRNA packaging[54, 105-106]. After pgRNA packaging, the viral polymerase initiates HBV reverse transcription converting pgRNA into the dsDNA genome[107]. This genome maturing process seems be inextricably linked with the phosphorylation at C-terminal sites of core proteins because mutation of the target sites of phosphorylation abolish generation of mature viral DNA[82]. Only mature nucleocapsids, but not immature nucleocapsids are enveloped by the viral envelope proteins and secreted as virions, which seems that a single-strand blocking signal triggered by ssDNA or pgRNA can prevent the envelopment of immature[108-109]. However, the signal on mature nucleocapsids for envelopment remains to be defined.

1.1.3.5 Virus assembly and release

After the synthesis of viral envelope proteins in the endoplasmic reticulum (ER), the assembly of empty subviral particles (SVP) is initiated by the integration of SHBs in the ER. Cryo-EM studies have revealed that the three envelope proteins assemble and closed pack as a mixed population

of homo-or hetero-dimers[110]. In the process, SHBs monomers rapidly form a disulfide-linked dimer and further assembles into filamentous particles with assistance of protein disulphide isomerase (PDI) within the ER. Then, SVPs are transported to a pre-Golgi compartment (ERGIC) depending on the action of the dynamin-2 GTPase[111-113]. Within the ERGIC lumen, filamentous particles are converted into spherical particles. Finally, SVPs are secreted out cells via the general secretory pathway, independent of glycosylation[114-115].

While the majority of spherical SVP is secreted via ER and Golgi vesicles, the assembly and egress of filaments and infectious virions are budding associated to the multivesicular bodies (MVB). First, nucleocapsids come in contact with the matrix domain (MD) 1 in the cytosol and are directed into the budding sites. Simultaneously, the L-protein interacts with γ2-adaptin which may contribute to HBV envelope protein trafficking from the ER/Golgi complex to the endosomes[116-117]. In the meanwhile, the ubiquitinated γ2-adaptin can be recognized by functional Nedd4 which can interact with core proteins at the position 96 lysine residue[116]. After that, the ubiquitinated complex, composed of Nedd 4, γ2-adaptin, and HBV envelope proteins, recruit the ubiquitin-binding endosomal sorting complexes required for transport (ESCRT)-II complex, followed by the recruitment of ESCRT-III and Vps-4 to mediate ER intraluminal budding and membrane fission[118-121].

Recent studies have demonstrated that budding and release of HBV viral particles heavily depend on the functions of MVB[119-121]. In support of this notion, virus assembly appeared in large intracellular compartments of HBV infected cells and liver biopsies from HBV-infected patients[122]. Another clue hinting at MVBs supporting virus budding is the fact that HBV is an ESCRT dependent virus[119, 121]. Besides, several studies showed that the HBV envelope proteins may associate with autophagy protein LCs in an autophagic pathway to travel out of the plasma membrane via the endosomal system[123]. However, it is still poorly understood exactly how and

where in the host cell HBV capsids recruit the envelope and the virus particles egress out of the infected cells.

1.1.4 Animal models of HBV infection

Despite decades of research, there is still limited knowledge about the virus-host interaction and immune system response during the natural HBV infection process because of the narrow host range and tissue tropism of HBV. Thus, effective animal models are necessary for the HBV research and clinical testing of antiviral agents. Currently, the animal models are mainly divided into the HBV-related virus models, natural infection models, and mice-based models.

The Peking duck and the woodchuck model belong to the HBV-related virus models used for studies about the replication mechanism and the preclinical evaluation of most antiviral drugs for HBV infection. However, there exist still some differences in the infection progress between these viruses and human HBV. The natural infection models, including Chimpanzees and Tupaia, are susceptible to infection with human HBV and support the full HBV replication cycle. Chimpanzees are capable of establishing acute and chronic HBV infections similar to those of infections in human[124-127]. Still, this model has been restricted mainly due to the significant ethical concerns and high costs. Compared to chimpanzees, Tupaia, as non-rodent mammals, are more often used for the study of HBV infection both *in vivo* and *in vitro*[128-129] HBV infection in Tupaia tends to be mild and transient at low viral replication[130].

Mice are the best characterized and most convenient laboratory animal model. However, they cannot be infected with HBV. To overcome these limitations, transgenic mice with a single expression of HBV proteins, such as HBsAg, HBeAg, and HBx, are used to study the role and oncogenic potential of HBV proteins[131-133]. Mice can replicate HBV, and secrete infectious HBV virions from integrated, overlength HBV DNA[134]. There is also no establishment of cccDNA in HBVtg1.3 transgenic mice[134]. As an alternative, adenoviral (Ad) vectors have been developed to

transfer overlength HBV DNA into the mouse liver to mimic HBV infection[135]. This model opens the possibility to investigate the mechanism of immune-mediated viral clearance. However, a persistent infection is generally not achieved due to the strong response against the adenovirus itself[136]. Compared to adenovirus transduction, adeno-associated viral (AAV) infection does not induce an obvious immune response and permits the establishment of persistent HBV infection[137-138]. All HBV genome transfer approaches allowed studying the elimination of the HBV transcript template in fully immune-competent mice but failed to permit the study of HBV cccDNA. To mimic the complete life cycle in mice models, chimeric mice with human hepatocytes have been developed. In this model, mice with immune deficiencies have been used, including $Rag2^{-/-}$ (recombinant activation gene 2), Sci (severe combined immunodeficiency) lacking functional B and T cells or Sci/beige mice also lacking NK cells functions[139], and $Fah^{-/-}/Rag2^{-/-}IL2rg^{-/-}$ knocking out Rag2 and IL2rg[140]. Aside from basic investigations on the biology of the HBV infection, human chimeric mice likely represent an ideal object for testing antiviral compounds on the influence of cccDNA clearance[141].

1.1.5 Therapeutic approaches

Currently approved antiviral therapies for chronic HBV infection include pegylated interferon-2α (IFN-α) and nucleos(t)ide analogues. After 24-48 weeks of therapy of interferon, viral replication is sustainably reduced and thereby therapy reduces the development rate of HCC. HBV's response to the IFN-α treatment depends on its genotype. A has the highest response rate, followed by HBV genotype B, C, and D[142-144]. Compared to the IFN-α treatment, nucleos(t)ide analogues have proven tolerable for long-term treatment. Nucleos(t)ide analogues (NUCs) are HBV polymerase inhibitors and prevent HBV DNA synthesis[145]. Lamivudine is the first registered nucleoside analogue for the treatment of chronic HBV infections. Following Lamvudine, Adefovir[146], Entecavir[147], Tebivudine[148], and Tenofovir disoproxil fumarate[149] have been

developed. One or a combination of these NUCs can control progeny release and viremia, while they cannot completely eradicate HBV infection as cccDNA still persists in hepatocytes, leading to a relapse of the HBV infection if the patients discontinue the treatment. Another concern in clinical practice is the emergence of resistance which limits the antiviral efficacy of NUCs.

To completely eradicate HBV infection, new drugs that target distinct steps of the HBV life cycle have been developed. These include inhibitors of the viral entry, new polymerase inhibitors, capsid and assembly inhibitors, virus release blockers, and disruptors of cccDNA formation and transcription[150-151]. In addition, innovative therapies aiming at enhancing the anti-HBV immune response have been considered as alternatives for curing hepatitis B (for review, *see Gehring and Protzer*)[152]. Antiviral agents are being tested, including TLR agonists, B cells and T-cells therapy, checkpoint inhibitors, and therapeutic vaccines[67, 153-154].

1.2 Application of metal nanoparticles in the detection of hepatitis B virus infection

(*Chapter 1.2 is based on the article[155]: "Applicability of Metal Nanoparticles in the Detection and Monitoring of Hepatitis B Virus Infection". Viruses 2017, 9(7), 193; https://doi.org/10.3390/v9070193*)

Infections with the hepatitis B virus (HBV) often become chronic, especially when people are infected at a young age. Chronic HBV infection is strongly associated with the development of liver diseases such as liver cirrhosis and hepatocellular carcinoma, resulting in about one million deaths each year[156-158]. Although currently no curative therapy for chronic HBV infection is available, treatment of patients with nucleo(s)tide analogs or interferon can suppress viral replication and reduce the risk of developing end-stage liver disease.

Several physico-chemical and biochemical methods have been developed to diagnose and quantify HBV infection[159-163]. In most infected patients, HBV DNA can be detected by PCR, and secreted HBV antigens such as the envelope (HBsAg) and core proteins[159, 163], can be detected by Enzyme-Linked ImmunoSorbent Assay (ELISA)[160]. Although PCR- and ELISA-based methods have proven to have a good specificity, they are not always sensitive enough to detect HBV antigens in patient samples. For instance, in occult HBV infection, HBV DNA can be detected in patient serum in the absence of detectable HBsAg. Notably, occultly infected patients are still at increased risk of developing HBV infection-related liver disease and may benefit from therapy. In addition, in blood transfusion practice, the detection limits of currently available standardised tests for HBV antigens can cause safety risks, especially because blood samples are often pooled before testing to reduce testing costs.

Nanoparticles have been developed for various applications in the treatment and imaging of liver diseases. Typically, such nanoparticles are coated with biological components (e.g., antibodies, oligonucleotides, aptamers, etc.) that grant them the ability to interact with one specific protein or

DNA fragment. For example, gold particles coated with antibodies specific for certain proteins can be used to localize these specific proteins at a sub-cellular level by electron microscopy. Nano-sized materials combined with biomolecules can contribute to the improvement of bio-analytical methods in terms of sensitivity and specificity[164]. In course of the development of this nanotechnology, various nanoparticles, including e.g. quantum dots[165], carbon nanotubes[166], and nanowires[167], were applied in bio-analytical assays.

The application of nanoparticle-based detection methods may provide a more sensitive alternative for the diagnosis and monitoring of viral infections. In this review, we provide an overview of recent advances in the development of diagnostic tools with specific focus on the application of gold and iron oxide nanoparticles that have gained much attraction in recent years[168-170] in detection and quantification of HBV infection.

1.2.1 Gold nanoparticles

Gold nanoparticles (AuNPs) have often been used as carriers for various biomedical applications, due to their biocompatibility, their optical and electronic properties, and because they are relatively easy to manufacture[171]. AuNPs can be functionalised with various biological macromolecules, such as antibodies, oligonucleotides, and aptamers, to detect a variety of (bio)molecules[172]. For instance, antibody-coated AuNPs can be used to stain substrates for electron microscopy. This process can be applied to determine the (sub)cellular localisation of (viral) proteins[173-174].

Over the last decades, various methods have been developed that employ the unique physical properties of AuNPs to detect and quantify biological molecules in samples. These methods have the potential to improve the sensitivity, ease of operation, and applicability of HBV detection[175]. For instance, *Wu et al*. employed AuNPs dually marked with anti-HBsAg antibodies and human alpha-thrombin (HAT, an enzyme that can convert a bisamide substrate into a fluorescent reaction product). These AuNPs were used to detect HBsAg bound to anti-HBsAg coated on a conventional ELISA plate by enhanced fluorescence enzyme-linked immunosorbent assay

(FELISA)[176]. Under optimal conditions (HBsAg was dissolved in PBS), this method allowed detection of HBsAg concentrations of 5×10^{-4} IU/mL, which is about 10^4 times lower than the detection limit of other fluorescence-based methods, and 10^6 times lower than those of the conventional ELISA[176].

One of the unique physical properties of the AuNPs is their specific optical behaviour when exposed to electromagnetic radiation. This causes an oscillation of the electrons, called surface plasmon resonance (SPR), which depends on the size and shape of the nanoparticle as well as the dielectric constant of its environment[177]. Consequently, interactions between molecules covered on the AuNP and molecules in the environment cause changes in SPR frequencies of the AuNP that can be detected and used to quantify specific biological molecules in their environment. Several bioanalytical applications based on AuNP SPR have been designed so far[178-180]. AuNP SPR has also already been used to quantify hepatitis B surface antigens (HBsAgs) in blood, serum, and plasma by directly measuring the shift in the SPR peak of anti-HBsAg coated AuNP[181]. The authors could thus detect HBsAg concentrations of 0.1 IU/mL[181].

Interestingly, changes in the SPR of AuNPs can be observed in the visible part of the spectrum, allowing determination of a reaction by colour shifts visible to the human eye. Typically, for this format, AuNPs are immobilised on paper strips and used to detect PCR-amplified pathogen DNA, which greatly enhances their applicability in resource-poor settings. For example, AuNPs have been combined with inkjet printers, with dye-sensitised TiO_2 photodetectors as a mean of detection, to generate colorimetric biosensors with a limit of detection (LOD) of 1 nM DNA[182]. Recently, this method was further enhanced to simultaneously detect two different pathogens in one reaction [183]. For example, *Duan et al.* employed immobilised HBV and HCV antigens, SPA-labelled AuNPs, and a silver staining step to increase the optical signal. Thereby, they were able to simultaneously detect antibodies to HBV and HCV antigens[184]. The method was tested on 305 serum samples, of which antigen concentrations were previously determined by ELISA, showing

a comparable sensitivity and a LOD of 3 ng/mL antibody[184]. Additionally, *Song et al*. used oligonucleotide-directed precipitation of AuNP on a plate carrier to identify YMDD mutations in patient-derived HBV DNA[185]. The release of AuNPs from a carrier can also be monitored by dark-field microscopy. *Jang et al*. used AuNPs coupled to multiple pathogen-specific oligonucleotides with restriction enzyme specific bridging sequences to simultaneously detect femtomolar amounts of the hepatitis A virus (HAV), HBV, and the human immunodeficiency virus (HIV) (c)DNA using sequential incubation with different restriction enzymes[186].

Electrochemical features of the AuNPs make them attractive carriers to grant specificity to electrochemical biosensors (reviewed in:[187]). AuNP-based electrochemical biosensors have been designed for DNA[188-190] and protein[191] quantification and analysis. The method is based on the complex formation between oligonucleotide- or antibody-covered AuNPs and specific DNA fragments or proteins at an electrode surface that results in the production of the detectable amperometric, potentiometric or impedimetric signals (**Fig. 1.6**). Notably, the detection of viral DNA does not require a (PCR) amplification step. So far, several electrochemical biosensors have been used to detect HBV antigens. Streptavidin-conjugated AuNPs have been combined with a biotin-labelled, HBV DNA-specific DNA probe and applied for voltammetric detection of HBV DNA with a LOD of 2×10^{-12} M viral DNA[192]. *Chen et al*. designed and tested an impedance biosensor for HBV DNA, which had a LOD of 111 copies/mL[190]. Similarly, several other electrochemical biosensors have been developed to detect HBsAg with a high sensitivity[191-197]

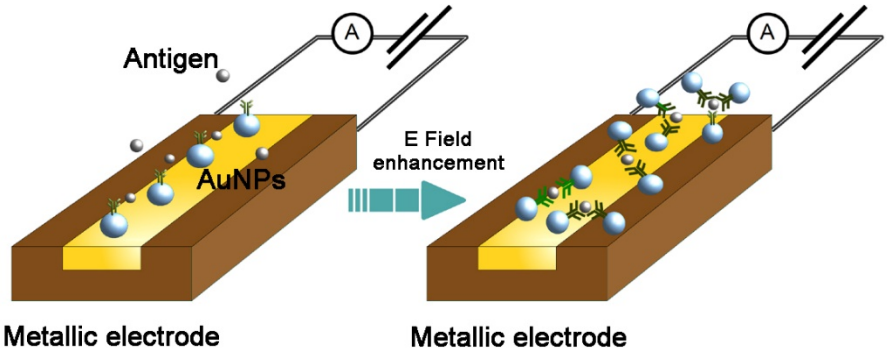

Fig. 1.6 Schematic representation of gold nanoparticles applied in an electrochemical biosensor. The figure is modified from [155]

Because they are easy to operate and do not require reagents or machines to be read out, lateral flow assay (LFA)-based detection methods are often applied in point-of-care diagnostics[175]. Several studies suggest that the main disadvantage of such tests—their low sensitivity—can be improved by AuNP-based signal amplification[198]. *Kim et al*. developed an AuNP-based LFA that could detect 500 ng/mL HBsAg in whole blood, which was comparable to a commercially available HBsAg LFA (Humasis)[199].

Raman spectroscopy terms the analysis of the scattering of low energy electromagnetic radiation by inelastic collision with an analyte[175]. Adsorption or immobilisation of an analyte on AuNPs can greatly (10^6 x) enhance the probability of Raman scattering, a phenomenon called surface-enhanced Raman spectroscopy (SERS). Intriguingly, SERS based detection methods have been developed with a sensitivity in the order of single molecules[172, 200]. A gold nanostructure-SERS based HBsAg assay was developed, which had a sensitivity of 0,01 IU/mL, a satisfactory specificity, and a broad linear range[201].

1.2.2 Magnetic nanoparticles

Because biological materials lack magnetic characteristics, magnetic nanoparticles (MNPs) can be employed to detect specific molecules in biological samples without interfering with the signal detection[202]. MNPs based on iron oxide are one of the most widespread NP formulations applied in biomedical research[203] and have been used in various electrochemical, optical, piezoelectric, and magnetic field sensors[204-210]. For the synthesis of MNPs, several types of magnetic iron oxides, including magnetite (Fe_3O_4), hematite (α-Fe_2O_3), and maghemite (γ-Fe_2O_3 and β-Fe_2O_3), are utilised[211]. As the magnetism of such particles relies on superparamagnetism, they are often referred to as superparamagnetic iron oxide nanoparticles (SPIONs). A widely used and straightforward application of such particles consists of magnetic-activated cell sorting (MACS), in which specific cells are labelled with antibody-conjugated magnetic particles and subsequently sorted by exposure to a magnetic field. The relative ease with which MNP-bound molecules can be sorted has also been put to use in the development of HBsAg-specific aptamers. These were subsequently used to detect HBsAg by ELISA, with a LOD of 0,1 ng/mL[212].

Most MNP-based antigen detection methods are based on changes in the spin-spin relaxation time (T_2) of water molecules surrounding an MNP upon clustering of the MNP, induced by a specific target **(Fig. 1.7)**. Changes in T_2 can be quantified using conventional MRI scanners, or nuclear magnetic resonance (NMR) relaxometers. Notably, such devices are becoming increasingly practical to work with (i.e., bench top-format) and sensitive. Recently, Wang et al. demonstrated that using MNPs and an ultra-low field (ULF) NMR technique, they could detect protein concentrations of 10 pg/mL, below the LOD of conventional ELISA[213]. More recently, chip-based NMR detection systems have been developed, which can process multiple microliter volumes samples[209].

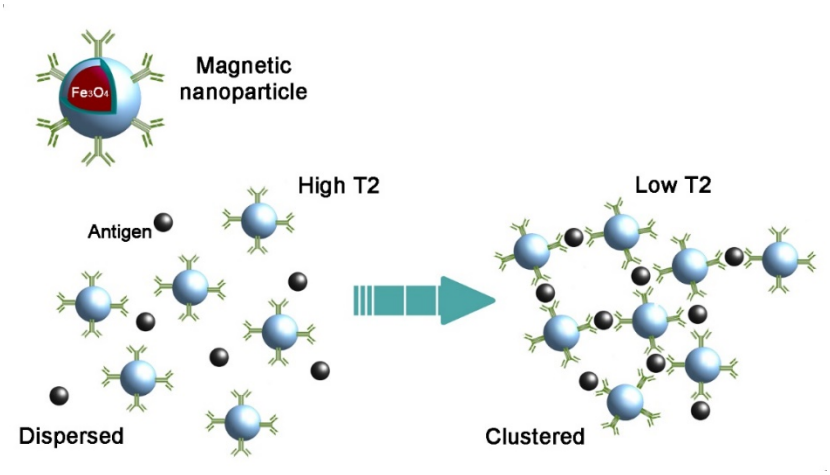

Fig. 1.7 Schematic representation of MNP clustering in the presence of a specific antigen. Following interaction between functionalized MNPs and an antigen, the clustering of MNPs induces a change in the T_2 of the surrounding water molecules, which can be detected by diagnostic magnetic resonance. The figure is modified from [155]

MNPs can also be employed for electrochemical detection of interaction with a specific ligand, e.g. through direct contact with the electrode, transfer of electrons generated in redox-reactions, or formation of a film on the electrode surface[205]. *Fatemi et al*. used MNPs to capture PCR-amplified HBV DNA and subsequently detect the presence or absence of DNA by cathodic stripping voltametry [214]. Although this method requires PCR-amplified DNA, its potential for miniaturisation (i.e. lab-on-a-chip) application is promising[214]. *Nourani et al*. applied anti-HBsAg coated MNPs to capture HBsAg and an HRP labelled secondary antibody to convert aminophenol into electrochemically detectable reaction products, with an LOD of 0.9 pg/mL[214-215]. Furthermore, MNPs have been applied to capture HBV DNA before analysis on a commercially available microfluidic electrophoresis system (Experion, Bio-Rad, USA)[216].

The magnetic properties of MNPs have also been utilised to assemble oligonucleotide-labelled MNPs on an electrode surface by application of a magnetic field. This electrode was subsequently applied to detect HBV DNA by impedance spectroscopy (an electrochemical technique to characterize film formation on conductive surfaces[217], with an LOD of 2,5 nM HBV DNA[218]).

Similarly, *Zhang et al*. constructed an MNP-based HBsAg lateral flow assay. Using human serum samples, they demonstrated that the LFA strips had an LOD of 5 pg/mL for manual (i.e. naked eye) detection and of 0.1 pg/mL for detection by mechanical analysers[219].

1.2.3 Combinations of different nanoparticles

Detection methods employing different nanomaterials can increase their effectiveness and applicability by combining properties of individual nanoparticles[220]. *Mashhadizadeh* and *Talemi*[221] combined antisense DNA probes, immobilised on AuNPs and linked to a carbon paste electrode, to measure the competition between target (HBV) DNA and MNPs by assessing the change in interfacial charge transfer resistance (R_{CT}). The LOD of this method amounted to 3.1 (± 0.1) × 10^{-13} M HBV DNA, considerably lower than detection methods employing either nanoparticle alone.

AuNPs and MNPs have also been combined for the colorimetric quantification of target DNA or RNA. For one, AuNPs were labelled with oligonucleotides that, upon hybridisation to a specific target RNA or DNA sequence, undergo a click-chemistry reaction, which could be amplified by thermal cycling. Subsequently, AuNPs were precipitated using MNPs specific for the reaction product. The (visible) change in the reaction supernatant SPR (i.e., colour) served as a readout[222]. The technique could detect several copies of target DNA, comparable to PCR-based methods. However, the procedure was not validated for detecting HBV DNA. *Alizadeh et al*. designed an electrochemical HBsAg immunosensor by assembling anti-HBsAg-coated MNPs on an electrode as a supporting matrix. Peroxidase-labelled AuNPs were then used to generate a voltametrically detectable signal[223], with a LOD of 0.19 pg/mL HBsAg. Additionally, Shen et al. combined AuNps with MNPs to detect HBsAg by anodic stripping voltammetry, with a LOD of 87 pg/mL[224].

1.3 Open questions

Current standard treatments, alpha-interferon and nucleos(t)ide analog (NUC), are only partially effective for treating chronic HBV infection due to the persistence of cccDNA. HBV is classified as a pararetrovirus due to transcription of a viral RNA intermediate during the HBV replication. Nuclear HBV cccDNA serves as a transcription template and initiates new virus replication when therapy is stopped[225-226]. Therefore, new antiviral strategies must be explored to eradicate cccDNA in HBV-infected cells. A number of studies have reported that killing the infected hepatocytes will be necessary to eradicate HBV and thus for finite treatment. To distinguish infected from naïve cells, however, specific bio-markers are needed. The most prominent one is HBsAg, that consists of subviral particles (SVP) and virions released from infected cells. While spherical SVP are secreted via ER and Golgi, many recent studies have reported that the endosomal sorting pathway via the formation of multivesicular bodies (MVBs) drives the release of infectious virions and filamentous SVP[118, 120-121, 227-228]. That means that similar to a retrovirus, HBV hijacks the ESCRT-complex of the host cell triggering membrane fission at the budding site as the final step of the HBV life cycle[65, 112, 118, 120-121, 227-228].

Immunofluorescence study and the immunohistochemical (IHC) staining have reported membrane-located and ‘patchy’ distribution patterns of HBsAg in liver biopsies from chronic hepatitis B-patients[229-232]. These studies may indicate that the viral envelop proteins might be involved in hijacking the ESCRT-MVB pathway for virus exit, thus co-localizing with the plasma membrane. Nevertheless, it is still unclear how HBV envelop proteins are translocated to the plasma membrane. As mentioned above, more sensitive detection methods and imaging tools of HBV infection are obviously necessary for identifying patients in need of therapy and preventing transmission[159, 163, 233].

1.4 Aim of the study

The thesis presented addresses the hypothesis that HBV envelop proteins trans-locate to the plasma membrane where they can be used as biomarker to identify HBV-infected cells or cells carrying an HBV integrate and maybe targeted therapeutically.

The first aim of this study was to verify the surface localization of HBV envelope proteins on infected hepatocytes. For this purpose, those cells with stable HBV replication, HBsAg expression, and natural HBV infection should be stained by characteristic anti-HBs antibodies and new artificial antibodies prior to fixation under confocal microscopy. In addition, ultrastructural analysis should be performed to prove that trans-membranous HBV envelop proteins are stained and not only viral or subviral particles secreted or bound back to the plasma membrane. If this holds true, membrane-associated HBsAg would be considered a bio-marker to target infected hepatocytes and provide promising immunotherapeutic strategies to eliminate chronic hepatitis B. This should be investigated using immune-therapy targeting HBV envelop proteins.

The second aim of this thesis was to use magnetic iron particles (SPIONs) bound to HBsAg-directed antibodies to detect and target HBV. We attempted to prove the functionality of MoMab-SPIONs, a possibly powerful tool for detection of active HBV replication in diagnostics. To test the target efficacy of MoMab-SPIONs *in vivo*, MoMab-SPIONs should be intravenously administered in different mouse models, including the Alb-PSX mice mirroring HBsAg expression, HBV 1.3 transgenic mice, and immunodeficient mice with xenografts of human hepatoma cells. They shall be detected by histological analyses and by imaging of SPIONs-conjugates with computed tomography and Magnetic Resonance Imaging (MRI).

2. Results

2.1 Establishment and characterization of detection and imaging tools

2.1.1 Generation and characterization of the chimeric anti-HBs antibody 5F9

The murine monoclonal antibody 5F9, which recognizes the major hepatitis B virus SHBs, was previously generated and characterized by F.G. Shiraz and U. Protzer[234]. It has been reported that the 5F9 antibody interacts with the HBsAg 'a' determinant, an immunogenic loop, and protects hepatocytes from infection by neutralizing HBV particles[235]. To obtain human chimeric antibody, the heavy and light chain variable regions of the 5F9 antibody were cloned in-frame with the constant regions of human IgG1 to construct the chimeric monoclonal antibody 5F9 (c5F9). The c5F9 antibody was produced by co-transfection of plasmids DNA encoding the c5F9 heavy- and light-chains in HEK293T cells (O.Quitt thesis, **Fig. 2.1.1)**.

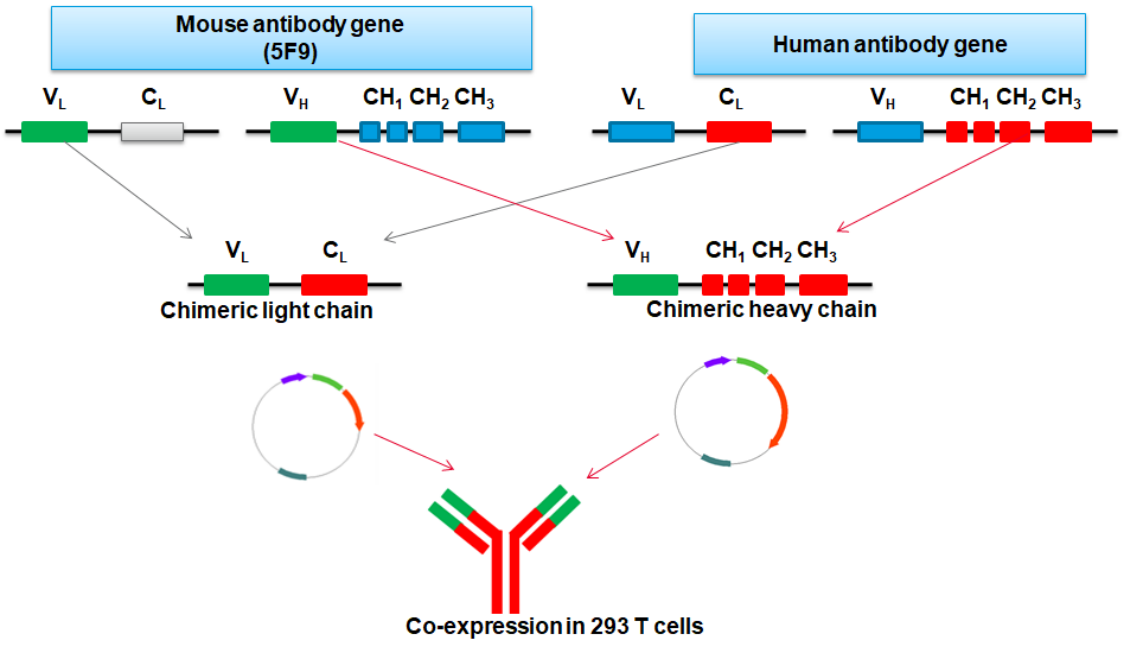

Fig. 2.1.1 Schematic representation of the chimeric 5F9 antibody production. The antibody contains a murine Fab region and a human Fc region. Both plasmids were co-transfected into HEK-293 T cells. After 3 days, the supernatant was harvested and purified.

2.1.2 Evaluation of expressed c5F9 from HEK293T cells by anti-HBs ELISA

To assess expression of c5F9, the supernatant from c5F9 plasmids transfected HEK293T cells was analyzed by ELISA (anti-HBs ELISA). In this ELISA method, we immobilized HBsAg on the ELISA plates and detected by the supernatant of transfected cells as a primary antibody. After washing steps, goat anti-human IgG coupled to peroxidase were used to detect the primary antibody. The supernatant from non-transfected cells was implemented as a negative control mechanism. Therefore, it was treated with the respective antibody combination. The anti-HBs ELISA results showed that the supernatant from transfected cells expressing c5F9 has a 10 folds-higher OD450 value than the negative control value, which indicated c5F9 could bind the coated HBsAg. To optimize the cell culturing condition, we compared the antibody production and the cell viability in different concentrations of FCS in a DMEM medium. The results showed that a lower FCS concentration in DMEM can aid cells in producing more antibodies, while 5 % FCS medium facilitates keeping the cells stable for longer (about 4 days). Therefore, 5 % FCS can be regarded as the optimal concentration in our situation **(Fig. 2.1.2)**.

To improve expression of recombinant antibody, a stable cell line should be generated. Because two plasmids need to be co-transfected to produce c5F9, there are three types of transfected cells: cells expressing only heavy chain, only light chain or both chains required to form c5F9. After single cell dilution, cell clones were grown and screened by analyzing the corresponding supernatants through anti-HBs ELISA **(Fig. 2.1.3A)**. Two clones, 3A4 and 1C3, were selected to produce higher amount of the c5F9 antibody **(Fig. 2.1.3B)**.

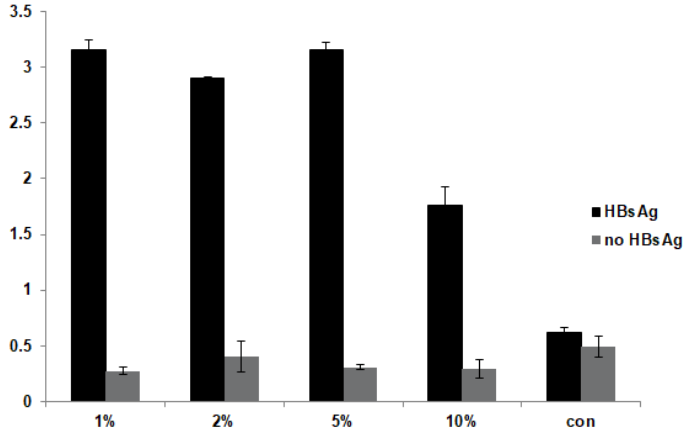

Fig. 2.1.2 The optimum concentration of FCS in the culture medium. After the co-transfection of plasmid DNA to initiate c5F9 production, HEK-293 T were cultured with different concentrations of FCS. 3 days post-transfection, the corresponding supernatant was harvested and assessed by anti-HBs ELISA for specificity. Con indicates the supernatant from non-transfected cells.

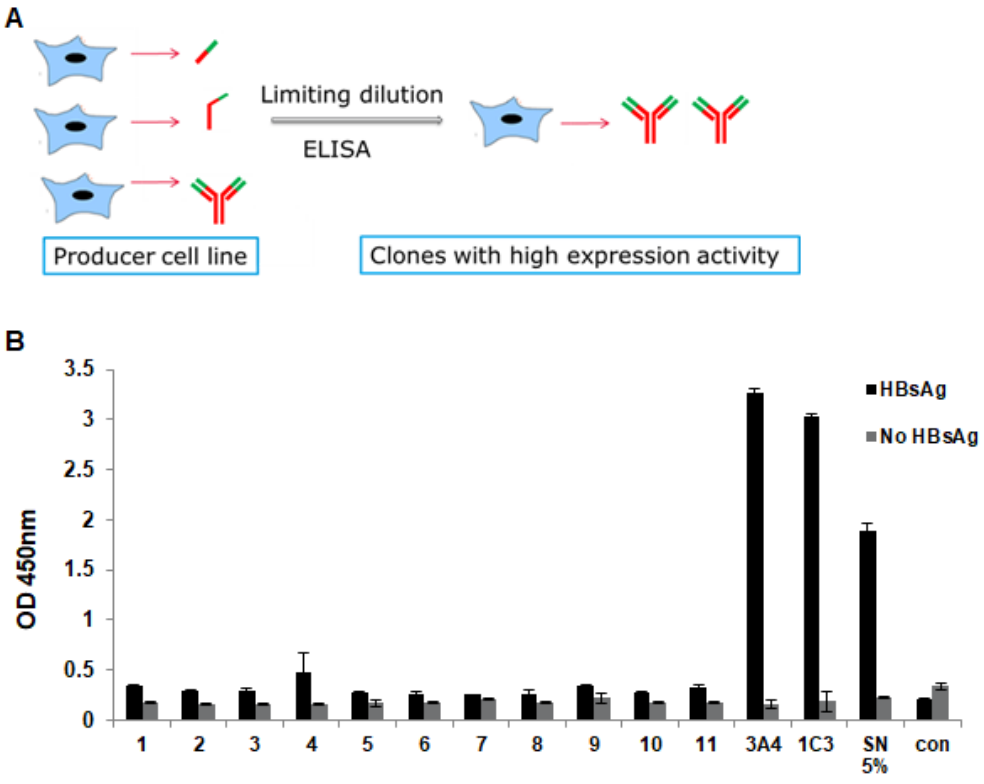

Fig. 2.1.3 Selection of clones with high expression activity. (A) Schematic overview of the clone selection by limiting dilution. Both plasmids were co-transfected into HEK-293T cells. As shown here, three types of transfected cells were produced in the producer cell line. (B) Comparison of the antibody expression for clone selection using ELISA. Clone 3A3 and 1C3 were selected since they were able to

produce higher amounts of the monoclonal antibody c5F9 compared to other clones. The producer cell line was cultured in 5 % FCS DMEM.

2.1.3 Purification of chimeric monoclonal antibody c5F9

Supernatants from these cell clones were initially collected in a volume of 2 liters. After concentration and dialysis in PBS, 100 ml in total volume were obtained. Next, the 5F9 antibody was purified by Protein-A affinity chromatography, and the eluted fractions were further analyzed by anti-HBs ELISA **(Fig. 2.1.4)**. The ELISA results verified that the fraction of A2-A4 contained the antibody c5F9 at high concentrations in comparison to both flow through and the concentrated supernatant. The purity of these fractions including the lower antibody concentration A2-A7 was assessed by SDS-PAGE followed by Coomassie staining, as well as by Western blot analysis **(Fig. 2.1.5)**. The denatured samples resulted in two prominent bands typical for antibodies: the heavy chain with 55 kDa and the light chain with 25 kDa. Since the A2-A3 fraction peaked in the UV detector during chromatography, other bands in A2-A3 in the Western blot analysis might represent the non-denatured or partially denatured antibody.

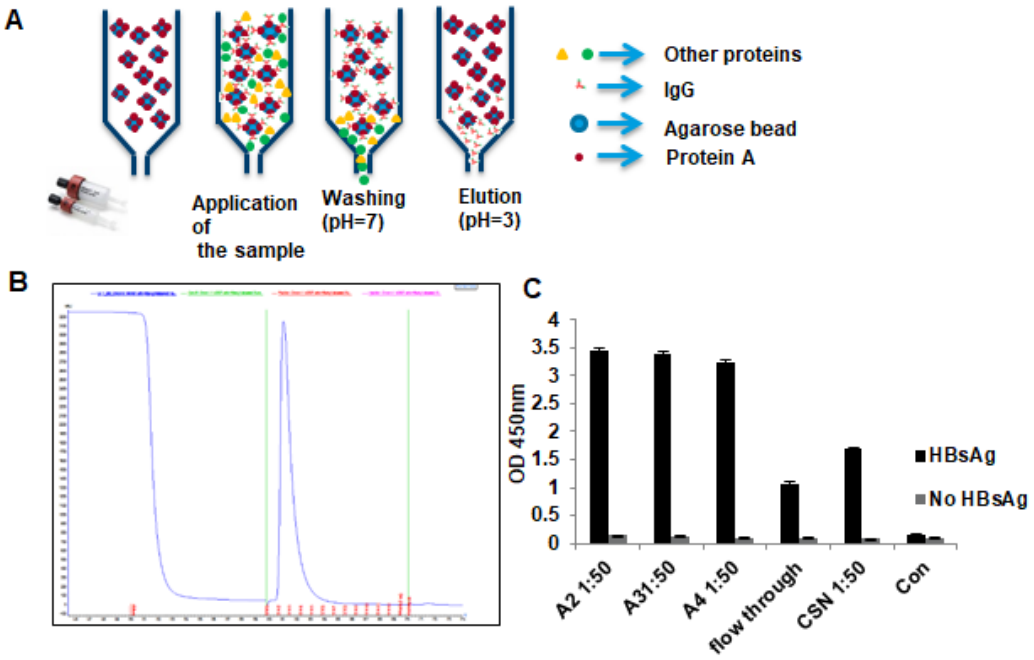

Fig. 2.1.4 Purification procedure of the antibody 5F9 by protein A column and high-performance liquid chromatography (HPLC). (A) Schematic representation of antibody purification by affinity chromatography with immobilized Protein A. (B) The absorption of the chromatographic separation was detected by UV detector and plotted output versus retention time in HPLC**.** The concentration of antibodies in each fraction was presented by a blue peak in the chromatography. (C) Each fraction was diluted to 50 folds and assessed by anti-HBs ELISA. CSN presents the concentrated supernatant and is diluted to 50 folds like each fraction. Con indicates the supernatant from non-transfected cells. Flow through is the washing fraction after sample application.

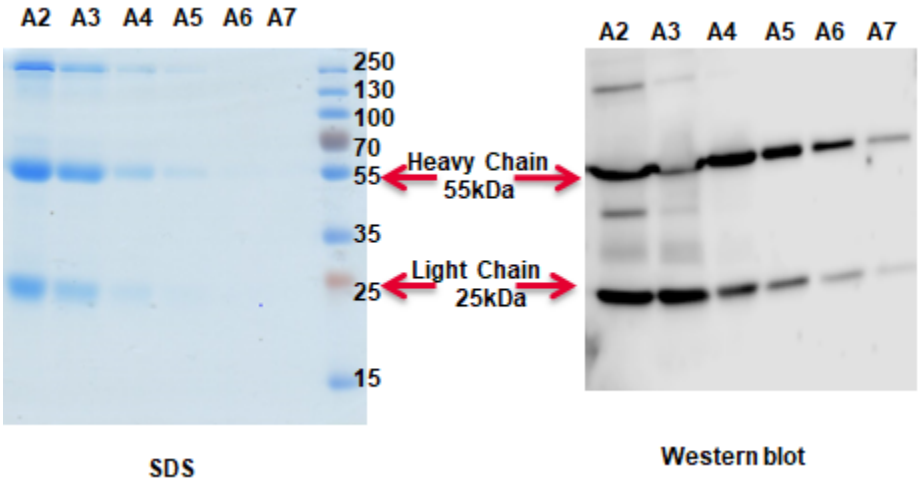

Fig. 2.1.5 Coomassie staining and Western blot analysis of all fractions after purification. Each fraction (A2-A7) was collected by HPLC and further analyzed by SDS-PAGE. Left: Coomassie staining of fraction A2-A7, right: Western blotting analysis of fraction A2-A7 stained with anti-human antibody. The antibody heavy chains (55 kDa) and light chains (25 kDa) are clearly visible. The other bands in A2-A3 might be non-denatured or partially denatured antibody.

2.1.1 Specificity of the chimeric monoclonal antibody c5F9 for HBsAg

To confirm the antigen-binding ability of the purified chimeric antibody c5F9, we compared c5F9 with another murine monoclonal antibody HB01 (provided by Prof. Dr. Dieter Glebe, Giessen). The Western blotting analysis demonstrates that c5F9 could recognize the reduced HBsAg at a comparable level to HB01 **(Fig. 2.1.6 A)**. Next, we immobilized different sources of HBsAg in a series of dilutions to test c5F9 binding activity. Subsequently, c5F9 was detected by a goat anti-

human IgG peroxidase secondary antibody. The results showed that c5F9 could bind HBsAg expressed in yeast, CHO cells and human serum **(Fig. 2.1.6 B)**.

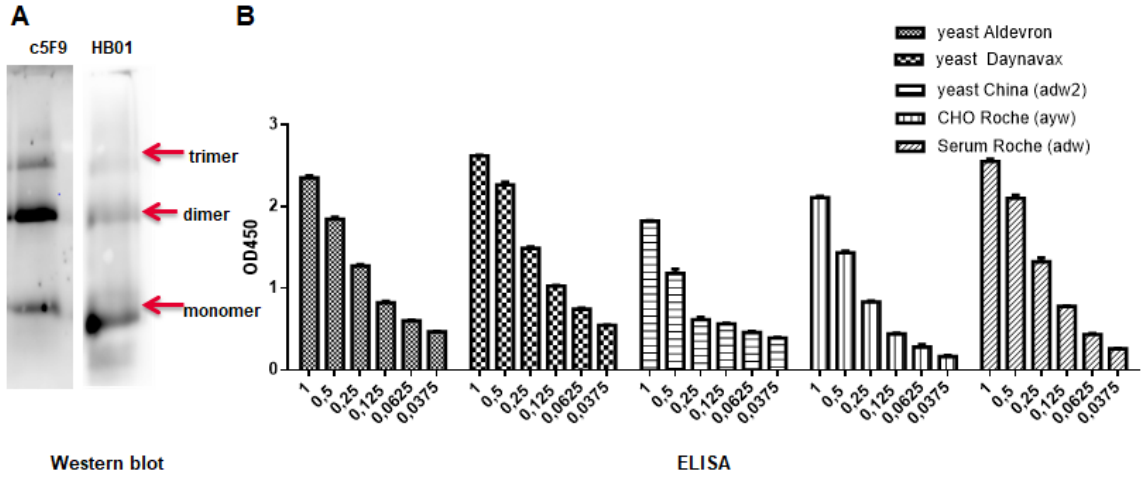

Fig. 2.1.6 Determination of the antibody affinity of c5F9 to divergent HBsAg. (A) HBsAg was mixed with a reducing loading buffer and heated at 95 ° C for 10 mins. The proteins were separated by SDS-PAGE and further stained by c5F9 and HB1 antibodies, respectively in Western Blot. (B) A series amount of HBsAg (µg/ml) were mobilized to the ELISA plates and detected by the same amount of c5F9. After incubation with the goat anti-human IgG labeled with HRP, the OD 450 value was measured by Tecan.

2.1.2 Establishment and characterization of the recombinant antibody MoMab

We have previously shown that the HBV-specific chimeric antigen receptor (S-CAR) can redirect T cells to kill HBV-infected human hepatocytes and result in a profound reduction of viral load *in vivo*[236-237]. In this study, the single-chain fragment (scFv) C8 was used for specifically binding the S domain of all HBV envelope proteins (S, M and L). For this purpose, we constructed a modified monoclonal antibody, called MoMab, which is composed of two single chain antibody fragments against HBsAg. The ScFv C8 was selected from a phage library expressing cDNA from B cells of a donor vaccinated against HBV[237]. We linked the scFv C8 genes to the constant region (CH2 and CH3) of a human IgG 1 **(Fig. 2.1.7A)**.

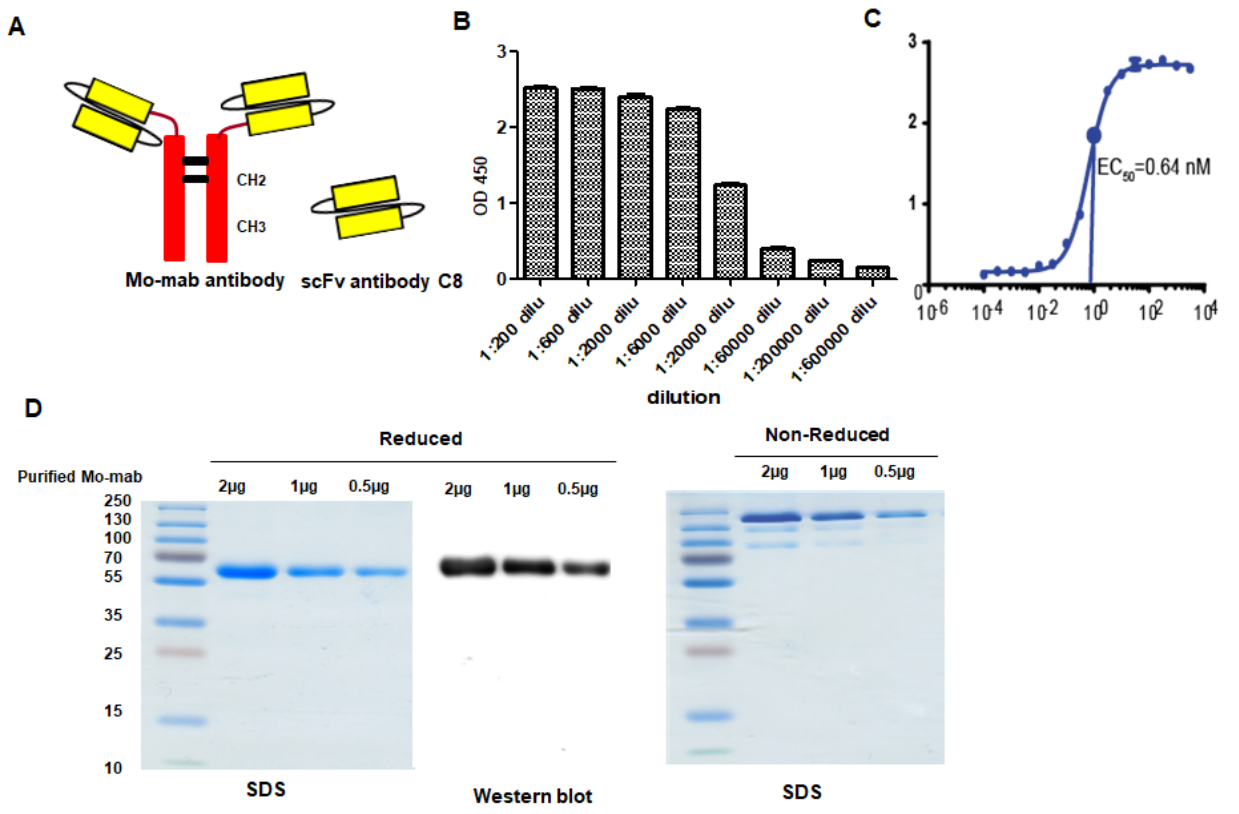

Fig. 2.1.7 Generation and characterization of the recombinant HBsAg-specific antibody MoMab (A) Schematic representation of the MoMab and scFv C8 construct. (B) Purified antibodies were analyzed by Anti-HBs ELISA in different dilutions (C) The EC50 values were calculated for MoMab separately from the fitted curves shown using Prism GraphPad 6 software. (D) Purified MoMab was analyzed by SDS-PAGE under reducing (left) and non-reducing (right) conditions. Denatured MoMab was detected by goat anti-Human IgG. In the reduced group, one distinct band with size 60 kDa is ScFv C8 with CH2 and CH3. Under non-reduced buffer treatment, the bands represent the dimers or trimers of MoMab after purification.

The expressed MoMab antibody was purified from the supernatant of transfected cells while its antigen specificity was investigated by anti-HBs ELISA. The purification of MoMab was performed by iron exchange chromatography (in VIVO, Berlin, Germany) **(Fig. 2.1.7B)**. The affinity of MoMab to HBsAg was measured by EC50 at 0.64 nM by using direct ELISA **(Fig. 2.1.7C)**. Coomassie staining (SDS-PAGE) showed that the purified MoMab did not contain light chains. Hence, the

purification was successful. Western blotting analysis also revealed that MoMab can be detected by anti-human IgG **(Fig. 2.1.7D)**.

2.1.3 Neutralization activity and epitope mapping of MoMab

We next assessed the capacity of MoMab to neutralize HBV. Concentrated HBV particles (MOI 100) were pretreated with different concentrations (1μg, 0.1μg, and 0.01μg) of MoMab. The commercial polyclonal antibodies Hepatect and Nadi were used as a positive control. After 3 hours, differentiated HepG2-NTCP cells were incubated by the HBV-antibody mixture for 24 hours. Following the washing with PBS, we exchanged the DMEM medium and collected the supernatant at 4 dpi, 8 dpi and 12dpi for HBsAg and HBeAg measurement. On the final day (12 dpi), we lysed cells to measure cccDNA, rcDNA and pgRNA. The HBV infection was evaluated by the level of all HBV infection markers we measured before. The inhibitory effect of MoMab was hence determined by the reduction of HBeAg, HBsAg, cccDNA, rcDNA and pgRNA. As the **Fig. 2.1.8** depict, the pretreatment with 0.1 μg and 1 μg MoMab resulted in completely inhibited HBV infectivity **(Fig. 2.1.8)**. Furthermore, even at the lower concentration alone (0.01 μg), MoMab was still capable of inhibiting HBV infection, causing a reduction to an approximately 40% infection rate. Taken together, MoMab, showed the predicted strong neutralizing ability against HBV infection.

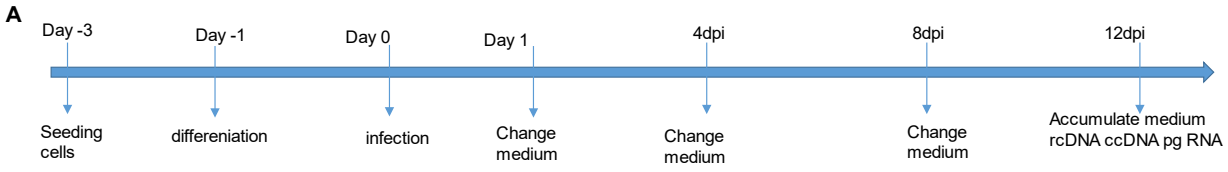

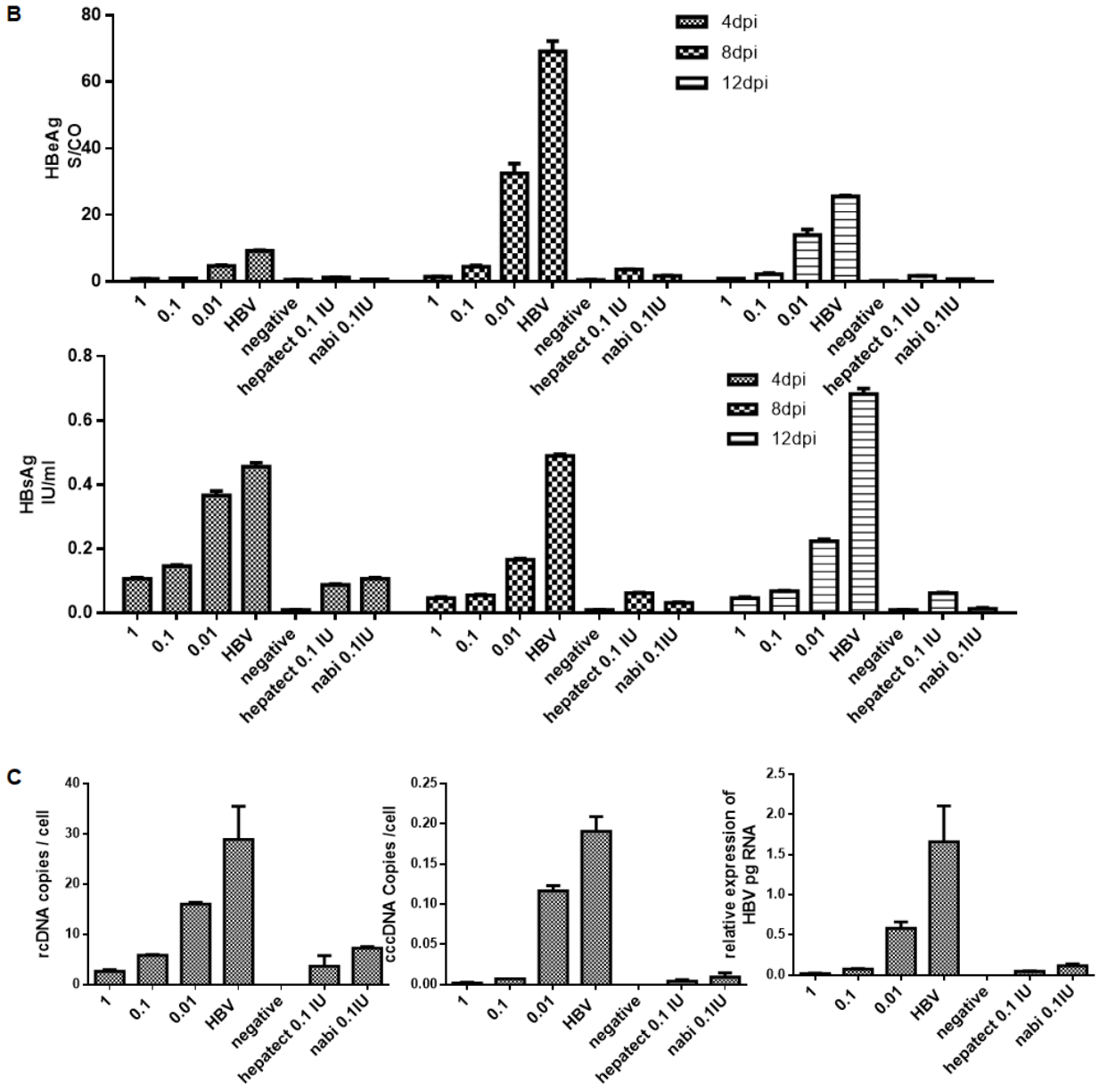

Fig. 2.1.8 The neutralization effect of MoMab on HBV infected HepG2-NTCP cells. (A) Schematic representation of the neutralization assay (B) The levels of the newly produced HBsAg and HBeAg in the cell supernatant at day 4, 8 and 12 post infection. (C) The relative expression levels of cccDNA, rcDNA, and pg RNA from cell lysate at 12 days post infection. The values were determined in triplicates, the results are given as the mean ± SD.

Next, we immobilized different sources of HBsAg in a series of dilutions to test MoMab binding activity. The detection by MoMab was verified using a goat anti-human IgG peroxidase as a secondary antibody. The results revealed that MoMab could detect HBsAg from different sources, the one from Aldevron, being the only exception **(Fig. 2.1.9A).** To further test the binding capacity with different HBV genotypes and subtypes, an ELISA was performed on plates coated with subviral particles of different HBV genotypes and detected by the MoMab and Murex antibody, respectively. The ELISA results were then normalized by the Murex antibody (the commercial kit) to evaluate the binding activity **(Fig. 2.1.9B)**. The results indicated that MoMab is capable of recognizing HBsAg of genotypes A, B, C, D, E, and G. Additionally, it showed a higher affinity to the subtypes adw2 and adrq than to ayw.

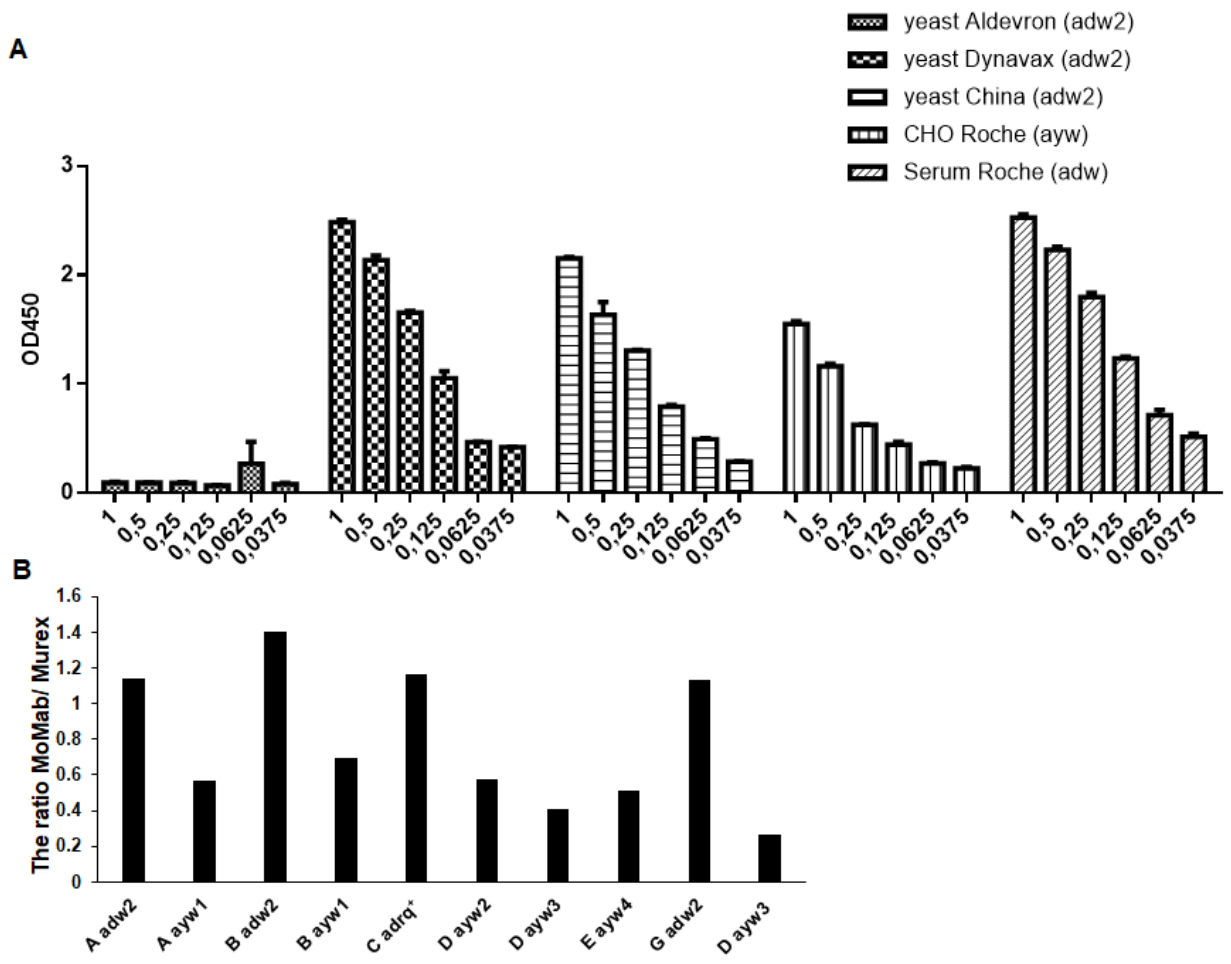

Fig. 2.1.9 Binding affinity and specificity of MoMab to different types of HBsAg. (A) A series amount of HBsAg (μg/ml) were mobilized and detected by the same amount of MoMab. After incubation with the goat anti-human IgG labeled with HRP, the OD 450 value was measured by Tecan. (B) HBsAg (1μg/ml) was immobilized and detected by MoMab and the commercial anti-HBs antibody Murex. The ratio of OD between MoMab and Murex level was presented.

As previously mentioned, a majority of antibodies, have their most effective neutralizing antibody response to the 'a' determinant[238-239] which is defined by a specific conformation of the antigenic loop (AGL) polypeptide. To precisely map AGL binding antibodies, *Camille Sureau et al*. used an alanine-scanning mutagenesis approach to design the SHBs mutants by site-directed mutagenesis[240-241]. Subsequently, viral particles with each mutant were normalized or calibrated

by anti-preS2 antibody since this antibody only recognized the linear epitope in the Pre-S2 domain of LHBs and MHBs[240]. In **Fig. 2.1.8**, MoMab has demonstrated its strong neutralization effect to HBV. Therefore, we hypothesized that MoMab could interact with the epitope within the 'a' determinant in order to neutralize viral particles. To identify the epitope of MoMab, we collaborated with *Camille Sureau* and examined its binding activity to each mutant by Sandwich ELISA. In the process, plates were coated with 2µg/ml MoMab to bind the same amount of these mutants. After that, a rabbit anti-PreS2 polyclonal antibody was loaded as detection antibody for binding the existing SHBs mutants. These results **(Fig. 2. 1.10)** revealed that MoMab is sensitive to the mutation of the disulfide bonds (C121, C124, C137, C138, C139, C149 and C147) and/or the near-by residues. Besides, we found that the residues K141 and D144, as well as the residue T148, appear to be part of the binding-region within the HBsAg. Interestingly, Y225 which is highly conserved in all HBV genotypes, except for genotype F, also plays an important role during the formation of the MoMab epitope.

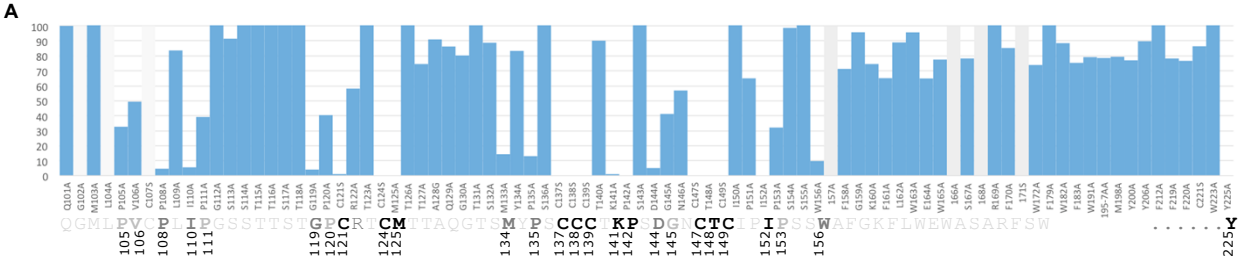

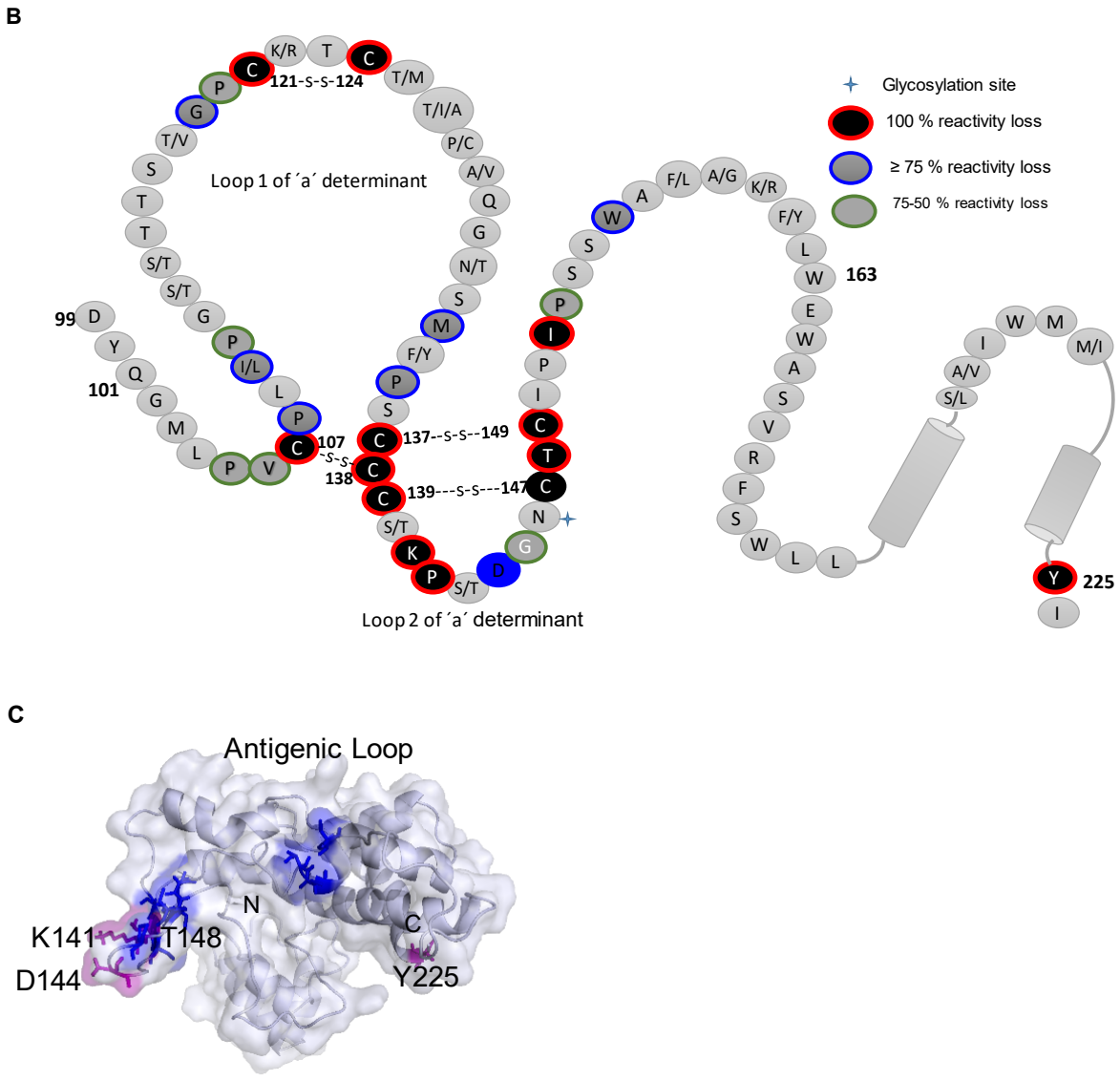

Fig. 2.1.10 The epitope of MoMab within S of HBV. (A) The histogram of the alanine-scanning of every amino acid in the AGL region on the binding of MoMab. The values were normalized using an anti-preS2 antibody. (B) Schematic representations of the essential residues within the 'a' determinant for HBsAg-binding by MoMab. (C) Overview of the residues relevant for the interaction with MoMab epitope (blue residues) highlighted by the proposed structure of HBV S. The proposed S structure is shown as a ribbon diagram with a transparent surface indicating the major residual determinants of the MoMab epitope (purple). The N- and C-terminus as well as the antigenic loop are indicated. The proposed structural view was modified using the PyMOL Molecular Graphics System, version 1.3 (Schrödinger, LLC).

2.1.4 Generation and characterization of MoMab-conjugated Superparamagnetic iron oxide nanoparticles (SPIONs)

To conjugate with MoMab, the dextran-coated magnetic nanoparticles were cross-linked to epichlorohydrin and aminated. Magnetic nanoparticles were then suspended in a phosphate buffered solution of MoMab (60 µg mL^{-1}). The dense core of the particles ranged in size of 5-10 nm[242]. Subsequently, dextran was coupled to the carboxyl groups of MoMab after activation by the water-soluble carbodiimide to produce the superparamagnetic conjugate MoMab-SPIONs. As a contrast electron dense agent, we used dextran-coated superparamagnetic iron oxide nanoparticles (SPIONs) prepared from iron salt solutions by co-precipitation in alkaline media at 80°C. The size of the prepared SPIONs were 43.1±3.1 nm. The conjugation of the nanoparticle surface with MoMab increased the size of the particles to 52.4±2.6 nm. The Z-potential was measured at –13.2 mV **(Fig. 2.1.11A)**.

As established, those elements with the odd protons and/or neutrons in their nucleus provide the primary origin of the magnetic resonance signal which can be monitored by nuclear magnetic resonance (NMR) and magnetic resonance imaging (MRI) applications. magnetic particles can alert the transvers relaxation time *T2* of the surrounding water molecules in the liquids and can be read out from NMR[243]. Therefore, the binding ability between HBsAg and MoMab-SPIONs was determined by temporally measuring T_2 of the conjugate suspension in water (i.e. "*switch assay*"). This switch assay was developed by *Tassa et al.* for the biosensing of molecules with sensitivity comparable to an immune enzyme assay[210]. After co-incubation with HBsAg (50, 100, and 200 ng mL^{-1}), the aqueous-phase magnetic conjugates were measured by NMR (CXP-300 NMR-spectrometer, Bruker, Germany) and the T_2 relaxation times were collected. In the presence of soluble HBsAg, the NMR magnetic relaxometry analysis of MoMab-SPIONs showed a significant change in the spin-lattice relaxation due to the binding between MoMab and HBsAg. Subsequent '*switch assays*' with the estimated T2 relaxation times of MoMab-SPIONs nanoparticles co-

incubated with soluble HBsAg demonstrated the formation of conjugate clusters that resulted in an increased T2 transverse time of relaxation. **(Fig. 2.1.11B)**.

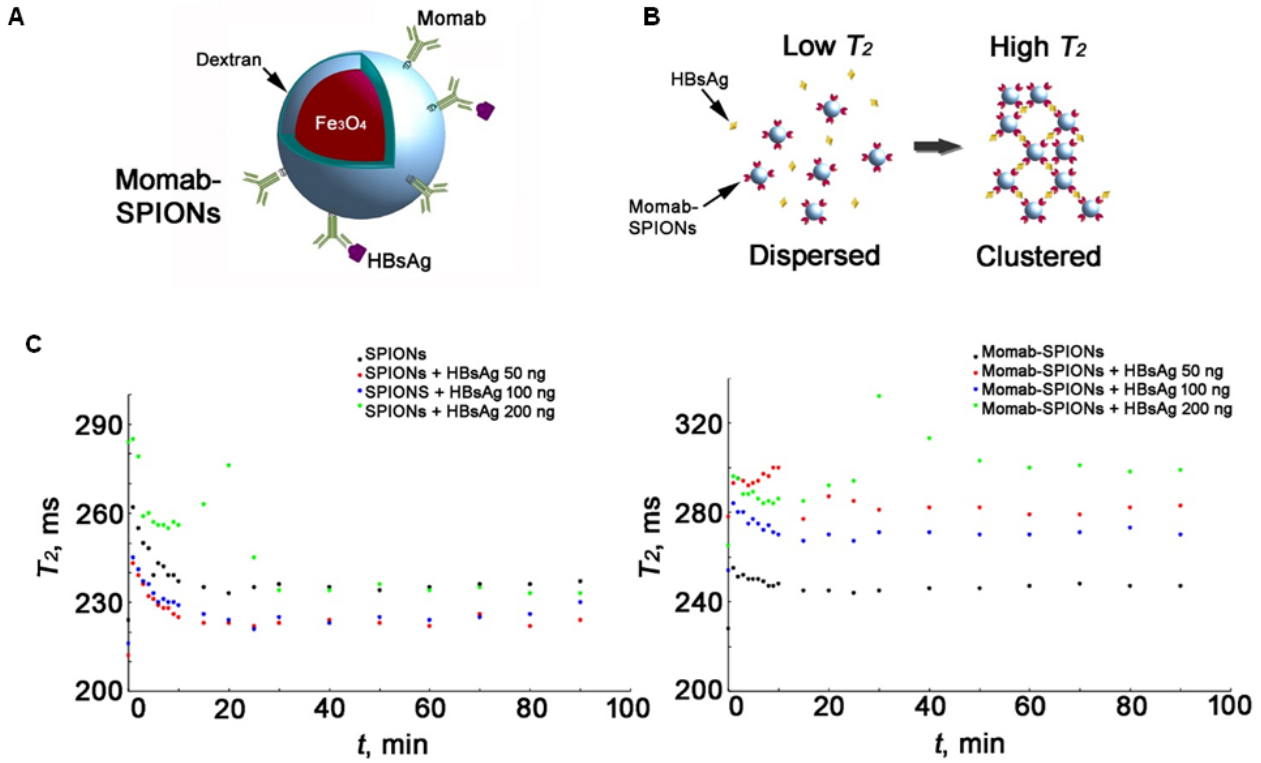

Fig. 2.1.11 Characterization of the specific activity of MoMab-conjugated SPIONs. (A) Schematic overview of the MoMab-SPIONs nanoparticles and the clustering induced by HBsAg. (B) The schematic illustration of the magnetic relaxation switch assay. (C) Magnetic relaxation switch assay on MoMab-SPIONs. Time evolution of spin-spin relaxation time (T2) of water protons based on the interaction of MoMab-SPIONs with HBsAg in a uniform magnetic field at a temperature shift from 20°C (left panel) to 37°C (right panel). The magnitude of the change in T2 relaxation time was increased dose dependent on the HBsAg in the volume, indicating the specific binding of MoMab coated SPIONS to HBsAg. Experiments performed by Dr. Boris P. Nikolaev and Yaroslav Marchenko (Pavlov First Saint Petersburg State Medical University).

This *switch assay* result signaled that the addition of HBsAg to magnetic conjugates increased the T_2 *t*ransverse time of relaxation from 240 ms to 300 ms in a homogenous magnetic field of 7.1 T due to the aggregation of conjugated nanoparticles by HBsAg. Besides, the *T2* relaxation

times of MoMab-SPIONs increased through the addition of HBsAg in a dose-dependent manner **(Fig. 2.1.11C)**. All experiments regarding the generation and characterization of MoMab-SPIONs have been performed in close collaboration with **Dr. Maxim A. Shevtsov, Dr. Boris P. Nikolaev and Yaroslav Marchenko** (Pavlov First Saint Petersburg State Medical University).

2.2 Analysis of the surface localization of the HBV envelope proteins

2.2.1 Membrane-localized HBV envelope proteins is not due to the attachment of circulating HBV virions

To analyze the distribution of HBV envelope proteins, confocal microscopy with immunofluorescence staining was applied to visualize the location of HBV envelope proteins on HepG2.2.15 cells, which constitutively replicate HBV. HepG 2 cells functioned as the negative control. To further test if the distinct membranous HBsAg exists on the HBV positive cells, we performed indirect immunofluorescence by labeling with different anti-HBs antibodies and counter-staining with Wheat Germ Agglutinin (WGA) as a cell membrane marker. To prevent the detection intracellular HBsAg, cells were antibody-stained at 4°C followed by PFA fixation without Triton-X100.

First, cells were stained with the anti-HBs antibodies 5F9 and c5F9 at 4°C to keep the cell membranes intact. Both antibodies contained the same binder Fab 5F9 to detect HBsAg. After counterstaining with WGA and labelling with an Alexa Fluor 647-conjugated goat anti-mouse or goat anti-human antibody, HBsAg was detected by the two selected antibodies. This proved that HBsAg was located on the surface of HepG2.2.15 cells, but not on HepG2 cells **(Fig. 2.2.1)**. Furthermore, we tested the ability of MoMab to interact with HBsAg on the cell surface using HepG2.2.15 and HepG2 cells. In the text line which included the Fab 5F9 antibodies staining, the localization of HBsAg on the plasma membrane was confirmed by overlapping with WGA **(Fig. 2.2.2)**. Indeed, well-characterized anti-HBs antibodies (the monoclonal antibody HB01 and the polyclonal antibody HBVax) also confirmed the membranous HBsAg with this distinct punctate pattern **(Fig. 2.2.3)**.

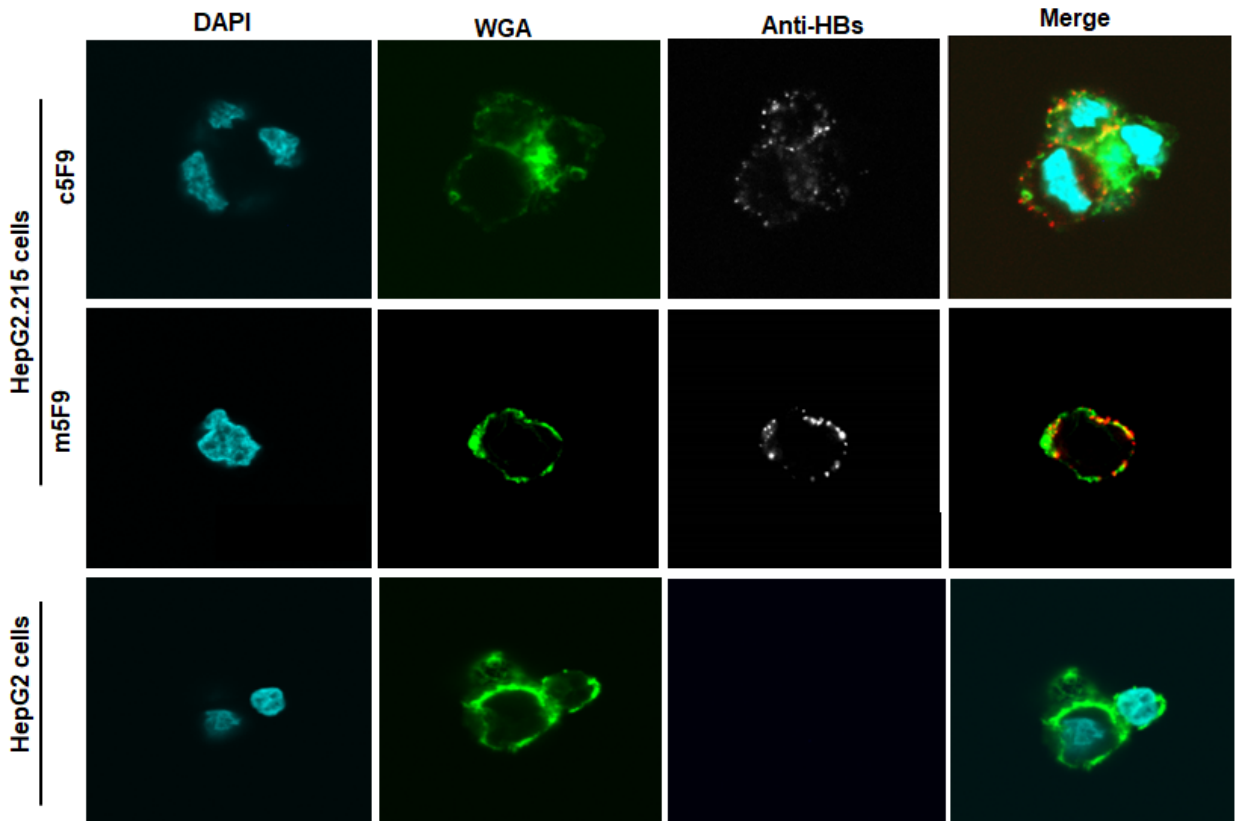

Fig. 2.2.1 Localization of the HBV envelope proteins on the surface of HepG2.2.15 cells by immunofluorescence using Fab 5F9. Non-permeabilized HepG2.2.15 cells and HepG2 cells were stained with m5F9 (murine) and c5F9 (chimeric) anti-HBs antibodies (grey/red) and counterstained with Wheat Germ Agglutinin (cellular membrane marker, green) as well as Dapi (nucleus, cyan). The plasma rim staining by WGA combined with the punctate membrane-localization of HBsAg (green and red) has been highlighted for non-permeabilized HepG2.2.15 cells compared to HepG2 cells. Scale bar = 10µm.

To test if the detected membranous HBsAg localization on the non-permeabilized HepG2.2.15 cells is ascribed the attachment of circulating HBV virions, HepG2 cells were pre-incubated with supernatant containing HBV virions before staining. Similar to the pure HepG2 cells, the indirect immunofluorescence of non-permeabilized HepG2 cells with HBV virions showed no HBsAg staining on the cell membrane **(Fig. 2.2.3)**. In conclusion, these results suggest that the membranous localization of HBsAg is not due to attachment of circulating HBV virions and that HBsAg partially ends up on the cell membrane of actively HBV-replicating cells.

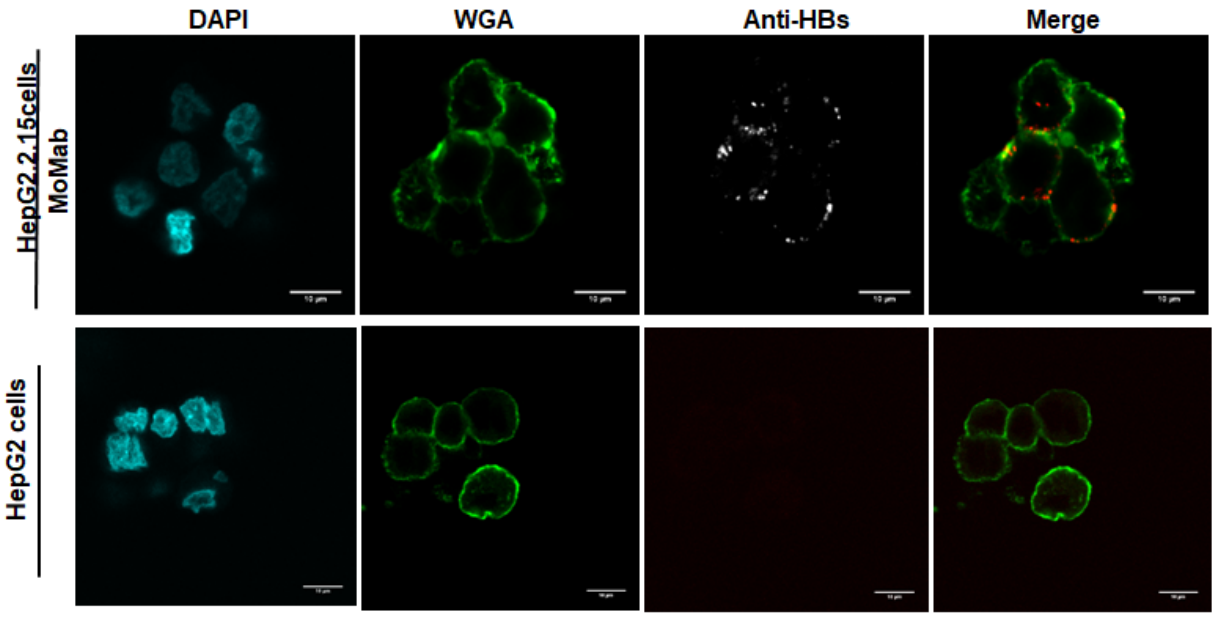

Fig. 2.2.2 Localization of HBV envelope proteins in HepG2.2.15 cells detected by indirect immunofluorescence using MoMab. Non-permeabilized HepG2.2.15 cells were stained with MoMab detecting HBsAg (grey) and counterstained with Wheat Germ Agglutinin (cellular membrane marker, green) as well as Dapi (nucleus, cyan). For negative controls, HepaG2 cells were stained with the respective antibody combination. Scale bar = 10µm.

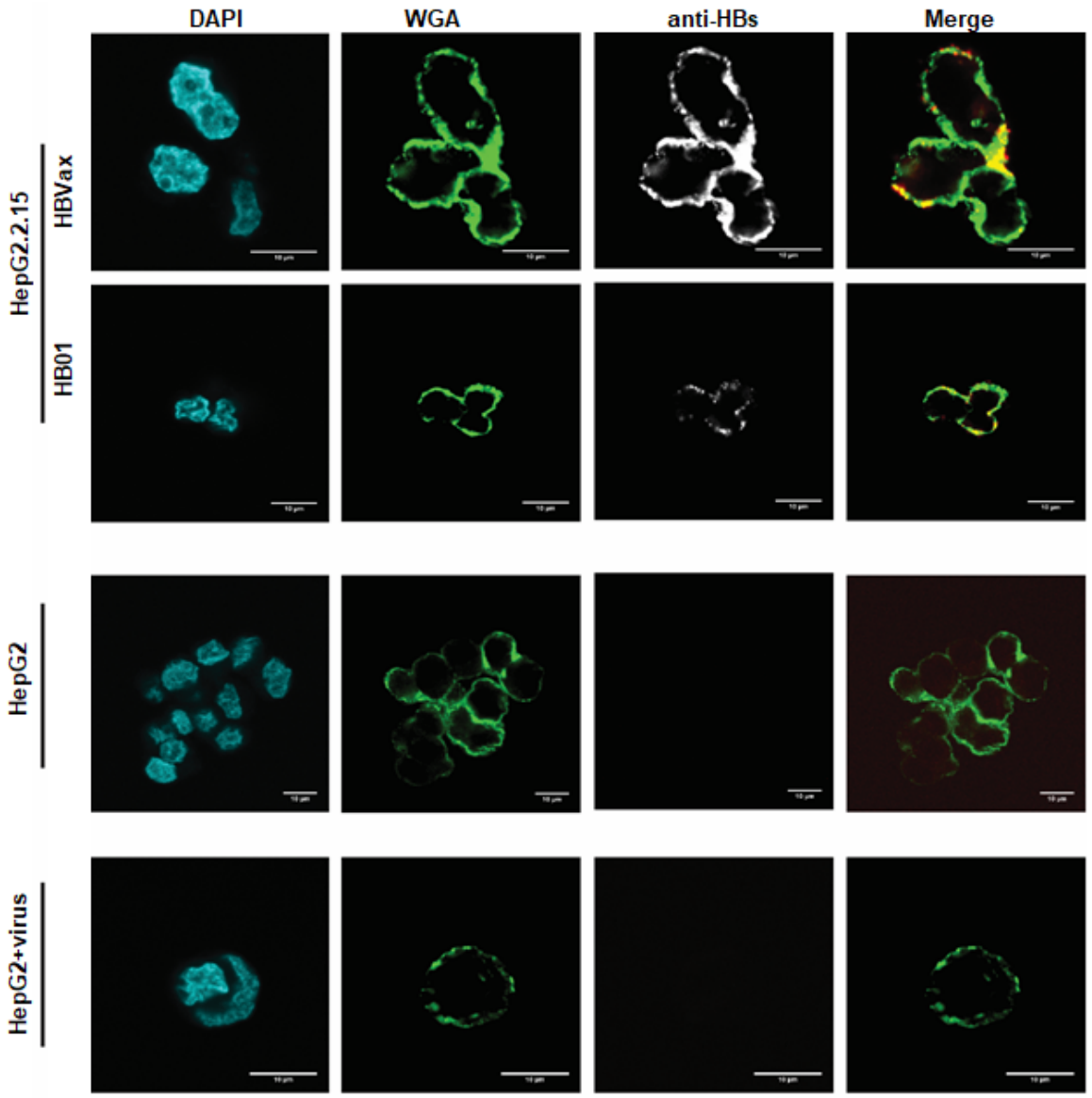

Fig. 2.2.3 Localization of HBV envelope proteins in HepG2.2.15 cells detected by indirect immunofluorescence using HB01 and HBVax. Non-permeabilized HepG2.2.15 cells were stained with HB01(murine monoclonal anti-HBs) and HBVax (rabbit polyclonal anti-HBs) detecting HBsAg (grey) and counterstained with Wheat Germ Agglutinin (cellular membrane marker, green) as well as Dapi (nucleus, cyan). HepaG2+virus group was recorded as HepaG2 cells containing the supernatant of HepG2.2.15 (HepaG2+virus) with the respective antibody combination. The HepaG2 cells were functioned as a negative control. Scale bar = 10μm.

2.2.2 The membrane-localized HBsAg does not rely on the production of subviral particles

Since HBV infection results in the production and abundant secretion of non-infectious subviral particles (SVPs)[244], these SVPs can likely affect the HBsAg localization. To address this issue, Huh7 cells were transient-transfected with SHBs-expressing constructs fused with mCherry. 48 hours post transfection (p.t), non-permeabilized cells were stained with MoMab and HB01 antibodies, respectively. As expected, the membrane detection by MoMab and HB01 only appeared on mCherry-positive cells and colocalized with WGA **(Fig. 2.2.4)**. After non-permeabilized surface staining, cells were subsequently permeabilized by Triton-X100 and co-stained with an antibody against Protein disulfide isomerase (PDI), an enzyme in the endoplasmic reticulum (ER). In addition to the membrane localization between WGA and anti-HBs, confocal microscopy showed that most of S-mCherry were accumulated in the perinuclear cytosol of cells and colocalized with the ER marker PDI (Fig.2.2.5). The result was thus in consistent with the previous, considered that HBV envelope proteins are derived from the endoplasmic reticulum[107, 245].

Next, HuH7 cells were transiently transfected with plasmids expressing either the small (S, SHBs) or large (L, LHBs) surface antigens, or all HBsAg isoforms combined (SML) **(Fig. 2.2.6A)**. To analyze the HBsAg secretion out of the cells, cells were harvested and lysed 24h, 48h, or 72h post-transfection and analyzed by Western blot using HB01 **(Fig. 2.2.6B)**. Additionally, HBsAg secretion from the corresponding supernatants was quantified by the Architect QT assay as well as Western blot **(Fig. 2.2.6C)**. The Western blot of the whole-cell lysates showed that the expression pattern of the S-, L-, and SML-constructs were comparable regarding the unglycosylated and glycosylated forms of S, M, and L **(Fig. 2.2.6B)**. In contrast, the Western blot and the Architect QT assay of the corresponding supernatants showed that the secretion of subviral particles is only induced by the expression plasmids of S and SML but not L **(Fig. 2.2.6B-C)**.

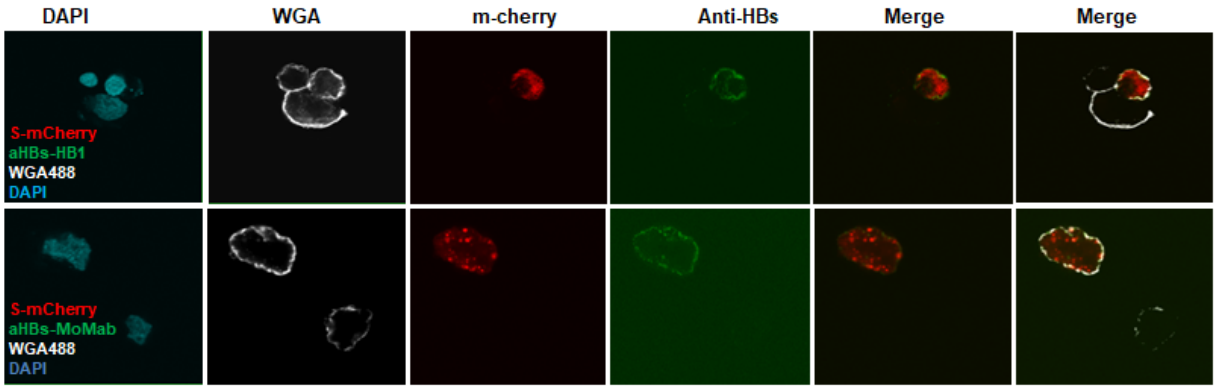

Fig. 2.2.4 Surface localization of S proteins fused mCherry in Huh 7 cells. HBsAg fused with mCherry was transiently transfected into HuH7 cells. After 48 hours, cells were evaluated for HBsAg cell surface distribution. Nuclei were stained by Dapi (cyan). Cells membrane was co-stained by WGA (grey). Analogously, mCherry was represented as the HBsAg expression in the HuH7 cells (red). Non-permeabilized cells were stained by MoMab (green), in comparison with HB01 (green). HBsAg was detected by MoMab and HB01 on the membrane of mCherry-positive cells, and colocalized with WGA.

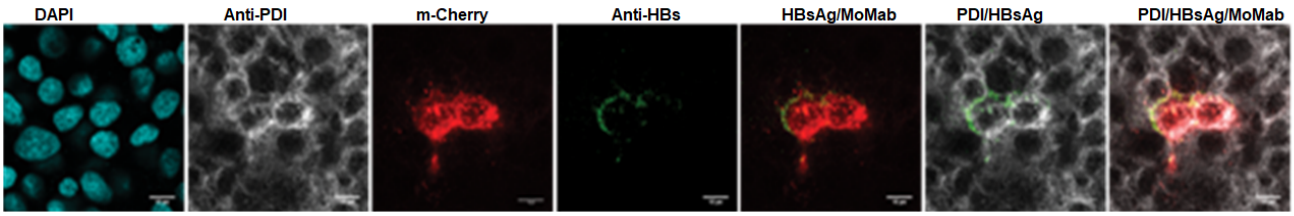

Fig. 2.2.5 Intracellular distribution of S proteins fused m-cherry in HuH7 cells. HuH7 cells expressed HBsAg fused to mCherry 48h after transient transfection. Non-permeabilized cells were stained by MoMab (green). Subsequently, we labeled MoMab with anti-human IgG conjugated with Fluorescence. In the following, cells were permeabilized and co-stained by anti-PDI (grey). mCherry represented HBsAg expression (red). Nuclei were stained by Dapi (cyan). In mCherry-positive cells, most of HBsAg accumulated in the perinuclear region and colocalized with PDI. Scale bar = 10µm.

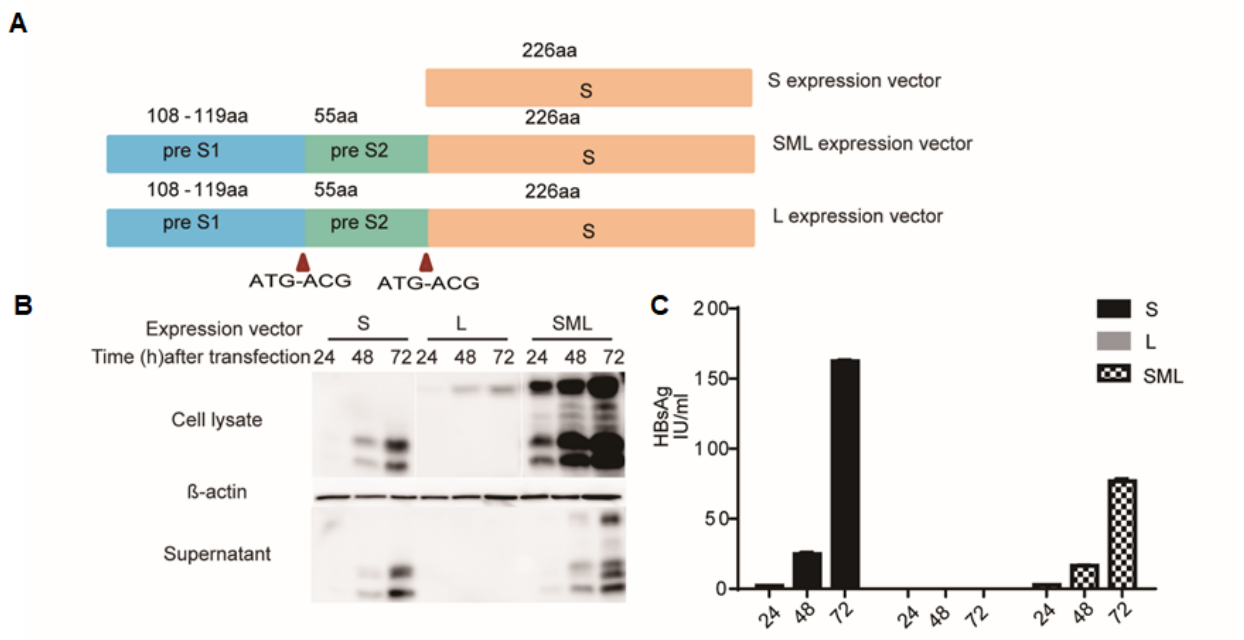

Fig. 2.2.6 Characterization of the expression of S, L, and SML in combination. (A) The S, L, and SML full-length proteins have been highlighted to show the preS1, preS2, and S regions, thereby indicating the position of the mutations in L that prevent the expression of S and M as well as the truncation of S. The mutation of methionine to threonine is shown in the text. Additionally, their position is indicated by red arrows. (B) Western blots of cell lysates and the supernatants of HuH7 cells transfected with S, L, or SML at 24, 48 and 72 h.p.t. using a monoclonal S-specific antibody (HB01) and a monoclonal anti-actin blot shown as a loading control for the cell lysates. The gels show the expected bands for S, M, and L in both the unglycosylated and glycosylated forms, except for L which is undetectable in the supernatants. C) HBsAg levels were monitored using a mix of monoclonal S-specific antibodies by means of an ELISA-based assay and the Architect QT assay. The results are depicted as IU/ml, showing a significant increase in HBsAg concentration over time for S and SML but not L.

To verify that the predominant pattern of speckled membrane-localized HBsAg can be confirmed by the tested S-, L-, and SML-expressing vectors, indirect immunofluorescence with the HB01 was performed on these transfected HuH7 cells. In line with our previous experiments, all HBsAg isoforms was associated with the plasma membrane in a distinct, punctuate pattern, even for the

L isoform that does not induce SVPs production/secretion **(Fig. 2.2.7)**. The observation that LHBs locates to the cell membrane confirmed that membrane-associated HBs was derived from endogenously expressed HBs and independent of the secretion of SVP.

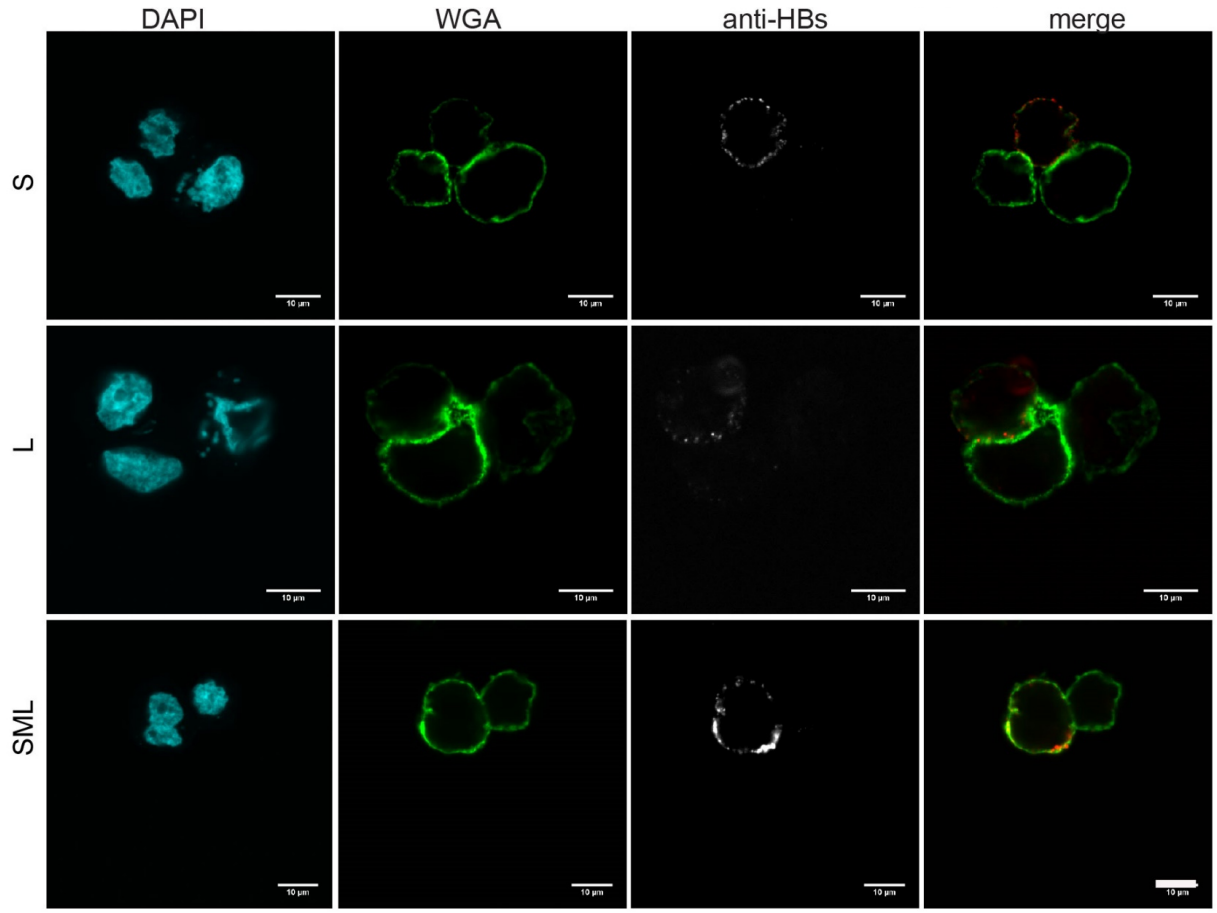

Fig. 2.2.7 HBV envelope proteins (S, L, and SML) colocalizes with WGA in HuH7 cells. The plasma membrane rim staining by WGA (green), combined with the punctate membrane-localization of HBsAg (white/red), has been highlighted for HuH7 cells transiently transfected with S, L or SML. The localization of HBsAg and WGA with the DAPI-stained chromatin (cyan) were recorded in a confocal laser-scanning microscope. Scale bars represent 10µm.

2.2.3 The correlation between the surface localization of HBV envelope proteins and the infection efficacy

To investigate the punctate localization of HBsAg within the plasma membrane during a natural infection, we infected hepatocytes' HepG2-NTCP cells with a multiplicity of infection (MOI) ranging from 200 to 1000. To confirm the infection efficiencies by increasing MOIs, the level of HBsAg and HBeAg in the supernatant at day 7 and day 9 post-infection were quantified by the Architet QT assay **(Fig. 2.2.8A)**. In addition, the expression of rcDNA, cccDNA, and pgRNA were evaluated by qRT-PCR **(Fig. 2.2.8B)**. The results proved that the production of the infection markers significantly increases when enhancing the MOIs **(Fig. 2.2.8A-B)**. Seeking to further explore the membranous distribution of HBV envelope proteins in HBV-infected cells, we performed the previous indirect immunofluorescence by labelling MoMab in the non-permeabilized infected cells at day 9 post-infection. First, the increasing amount of HBV used for infection strongly correlated with the detection of membrane-localized HBV envelope proteins **(Fig. 2.2.9)**. Additionally, co-staining with HBcAg confirmed that the speckled membranous HBsAg only appeared in the HBV infected cells, and thus it is commitment with HBcAg expression. However, HBc expression did not show any significant correlation with the HBsAg expression **(Fig. 2.2.10)**. Taken together, these data confirmed that the intensity of surface localization of HBV envelope proteins in infected HepG2-NTCP cells relates to the infection efficiency and infectious dose (MOI).

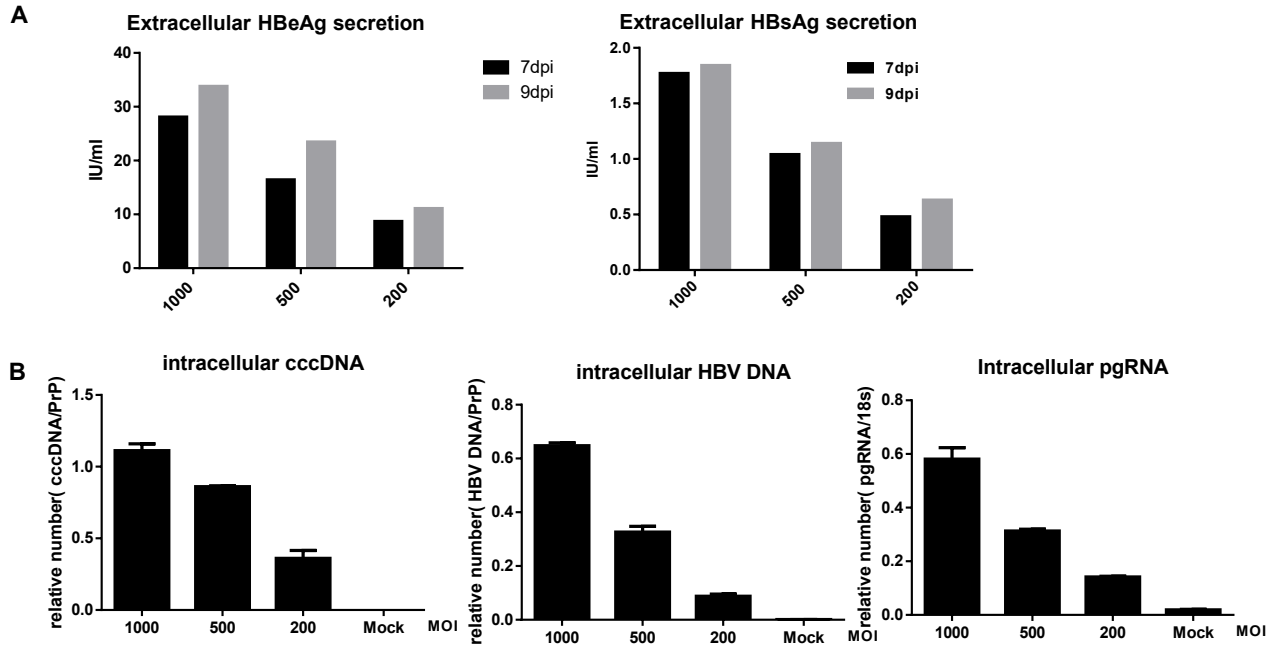

Fig. 2.2.8 Identification of HBV replication in HepG2-NTCP cells. HepG2-NTCP cells were infected with different MOIs ranging from 200 to 1000. (A) The culture supernatant was collected at 7 dpi- and 9-dpi by exchanging the medium on the respective day. A gradual increase of HBsAg and HBeAg secretion were observed in each infected group. (B) At 9 days after the infection, the total DNA and RNA were isolated from cell lysates and analyzed by real-time PCR to quantify the expression of cccDNA and rcDNA.

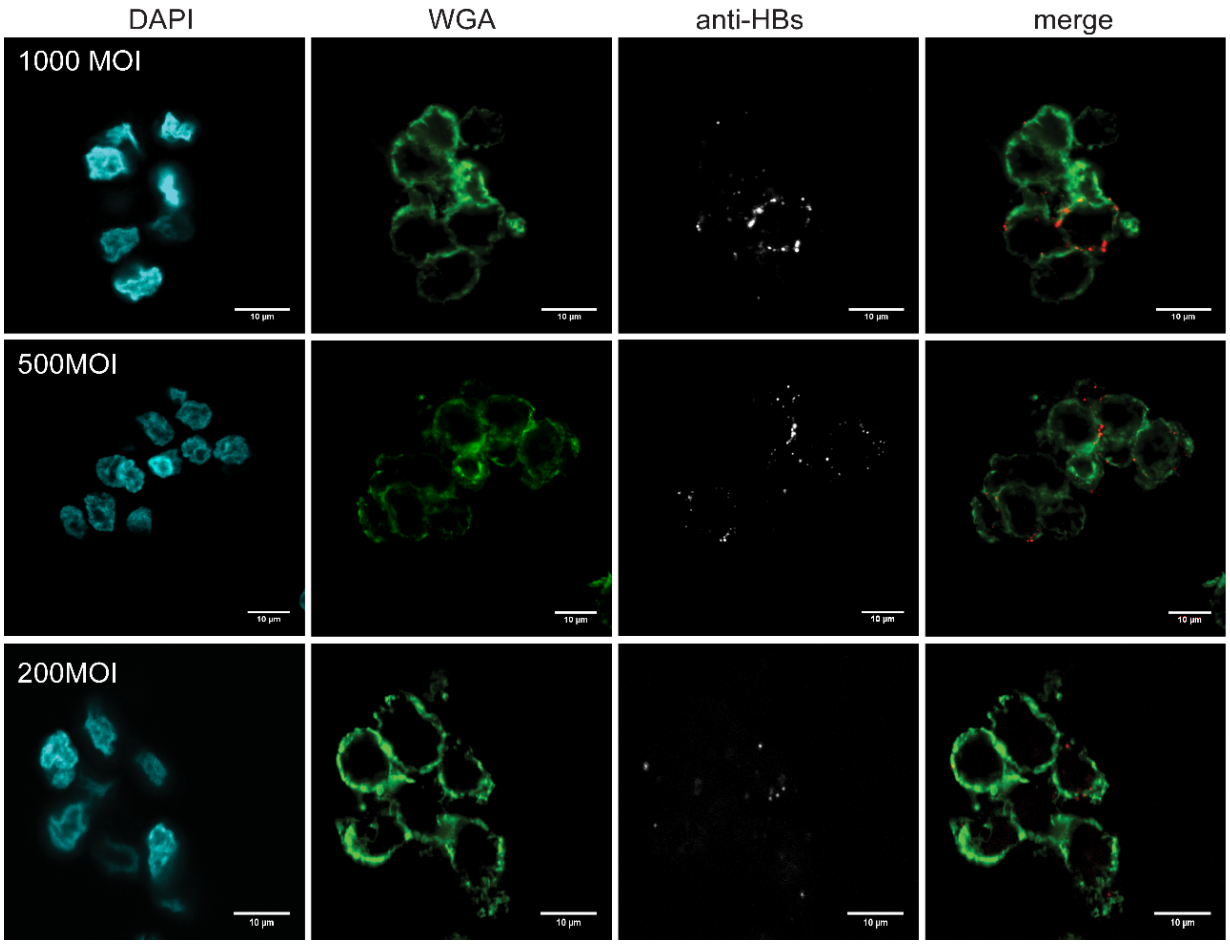

Fig. 2.2.9 Surface localization of HBV envelope proteins in HBV infected cells. Membrane-localization of HBsAg (white, red) related to the rim-staining of WGA (green) is indicated for HBV-infected HepG2-NTCP cells (MOI of 200, 500 and 1000) at day 9 p.i. The localization of HBsAg and WGA with the DAPI-stained chromatin (cyan) were recorded in a confocal laser-scanning microscope. Scale bars represent 10µm.

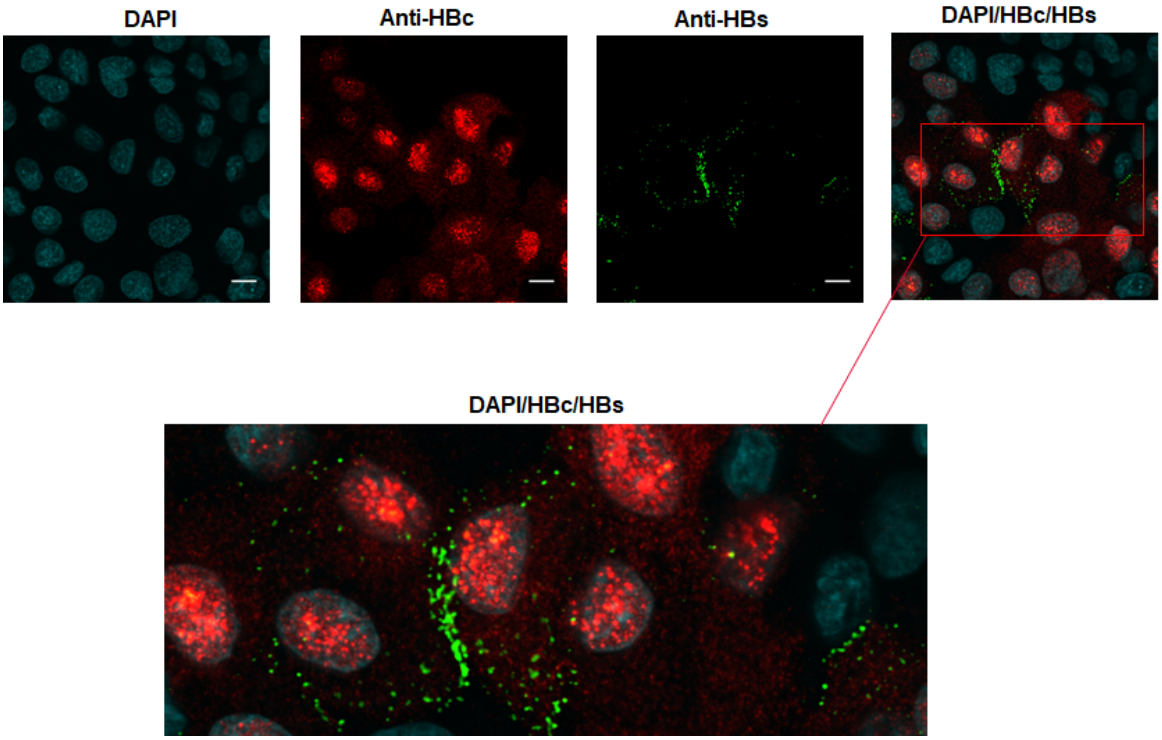

Fig. 2.2.10 Detection of HBV-specific proteins in infected HepG2-NTCP cells. The punctate membrane-localization of HBsAg (green, MoMab) combined with the diffuse HBc distribution (red) has been highlighted for HBV-infected HepG2-NTCP cells. The localization of HBsAg and HBc with the DAPI-stained chromatin (cyan) were recorded in a confocal laser-scanning microscope. Scale bars represent 10µm.

2.2.4 Ultrastructural analysis of HBV envelope proteins localization in HBV replicating cells

The results obtained by confocal microscopy in our previous experiments indicated that HBsAg is incorporated into the plasma membrane of infected hepatocytes. To further prove the punctate membrane-associated localization of HBsAg, we used a high-resolution TEM to visualize the localization of HBsAg. First, we pre-tested the immunostaining on S-mCherry transfected cells by confocal fluorescence microscopy. After combining the co-culture with murine antibody HB01, only mCherry-positive cells were detected by Alex Flour 488-gold conjugates with gold nanoparticles **(Fig. 2.2.11)**. This suggests that a gold-labeled secondary antibody can be used for the detection of a primary antibody in the TEM protocol. Therefore, we performed TEM visualization by staining the anti-HBs antibody and further detecting it with an immune gold-labeled secondary antibody.

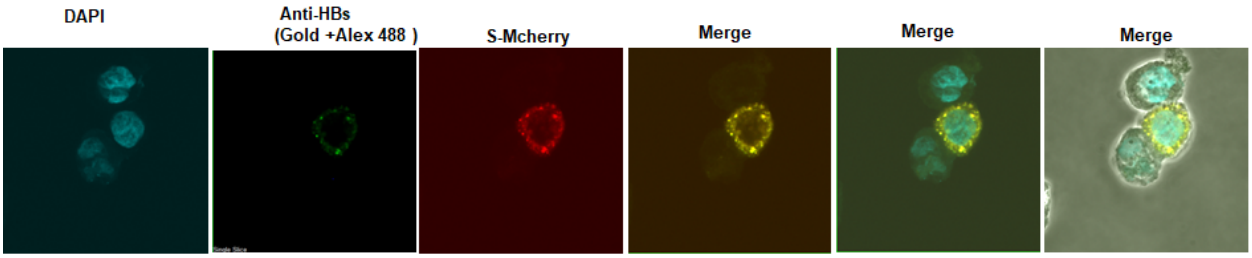

Fig. 2.2.11 The indirect detection of HBsAg by Alex Flour 488-gold conjugates in HBsAg fused mCherry HuH7 cells. MCherry S plasmid was transfected to HuH7 cells. At 48h post-transfection, immunofluorescent images of cells were performed by incubation with HB01 as the primary antibody and anti-mouse IgG conjugated with 12 nm gold particles and Alex Flour 488 as the secondary antibody. Nuclei were stained with DAPI (cyan).

Based on the previous results, HepG2.2.15 and HepG2 cells were labeled with the murine antibody 5F9 followed by staining with the secondary antibody goat anti-mouse covalently conjugated with gold nanoparticles. In line with our previous staining protocol, there was no

permeabilizing step prior to fixation. The data was documented by TEM. As illustrated in **Fig. 2.2.12**, the gold particles specifically bound to the surface of HepG2.2.15 cells but not to HepG2 cells, although only a small number of particles were observed. To increase the detection signal, we applied the polyclonal antibody HBVax as a primary antibody and increased the size of the gold particles conjugated with a secondary antibody as well **(Fig. 2.2.13)**. However, these approaches did not result in an increase of detectable membrane-associated HBV envelope proteins presented on the plasma membrane.

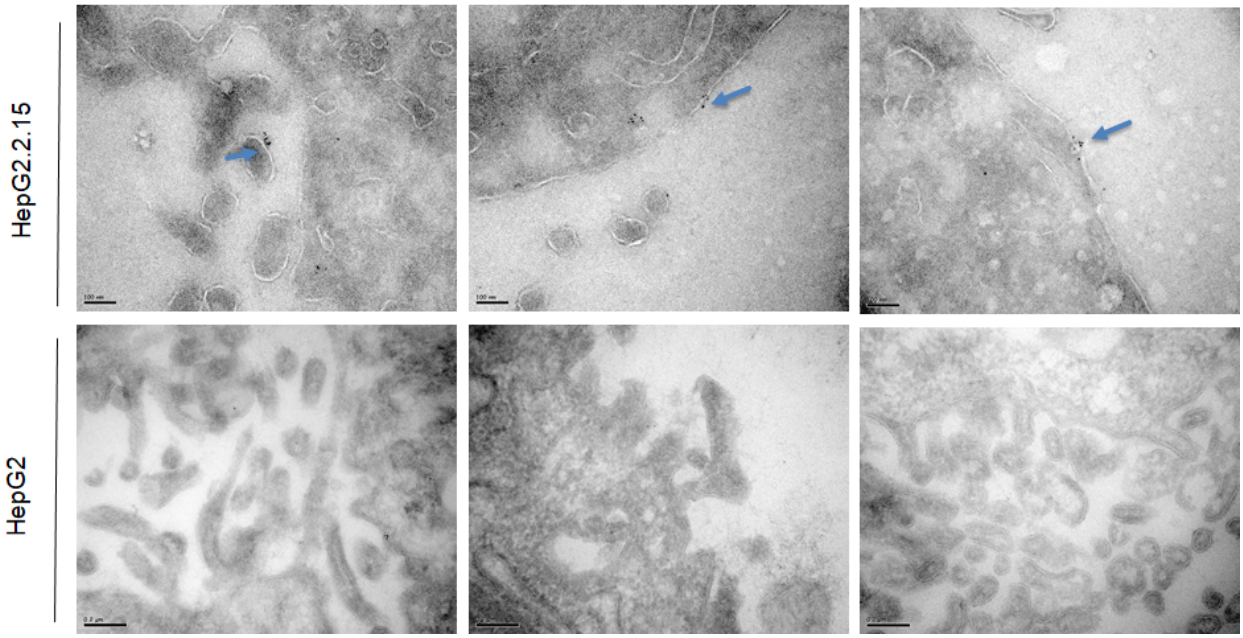

Fig. 2.2.12 Ultrastructural analysis of HBV envelope proteins g localization in HBV replicating cells by Monoclonal antibody. Non-permeabilized HepG2.2.15 cells were stained by murine monoclonal 5F9. The secondary antibody was a goat anti-mouse Fab fragment conjugated to 5-nm gold particles. The blue arrow highlights the gold nanoparticles on the cells surface. Scale bar is 100µm.

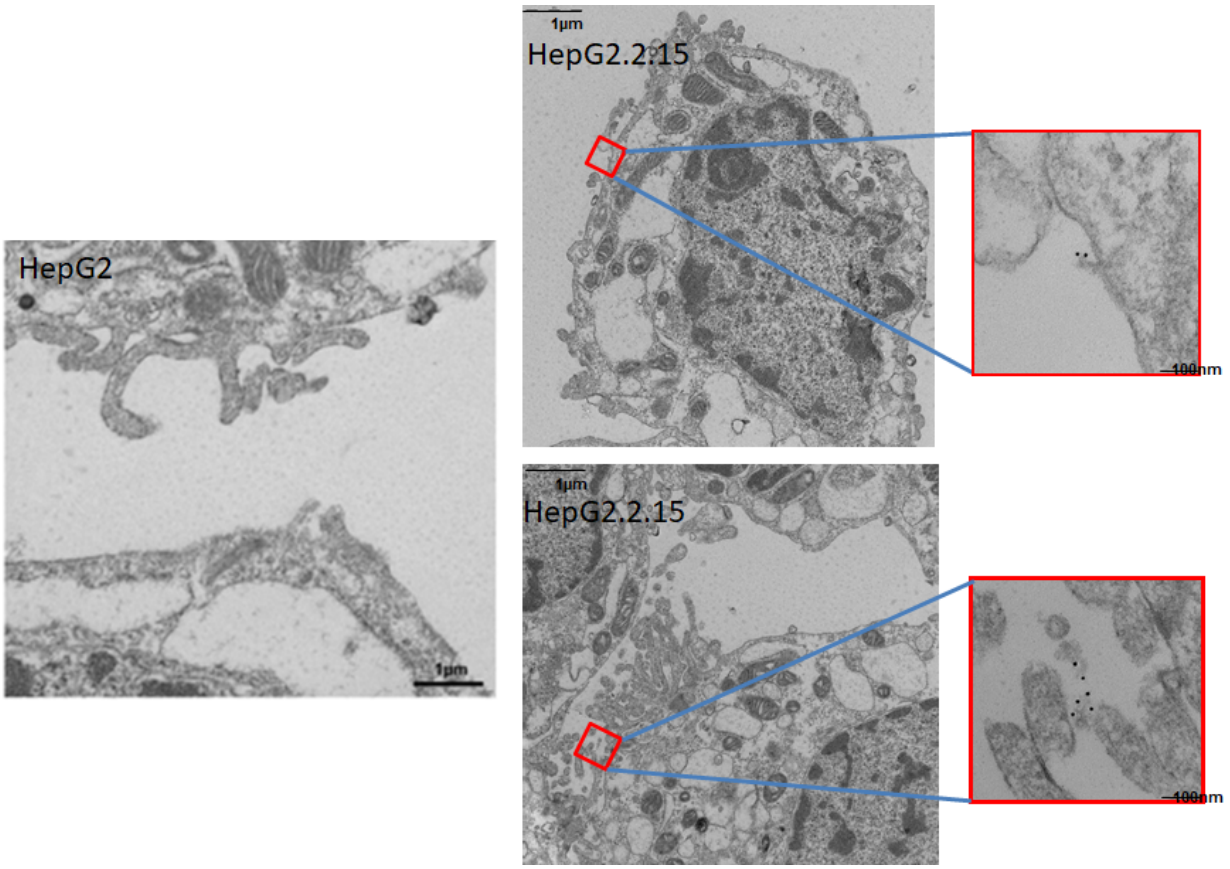

Fig. 2.2.13 Ultrastructural analysis of HBsAg localization in HBV replicating cells by polyclonal antibody. TEM image of HepG2.2.15 and HepG2 cells labeled with an anti-HBs polyclonal antibody HBVax and a secondary anti-rabbit antibody conjugated with 12nm gold particles. Scale bars for all TEM images are as indicated.

According to the results **(Fig. 2.2.12-13)**, the wash procedure or the size of the gold particles might account for the difficulty in HBV envelope proteins localization analysis by TEM. To improve the visualization of HBV envelope proteins by TEM, we explored new methods to directly label the primary antibody MoMab with SPIONs (around 50 nm). Therefore, we incubated MoMab-SPIONs on these cells before fixation, and then performed electron microscopy. TEM revealed that the MoMab-SPIONs bind HBV envelope proteins on the plasma membrane **(Fig. 2.2.14)**. MoMab-SPIONs formed cluster reflected by a punctuated distribution on the cell surface of HepG2.2.15, HepAD38, as well as HBV-infected HepG2-NTP cells (at 9 dpi), in accordance with

the distribution pattern of HBsAg shown by indirect immunofluorescence staining. As a control, the HepG2-NTCP cells treated with HBV-containing supernatant and immediately fixed after MoMab-SPIONs staining, were also subjected to electron microscopy. As expected, only a limited number of MoMab-SPIONS were detected on the cell membrane, possibly reflecting viral particles attaching to the cell surface proteoglycans and/or NTCP receptor prior to virus uptake.

In conclusion, the localization of HBV envelope proteins in the membrane of HBV replicating cells was confirmed by TEM using MoMab-labeled SPIONs. The accumulation at distinct membrane sites correlated with the punctuate staining pattern by confocal microscopy.

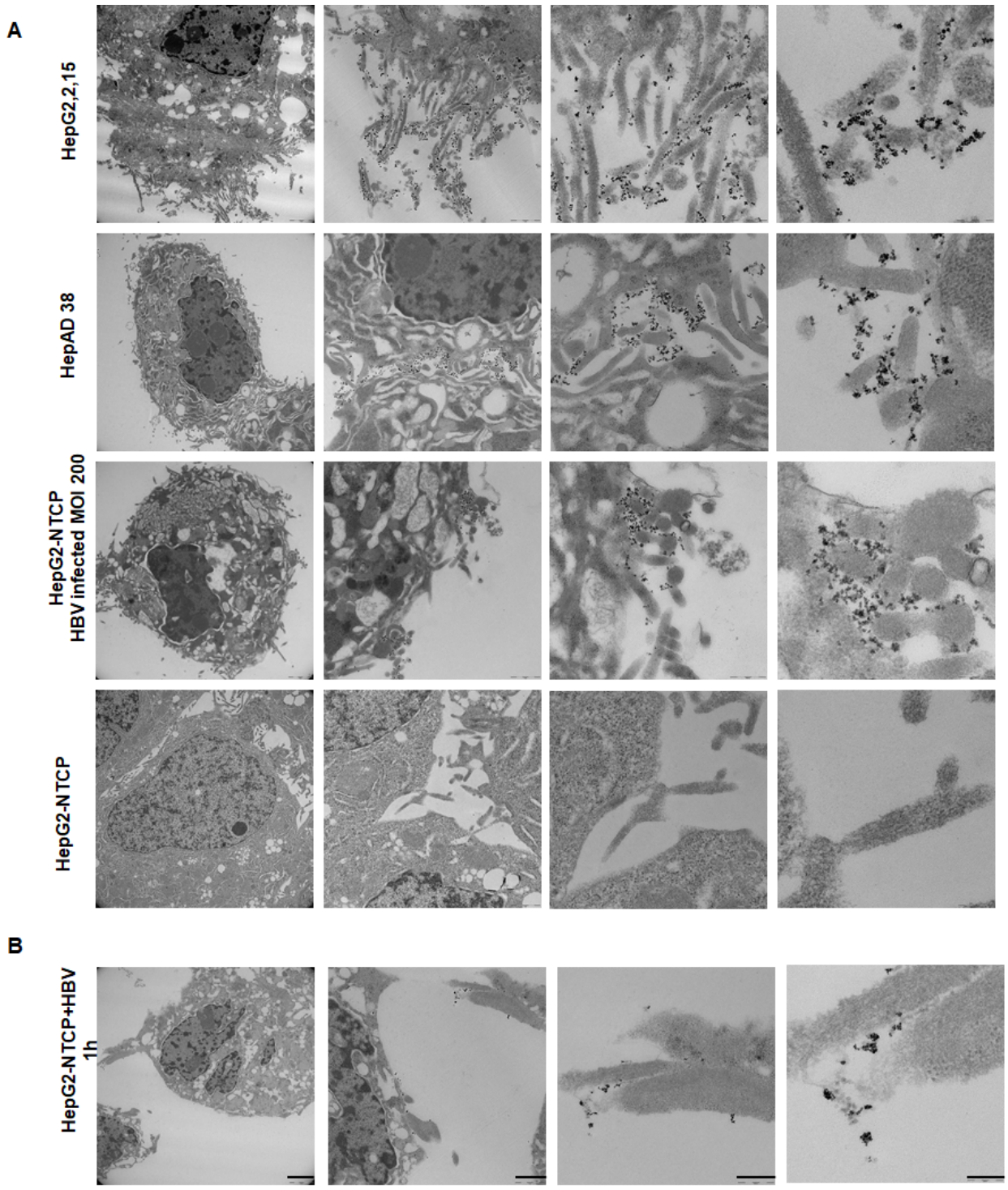

Fig.2.2.14 Ultrastructural analysis of HBsAg localization on HBV replicating cells. (A) Membrane-localization of MoMab-SPIONs on non-permeabilized HBV-positive cells (HepG2.2.15, HepAD38 and HepG2-NTCP cells infected with HBV with MOI 200) and HBV-negative HepG2-NTCP cells as mock control,

indicated by electron microscopy. Scale bars are shown. Scale bar = 2µm, 1µm, 500nm and 200nm, respectively.

2.2.5 The membranous HBsAg as target for immunotherapeutic approaches

As we and others[230] have shown that sHBs protein is localized on the plasma membrane of HBV replicating cells, it may serve as a therapeutic target. We hypothesized that membrane associated S- or L-protein can activate T cells grafted with an S-specific chimeric antigen receptor (S-CAR). To prove this hypothesis, S-, L-, and SML-transiently transfected HuH7 cells, as well as regular HuH7 cells (negative control), were co-cultured with S-CAR grafted T cells at an effector to target cell ratio of 1:2. Decoy T-cells that carry a ∆S-CAR without a TCR signaling domain served as a control. Target cell viability was monitored by the XCelligence real-time cell analysis system and is given as the normalized-cells index relative to the initiation of the co-culture with S-CAR T-cells and decoy T-cells. Controls were both, both HuH7 cells co-cultured with S-CAR T-cells and all transfected HuH7 cells with decoy T-cells (data not shown). As expected, co-culture with S-CAR T cells significant decreased the viability of HBsAg-transfected HuH7 cells **(Fig. 2.2.15A)**. Concomitantly, we observed that the T cells in the co-culture with HBsAg expressing Huh-7 cells produced INF-γ, indicating T cell activation **(Fig. 2.2.15B)**. However, neither IL-2 nor TNF-a were induced (data not shown). L-transfected HuH7 cells showed a comparable decrease in viability after having been co-cultured with S-CAR T-cells, but less induction of INF-γ secretion compared to HuH7-S and HuH7-SML.

To explore another immunotherapeutic strategy, we applied bi-specific BiMab antibodies which combined C8 scFv (anti-HBs variable domains) and CD3 or CD28 scFv binders to kill the HBsAg positive cells by redirecting T-cells from PBMCs. In this experiment, at 24h p.t., the S-, L-, and SML-transfected HuH7 cells were pre-seeded into 96 well-plates, followed by a co-culture with PBMCs in the presence of BiMabs (the combination of BiMab-SxCD3 and BiMab-SxCD28). Real-time measurement of the target cell viability was again performed by the XCELLigence system.

Killing of the target cells is recorded as the normalized-cells index from the starting point with the co-culture PBMC **(Fig. 2.2.15C)**. The results showed that BiMabs redirected T-cells to specifically eliminate HuH7 cells expressing HBV envelop proteins, especially L-expressing cells, while simultaneously sparing HBV-negative HuH7 cells. The corresponding supernatant was quantified by ELISA and revealed that the activated T-cells could produce a high level of INF-γ **(Fig. 2.2.15D)**. These data again indicated that S and L protein when expressed in HuH7 cells translocate to the cell surface, and maybe used as a therapeutic target.

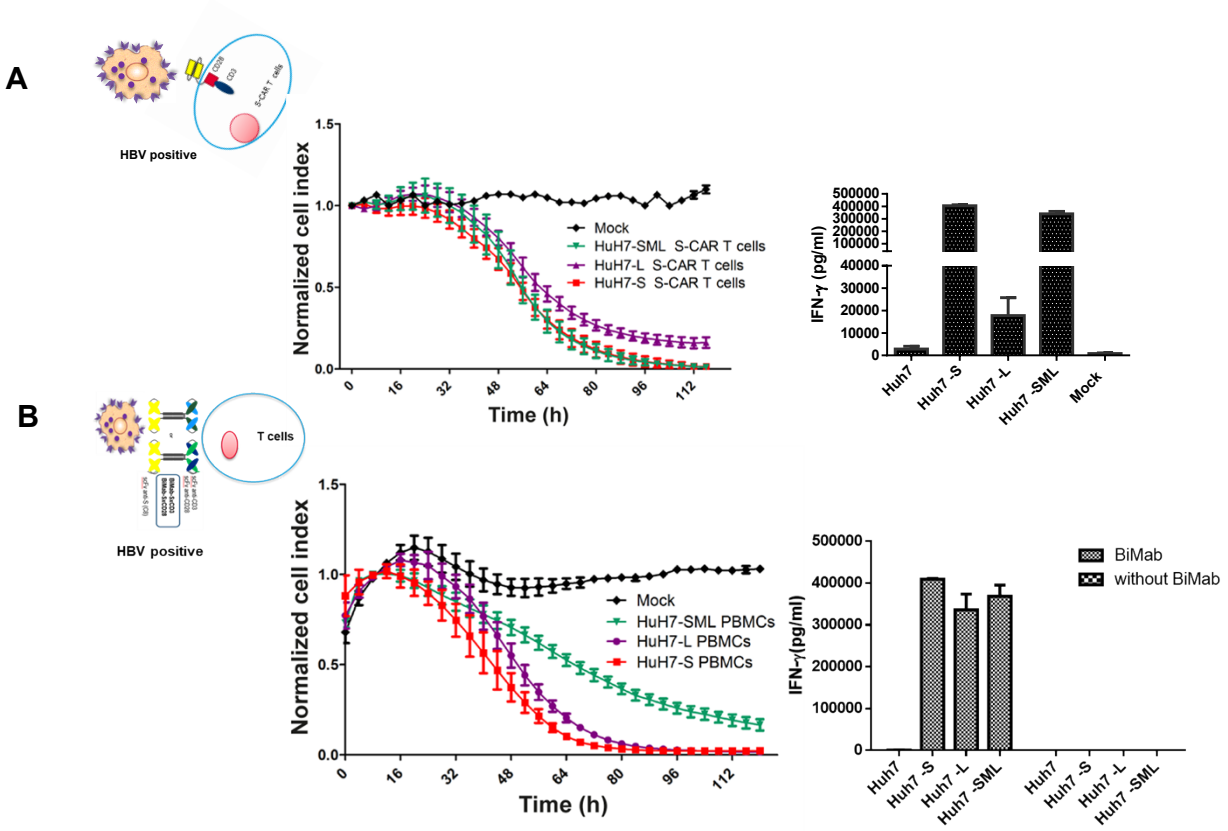

Fig. 2.2.15 Exploiting surface localization of HBV envelope proteins for therapy. A) Viability of HuH7 cells expressing the S-, SML- or L protein(s) co-cultured with S-CAR-grafted T cells. HuH7 cells were transfected 24 hs and transferred to 96-well plates. After 24 hs, these cells could be co-cultured by S-CAR T-cells (the chimeric T-cells receptor contains HBsAg specific single-chain antibody fragment as binder) at an E/T ratio of 1:2. Cells viability was measured by XCELLigence from the starting point of the co-culture and analyzed by xCELLigence RTCA analysis. The data is given as the normalized-cells index. Only HBsAg-positive cells were killed by S-CAR T-cells, especially L protein. Non-specific T-cells (mock T-cells)

failed to kill target cells. C) Redirecting T-cells from PBMC by BiMab in HBs-positive HuH7 cells. After HBsAg transient transfection 48hs, cells were co-cultured with PBMC in the presence of BiMab. Cell viability was measured by XCELLigence (B, D). Killing HBsAg-positive cells is accompanied by a specific secretion of IFN-γ.

2.3 Visualization and targeting HBV in vivo

2.3.1 HBV envelope proteins localizing to the plasma membrane *in vivo*

Previous studies indicated that membrane associated HBV envelope proteins in chronic hepatitis B patients strongly correlates with active viral replication of HBV (serum HBV DNA and HBeAg)[229-230, 246-247]. Thus, HBV envelope protein is a sensitive and specific marker of replication, even better than hepatocyte staining of HBcAg in HBeAg negative patients[230, 232]. To further study the characteristic HBsAg-distribution on hepatocytes, we collected and analyzed liver specimens from HBV 1.3 transgenic mice. Immunohistochemical analysis revealed a predominantly membranous distribution of HBV envelope proteins on hepatocytes from HBV-transgenic mice **(Fig. 2.2.1A)**. Also, in liver tissue of HBV infected chimpanzees we observed a distinct surface localization of HBV envelope proteins on hepatocytes, **(Fig. 2.3.1B)**.

In previous studies, indirect immunofluorescence on liver specimens from patients with chronic hepatitis B showed exclusively membranous, cytoplasmic, as well as mixed staining of HBsAg on hepatocytes[230, 232]. In this study, we analyzed HBV envelope proteins distribution in liver biopsies from patients with chronic hepatitis B related HCC. In agreement with **Fig. 2.3.1**, the results showed that HBsAg was consistently present on the cell membrane in the presence or absence of diffuse cytoplasmatic staining **(Fig. 2.3.2)**.

Taken together, our IHC results confirmed the hypothesis that HBV envelope proteins localize to the plasma membrane of hepatocytes *in vivo*

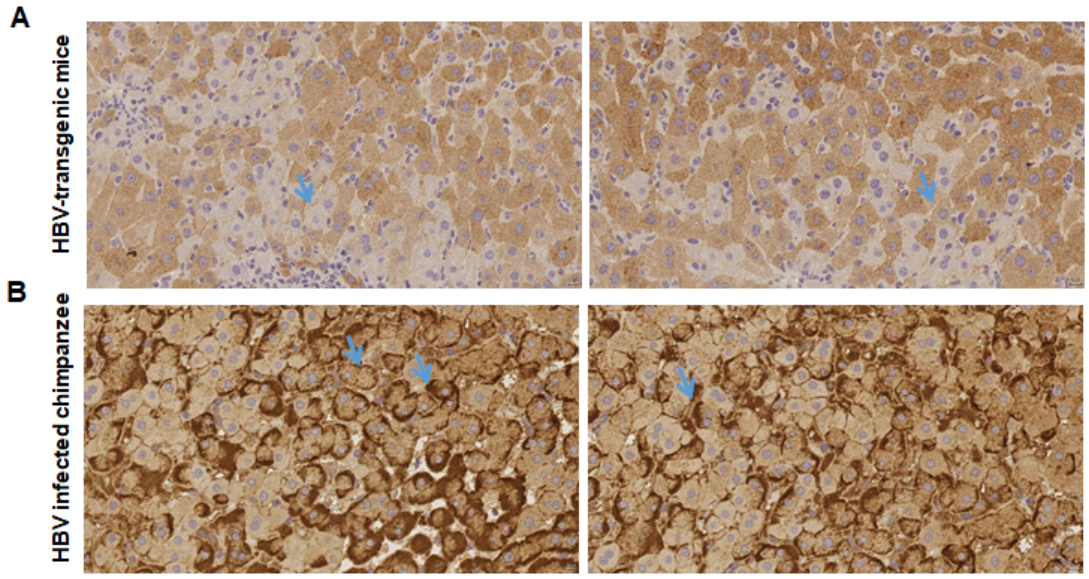

Fig. 2.3.1 Intrahepatic distribution of HBV envelope proteins *in vivo.* IHC analysis of HBsAg in liver specimens of two HBV-transgenic mice (A) and two HBV-infected chimpanzees (B). HBV envelope proteins were detected using the HBsAg-specific antibody 70-HG15 (specific for subtype AD/AY). Examples for membrane-associated HBV envelope proteins are highlighted by blue arrows

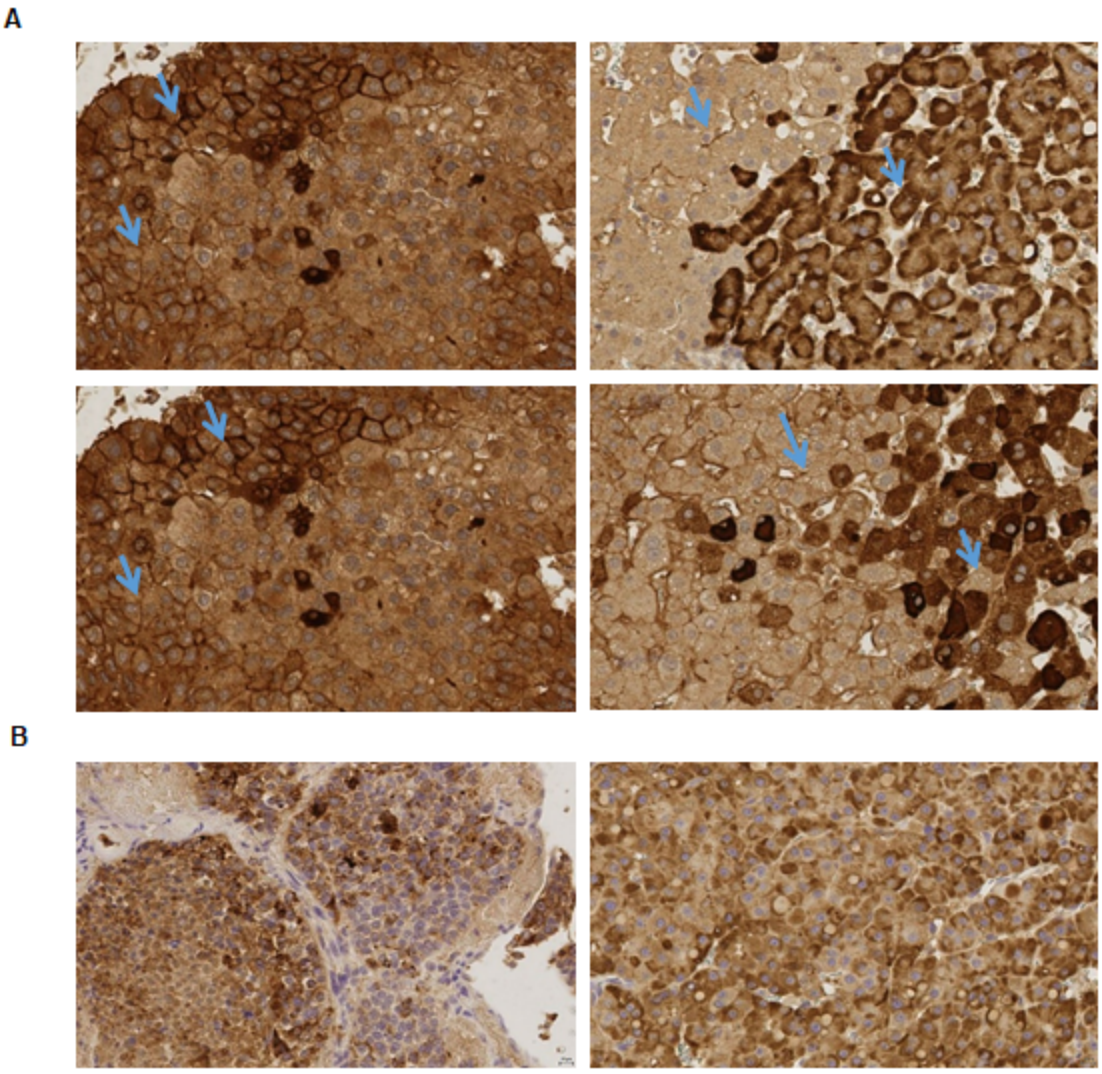

Fig. 2.3.2 Intrahepatic distribution of HBV envelope proteins in HCC samples. Hepatocytes of HCC-patients displaying both (predominantly) membrane-localized HBsAg (A) and cytosolic/diffuse intrahepatic HBsAg (B). HBV envelope proteins were detected using the HBsAg-specific antibody 70-HG15 (specific for subtype AD/AY). Membrane-associated HBsAg is highlighted by blue arrows.

2.3.2 Targeting HBV L protein in Alb-PSX mice by MoMab

Alb-PSX transgenic mice express LHBs under the control of an albumin promotor. They show predominant intrahepatic HBsAg expression with low or non-existent HBsAg secretion in the serum[248]. Four hours after intravenous injection with 50 µg MoMab **(Fig. 2.3.3A)**, we evaluated MoMab in mouse liver tissue by IHC. **Fig. 2.3.3B-C** illustrated that the free MoMab travelled into

the liver and specifically targeted HBV envelope proteins -expressing hepatocytes of transgenic mice, but not of wildtype C57BL/6 mice. In one mouse, in which HBsAg was detected in the serum, we observed a clear decrease of serum HBsAg from 43.35 IU/ml to 8.95 IU/ml after MoMab injection. No increase in serum ALT was observed in either of the mice. These results indicate that it is possible to target HBV envelope proteins expressing hepatocytes *in vivo* by using HBsAg specific antibodies.

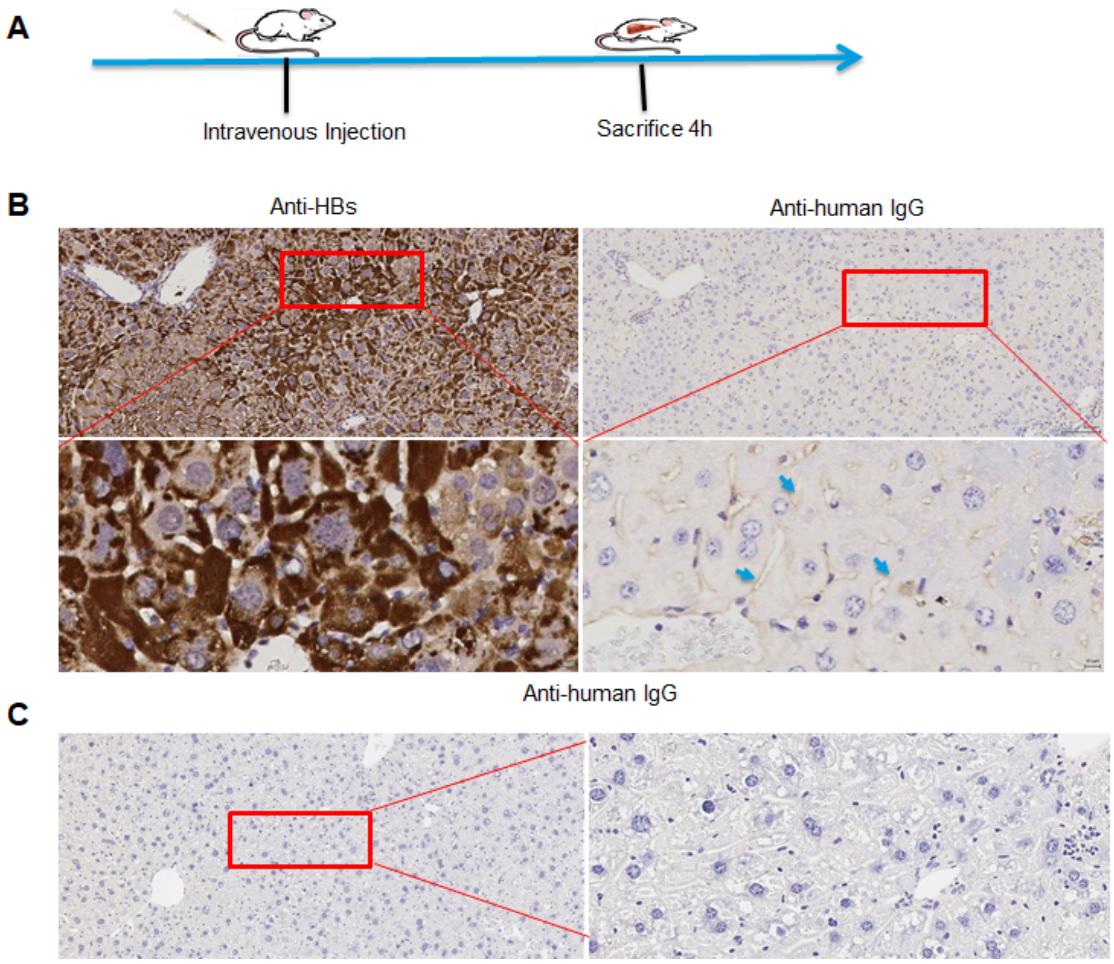

Fig.2.3.3 *in vivo* detection of membrane-associated HBsAg by MoMab. (A) 4 hours after intravenous injection of MoMab, Alb-PSX mice and wildtype mice were euthanized and livers were harvested for histology. (B) IHC analysis of the distribution of HBsAg and MoMab in the liver sections. The HBsAg was detected by antibody 70-HG15. MoMab was stained by anti-Human antibody. The blue arrows highlight MoMab on the membrane of HBsAg expressing cells. (C) MoMab staining was negative in liver sections of wildtype mice.

2.2.1 Targeting replicating HBV *in vivo* by MoMab-SPIONs

In this study, we assessed the feasibility of targeting HBsAg-expressing hepatocytes using intravenously administered MoMab-SPIONs. For this purpose, we injected non-coated SPIONs or MoMab-SPIONs via the tail vein into HBV1.3 transgenic mice with different HBsAg titers (three animals per group). SPIONs can shorten the T2 relaxation times of surrounding water protons inside various organs, leading to a negative contrast in MR images[242, 249]. At 4- or 24-hours post-injection, animals were assessed by MRI (T1 and T2 relaxation time). MRI image analyses were done by Dr. Maxim A. Shevtsov, After the administration of MoMab-SPIONs, SPIONs, and PBS (negative control), we detected the accumulation of those particles in the liver by hypotensive *T2*-weighted images. SPION detection was clearest on images obtained by the fast-low angle shot (FLASH) regimen. When MoMab-SPIONs were injected, we observed an increased accumulation of the magnetic conjugates in the liver as compared to the control non-coated SPIONs. Additionally, acquired T2*-weighted multigradient sequences (MSME regimen) were assessed, and the T2* values were calculated by a histogram. In the control PBS-injected animals, the T2* values constituted 18.03±1.39 s^{-1} **(Fig. 2.3.4)**. After infusion of SPIONs, there was a notable drop of T2* values to 7.63±1.56 s^{-1}, which were further decreased when MoMab-SPIONs were administered—to 1.43±0.68 s^{-1} ($P<0.001$). Besides, we compared the accumulation of the nanoparticles in brain, heart, lung, and liver tissues (as shown in **Fig. 2.3.5)**. As expected, most of the injected MoMab-SPIONs accumulated in the liver tissue, indicating the specific binding of the functionalized particles to the HBsAg-positive hepatocytes. Summarized, all results indicated that MoMab could drive SPIONs to HBsAg-positive hepatocytes which lead to the predominant accumulation of SPIONs in the liver of HBV transgenic mice.

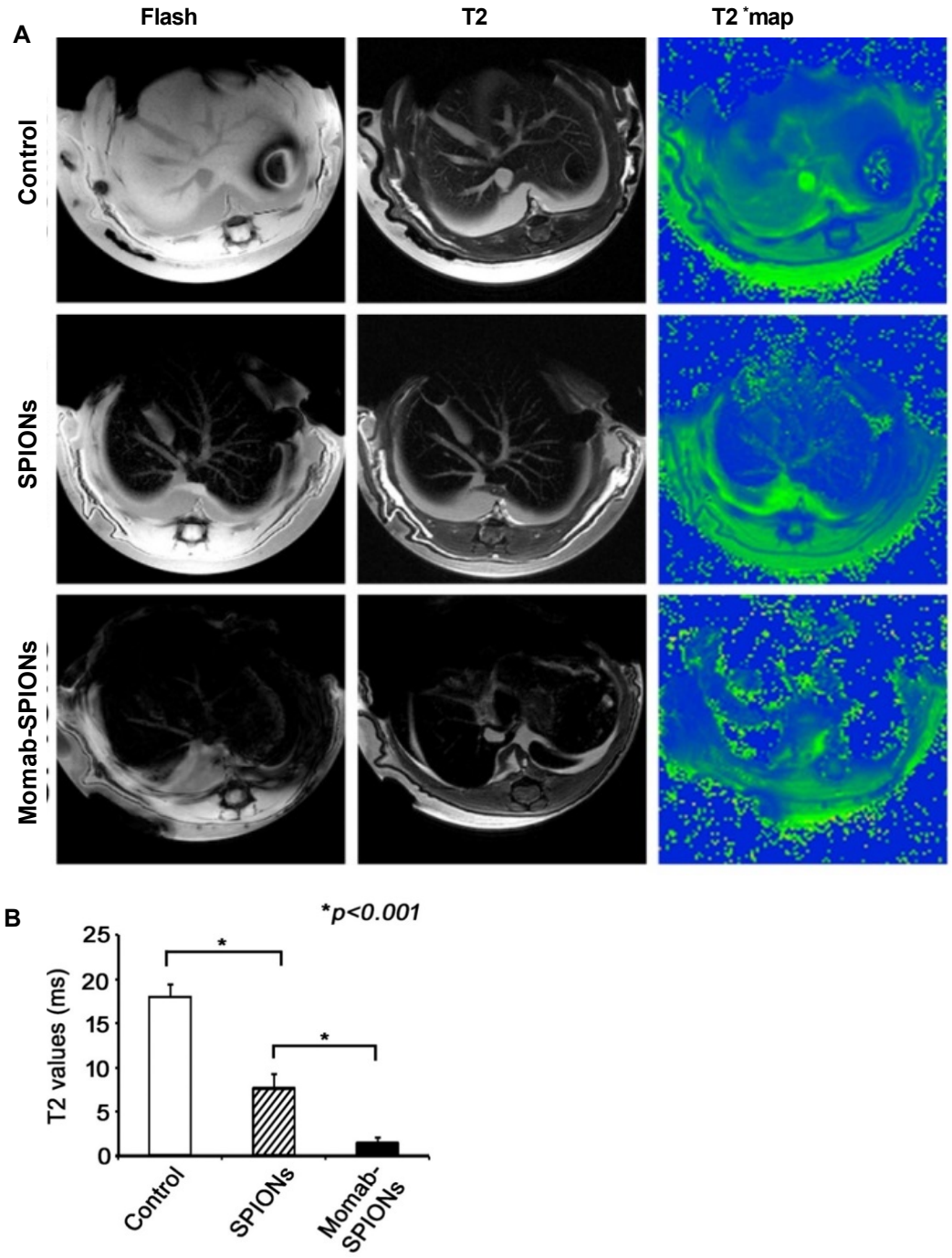

Fig. 2.3.4 MRI images of HBV-positive hepatocytes of HBV-transgenic mice. (A) MRI scans of control animals (treated with PBS), animals 24 hours after intravenous treatment with SPIONs (2,5 mg/kg) and animals treated intravenously with MoMab-SPIONs (2,5 mg/kg) after 24 hours. SPIONs accumulation was detected in the liver by T2-weighted imaging. The corresponding T2-map of the liver illustrated a decrease in T2-value. (B) Quantification of the T2 values in histogram of MRI images.

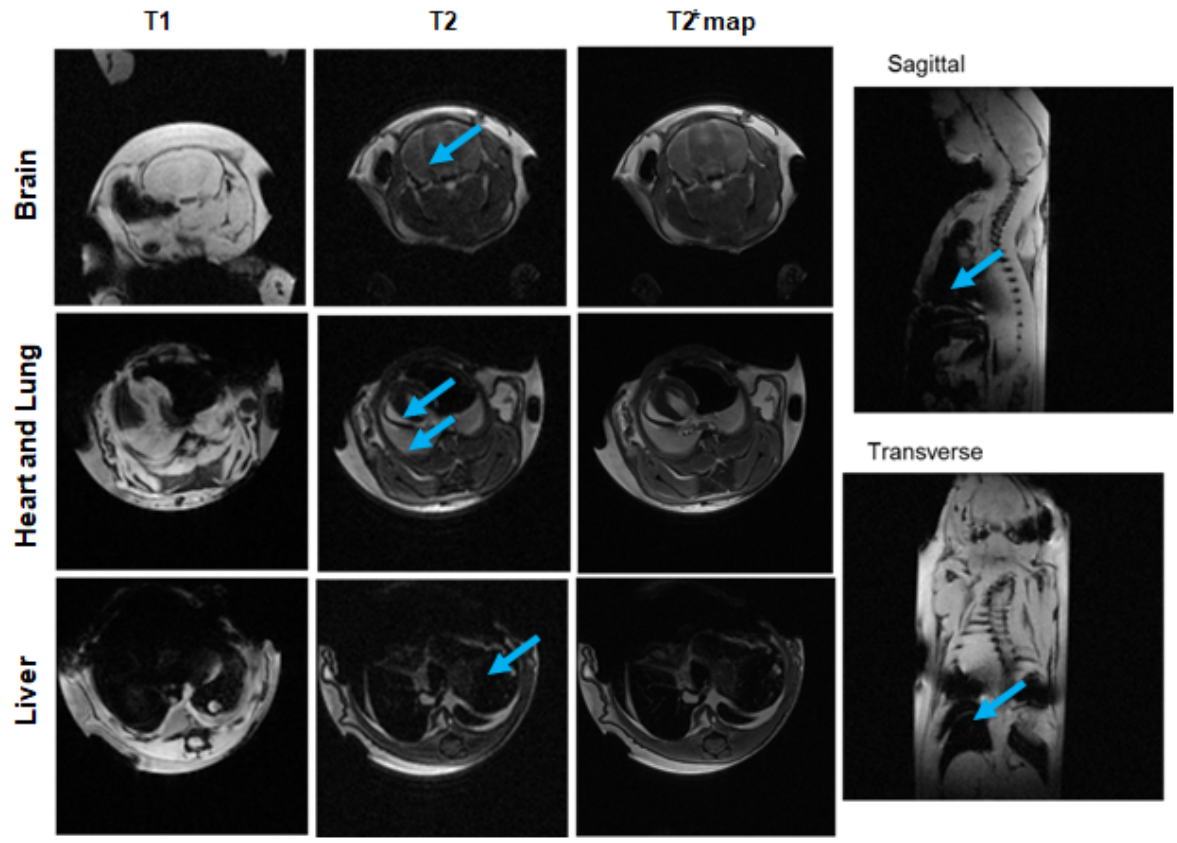

Fig. 2.3.5 The distribution of MoMab-SPIONs in the different organs. Magnetic resonance images for animals treated with MoMab-SPIONs (2,5 mg/kg) particles were obtained in T1-Flash, TurboRARE-T2 regimens in Brain, Heart, Lung and Liver. The retention of the nanoparticles mainly appeared in the liver, but not in the heart, lung and brain. The blue arrows are represented for the target organs.

Since CT also provides high-resolution images and is widely applied for the clinical diagnosis of various diseases[250], we assessed whether X-ray CT could be adjusted for the detection of superparamagnetic nanoparticles *in vivo*. The HBVtg1.3 mice were previously used for MRI-mediated SPION detection were scanned by X-ray CT. Various regions of interest (ROI) with different sizes and positions of the animal were assessed **(Fig. 2.3.6A)**. Finally, those ROIs were calculated into a histogram **(Fig. 2.3.6B)**. While comparing the accumulation of SPIONs and PBS

groups, no significant change (P>0.05) in MoMab-SPIONs could be detected. This indicated that the method of X-ray CT cannot be successfully applied for tracking the MoMab-SPIONs *in vivo*.

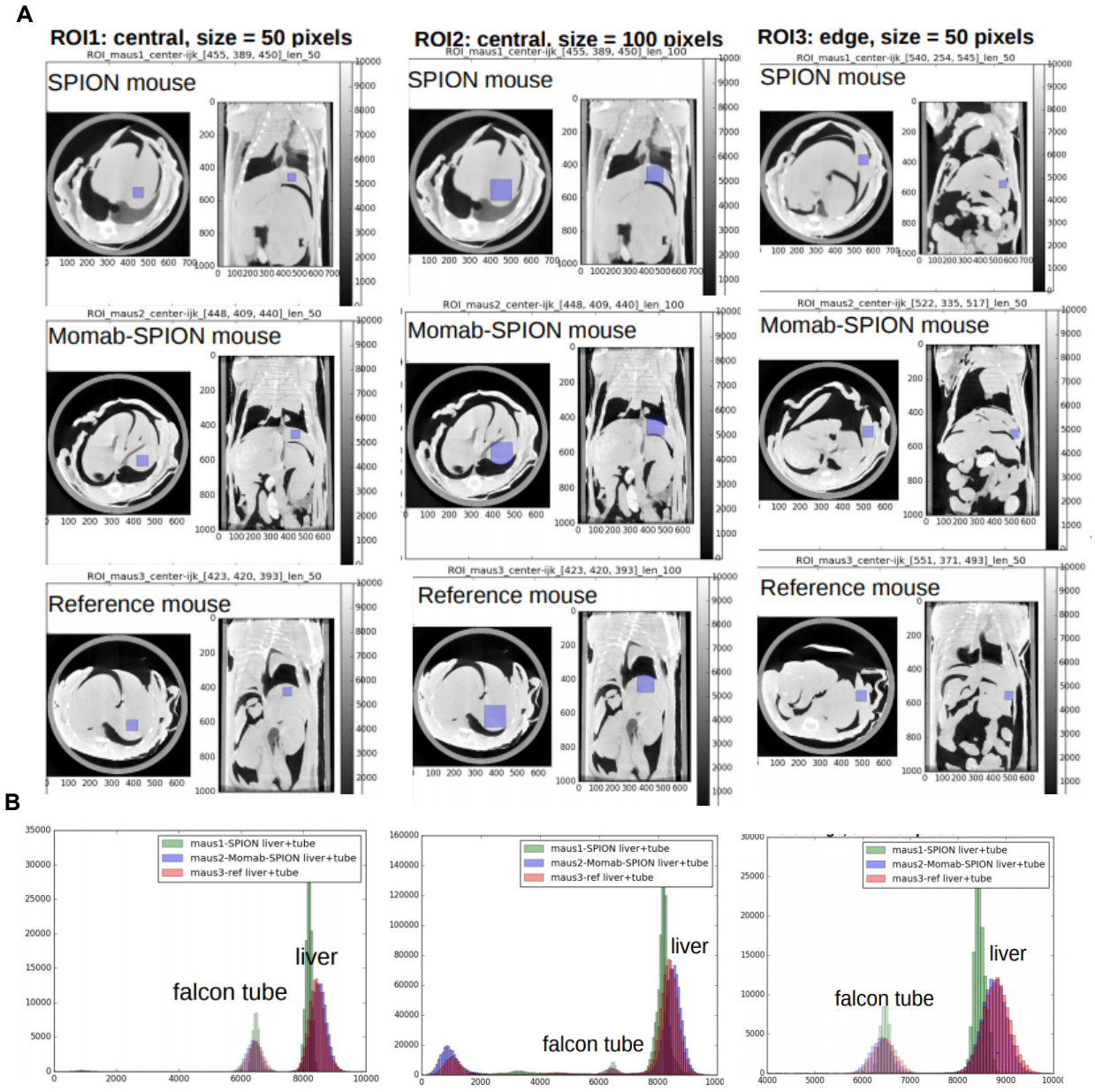

Fig. 2.3.6 X-ray CT image of HBV positive hepatocytes in the transgenic mice. (A) Selection of different ROI in the liver of each mouse. The ROI was marked by a blue square. The spread of grey levels ranged from 0 to 10,000 grey level values. (B) The input CT image to be histogram-equalized and its corresponding histogram evaluation. The y-axis represented the number of pixels, the x-axis is the grey level.

To confirm the specific targeting of MoMab-SPIONs to hepatocytes, we tested MoMab and iron distribution in liver and spleen sections by IHC. Intrahepatic Iron was visualized by Prussian Blue staining (**Fig. 2.3.7A**). Some clusters or blue dots in both the SPIONs and the MoMab-SPIONs group were observed, with no significant difference among these three groups being visible. MoMab contains a Human IgG constant region. Therefore, we attempted to stain MoMab using anti-human IgG by IHC, but MoMab detection in the liver still failed (**Fig. 2.3.7A**).

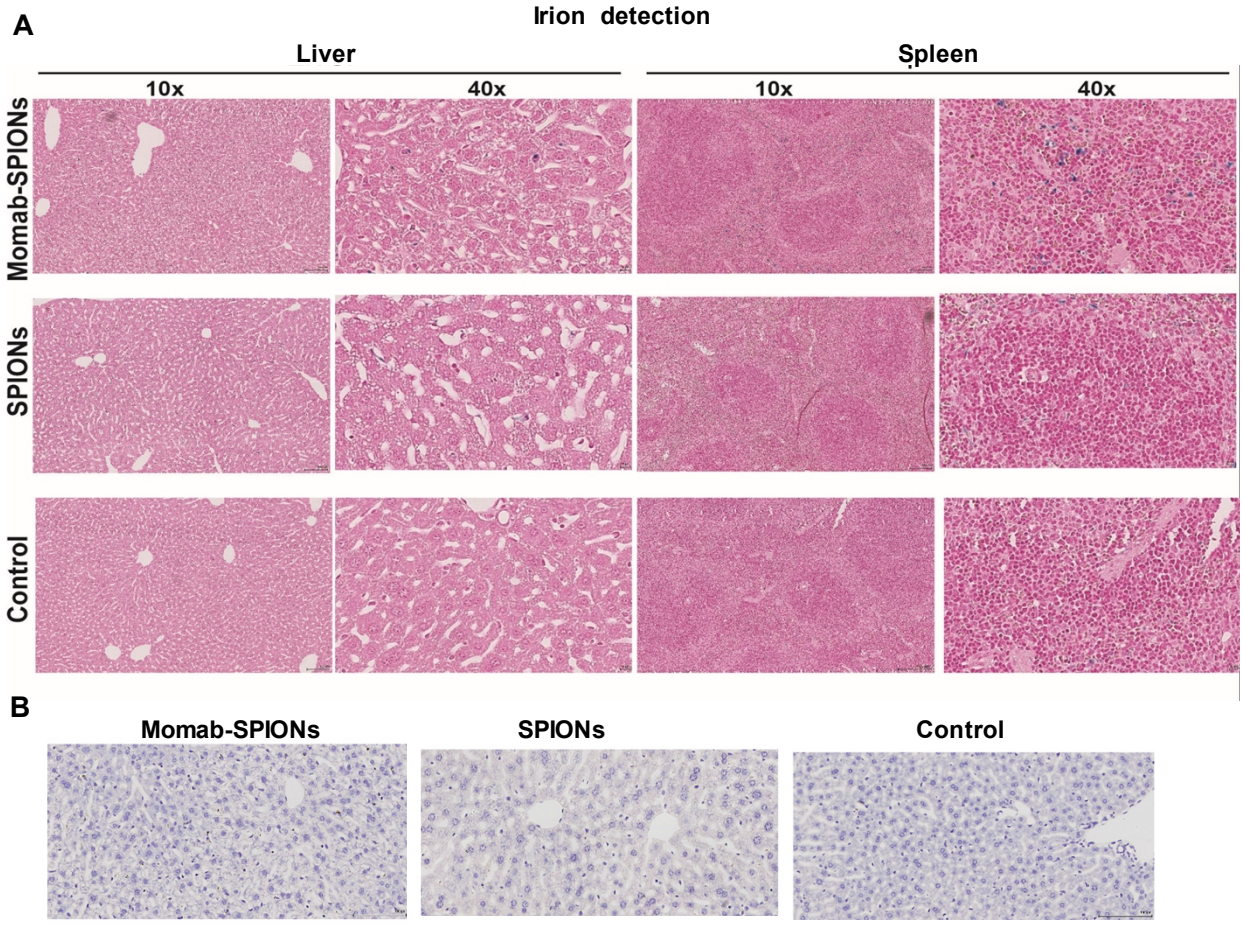

Fig.2.3.7 Histological distribution of MoMab-SPIONs in HBV transgenic mice. (A) Prussian blue staining image of liver and spleen tissues. (B) Immunohistochemistry staining of MoMab in liver sections by anti-Human IgG.

2.3.3 Targeting of HBV replicating hepatoma *in vivo*

Our previous results clearly demonstrated that MoMab-SPIONs targeted the surface of HBV-positive cells **(Fig. 2.2.15)**. Also, we detected a MoMab SPIONs signal in the liver of HBV-transgenic mice using an MRI scanner **(Fig. 2.3.5**), despite these mice expressing HBsAg in their whole liver and containing high levels of HBsAg-secretion in their blood. To confirm that MoMab-SPIONs can target the HBsAg-positive cells, we transplanted HBV-positive (HepG2.2.15) and negative (HepG2) human hepatoma cells in immunodeficient mice (Rag2$^{-/-}$ mice). All mice received HepG2.2.15 cells intrahepatic, and concomitantly HepG2.2.15 cells in the right- and HepG2 cells in the left leg by s.c. injection. 3 weeks after implantation, the size of the subcutaneous tumors was observed by eye. Additionally, the serum was collected for measurement of HBsAg and HBeAg levels (**Fig. 2.3.9C-D**). Detection of HBsAg and HBeAg in serum indicated successful grafting of HepG2.2.15 cells in those immunodeficient mice. in these mice

As shown in **Fig. 2.3.9**, the hepatoma cell xenografts showed typical histopathological features of tumor tissue. The morphology changes of hepatocyte–like cells were characterized by a high nuclear-to-cytoplasmic ratio and distorted trabeculae with increased thickness of the hepatocellular plates. To evaluate the expression of the HBV-infection markers HBsAg and HBcAg, we performed an IHC staining on tumor sections with anti-HBs and anti-HBc antibodies, respectively. As **Fig. 2.3.10** demonstrates, HepG2.2.15 cell xenografts were both HBsAg- and HBcAg-positive but this was not the case for HepG2 cell xenografts In summary, our data indicated that we successfully established a mouse model with both liver and subcutaneous tumors, which contained both HBV-positive and negative cells, respectively.

A

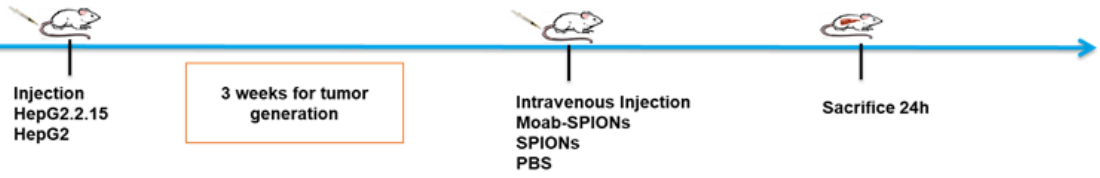

B

Injection Volumn	PRO-37552 SPIONs Mice 5	PRO-37553 PBS Mice 6	PRO-37554 SPIONs Mice 7	PRO-37555 Momab SPIONs Mice 8
In hepatic 100 ul	HepG2215	HepG2215	HepG2215	HepG2215
S.C. Left 100 ul	HepG2	HepG2	HepG2	HepG2
S.C Right 100 ul	HepG2215	HepG2215	HepG2215	HepG2215

C

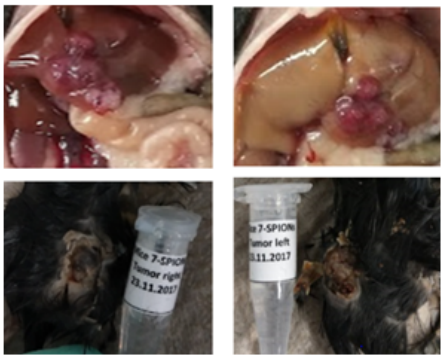

D

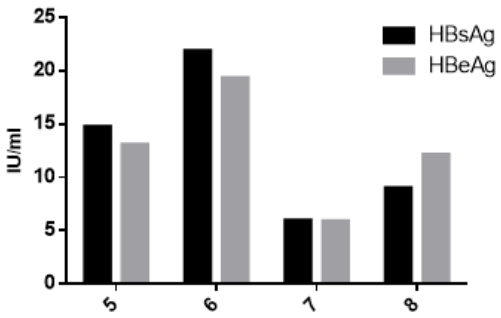

Fig. 2.3.9 Transplantation of hepatoma in Rag2-/- mice. (A)Schematic representation of the transplantation procedure (B) The injection route and volume contained 2x10^{6}cells of HepG2.2.15 and HepG2 cells. (C) The appearance of liver tumors and subcutaneous tumors. (D) HBsAg and HBeAg level in the mouse serum 3 weeks post-injection.

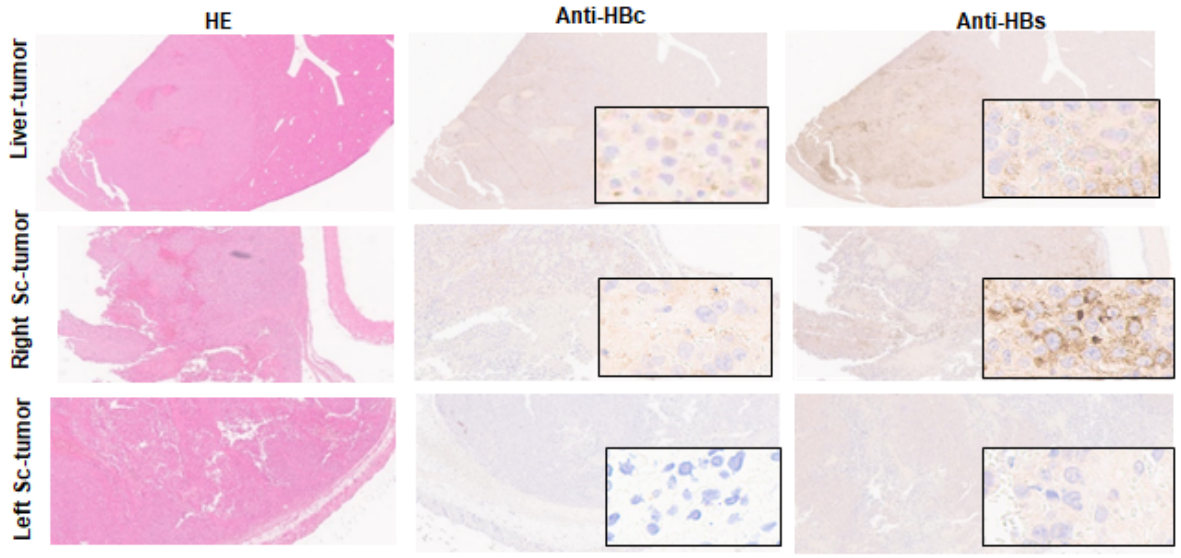

Fig. 2.3.10 Histological characterization of transplanted hepatoma in Rag$^{-/-}$ mice. Representative H&E sections of the tumors, with typical histopathological features of HCC. Histology section through margin of intrahepatic xenograft demonstrated a typical distribution of HBsAg and HBcAg in the liver and the right subcutaneous tumor. The left subcutaneous tumor is negative. The black box equals a 20x magnification.

After the histological confirmation of HBsAg-expression in the hepatoma, we assessed the feasibility of targeting HCC with magnetic nanoparticles. All nanoparticle injections were well-tolerated by the animals. We observed neither an increase of the ALT-level nor any behavioral abnormalities. The MRI images of hepatoma were acquired 24 hours after intravenous injection. The hepatoma presented on T1, T2, and T2-map images are shown in **Fig. 2.3.11A**. The retention of the nanoparticles in the tumor was assessed utilizing T2* sequences with the subsequent estimation of T2-values (**Fig. 2.3.10B**). The evaluation of the MRI images revealed a statistically significant signal change in the HBsAg-positive intrahepatic tumors 24 hours after i.v. injection of MoMab-SPIONs. The T2-values of the MoMab-SPIONs group amounted to 23±3 s^{-1}, which was significantly lower compared to the control or the unmodified SPIONs group with the values of 49.5±1.9 and 37.7±2.9 s^{-1} ($P<0.001$), respectively. Additionally, we could confirm the

accumulation of functionalized magnetic conjugates to the HBsAg-positive subcutaneous tumors while the same was not true for the HBsAg-negative s.c. tumors. The MoMab-SPIONs group delivered T2-values of 22.7±4.0 s^{-1}, while the control and SPIONs groups produced the values 48.7±3.3 and 37.5±2.3 s^{-1} ($P<0.001$), respectively. Comparing s.c. HBsAg-negative tumors with the SPIONs and MoMab-SPIONs groups, we did not observe any significant differences, although the T2-values were significantly lower than those of the control (PBS) group. This indicates the accumulation of the particles in the tumor tissues is caused by the EPR (enhanced penetration and permeability) effect.

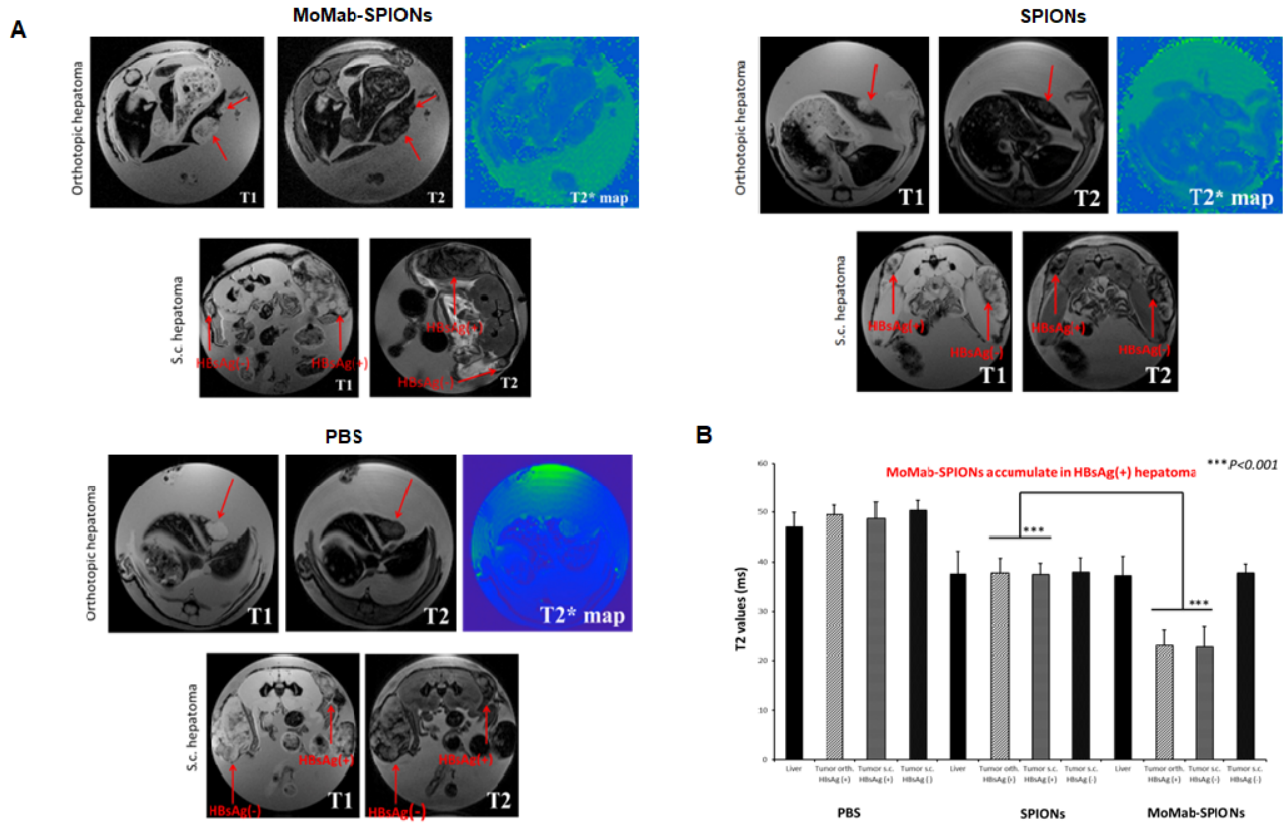

Fig. 2.3.11 Targeting of HBV-positive hepatoma using MoMab-SPIONs in Rag2$^{-/-}$ mice. (A) MRI of hepatoma after 24h of i.v. treatment with MoMab-SPIONs and SPIONs. The evaluation of the MRI images revealed a statistically significant signal change in the HBsAg positive orthotopic tumors after injection of MoMab-SPIONs but not in PBS and SPIONs group. The red arrow highlighted the xenografts or tumors. (B) Retention of the nanoparticles in the tumor was assessed utilizing T2* sequences with subsequent estimation of T2-values.

3. Discussion

The hepatitis B virus (HBV) cause chronic liver infections in humans who are subsequently at a high risk of developing liver cirrhosis and hepatocellular carcinoma (HCC). Current therapies, alpha-interferon and nucleos(t)ide analog (NUC), have limited effectiveness in treating chronic HBV-infections[251]. The main insufficiency of the standard treatments is the inability to completely clear the patient of HBV due to the fact that the cccDNA remains in the nucleus and acts as a template for new virus replication[225-226]. In chronically infected patients, HBV-specific T-cells show an exhausted phenotype or are completely absent, and therefore incapable of clearing the infection[252-253]. Hence, new therapeutic strategies are needed to prevent relapse of HBV-infection upon cessation of (NA) therapy. Typically, such approaches should aim at eliminating the cccDNA and/or inducing a strong immune response to kill infected hepatocytes. Recently, a study has reported that the compensatory cell proliferation after killing HBV-infected cells leads to the cccDNA-loss by cell division[254].

Previous studies have noticed a membranous localization of HBV surface antigens (HBsAg) in chronic hepatitis B patients with or without HCC[229, 231, 246, 255]. In line with this observation, there is increasing evidence that HBV-budding and -egress both depend on the function of the multivesicular body (MVB) with the assistance of the endosomal sorting complex required for transport (ESCRT)[120-121, 227, 245], by which other enveloped RNA-viruses bud from the plasma membrane[256-259]. Although the mechanisms of HBV-assembly, -budding and -release are not yet fully understood, new immunotherapeutic approaches that aim to kill HBV-infected cells by targeting the HBsAg expressing on the cell membrane have undergone preclinical testing[236, 260].

In the study at hand, we show that HBsAg is embedded in the membrane of hepatocytes by means of HBsAg specific antibodies (anti-HBs). Furthermore, we generated SPIONs functionalized with an anti-HBs antibody (MoMab), and showed that these SPIONS can target

membranous HBV envelope proteins and thus can be applied for the imaging of HBV-infected hepatocytes *in vitro* and *in vivo*.

3.1. Establishment and characterization of detection and imaging tools

3.1.1. Establishment and characterization of anti-HBs antibodies

The HBV envelope proteins or surface antigen (HBsAg) has been considered as the most essential target for the diagnosis and immune prophylaxis of HBV infection[261]. Anti-HBsAg antibodies that are induced by natural HBV-infection or by vaccination predominantly recognize the hydrophilic determinant of HBsAg, termed the 'a' determinant, and can neutralize circulating HBV-particles[239]. Hepatitis B immune globulin (HBIG) is an anti-HBsAg antibody preparation derived from human donors after vaccination with HBsAg. HBIG has been applied to prevent re-infection in hepatitis B-seropositive liver transplantation recipients and for passive immunoprophylaxis against HBV-infection. However, long-term treatment with HBIG may not only be hindered by its high cost but also by its tendency to cause genetic HBV-mutants[262]. Therefore, monoclonal antibodies and engineered antibodies have been generated to replace HBIG for therapeutic application[263-265].

A murine monoclonal antibody (5F9) has been previously produced and characterized in our lab[234-235]. The 5F9 recognizes both reduced and non-reduced forms of HBsAg, and can inhibit HBV-infection in vitro, indicating that it has neutralizing capacity. However, murine monoclonal antibodies mostly cannot be applied in humans because they provoke an anti-mouse antibody response in human recipients. Recently, humanized anti-HBs antibodies and human monoclonal antibodies have shown antiviral effects through the clearance of Ab-Ag complexes and the neutralization of circulating viral particles[264-268]. Therefore, we constructed a chimeric monoclonal antibody (c5F9) which contains murine variable regions and human IgG1 constant region **(Fig.**

2.1.1). c5F9 was expressed in human HEK 293 cells and purified by one-step Protein-A affinity chromatography. The purity of this preparation was confirmed by Coomassie staining after poly acrylamide gel electrophoresis (PAGE). Subsequently, the specificity of c5F9 against HBsAg was evaluated by ELISA and Western blot **(Fig. 2.1.3-5)**. Our results indicated that c5F9 could specifically interact with HBsAg expressed in yeast and CHO cells, and HBsAg derived from human serum **(Fig. 2.1.6)**. These results also indicated that c5F9 has the same immunoreactivity as the original murine 5F9 antibody. 5F9 has broad neutralizing activity since it displayed only reduced or no reactivity to a mutation of the second loop of the 'a' determinant (D144A, G145R, and N146S)[234, 269]. Thus, c5F9 can potentially be applied for diagnostic purposes and as an alternative for HBIG in passive immunotherapy.

It was previously demonstrated in our lab that T-cells grafted with an S-specific chimeric antigen receptor (S-CAR) based on the single chain antibody fragment (scFv) C8, recognize surface-localized HBsAg. Thereby, S-CAR T cells can specifically recognize and kill HBV-infected human hepatocytes *in vitro*, and lead to a profound reduction of viral load *in vivo*[236, 260]. Therefore, we developed a new monoclonal antibody, called MoMab, that contains a double scFv C8 binder which inserted into the constant region (CH2 and CH2) of a human IgG1 **(Fig. 2.1.7)**. In this thesis, the MoMab antibody was expressed in CHO cells, and purified by iron-exchange chromatography. The binding and neutralizing activity were subsequently assessed **(Fig. 2.1.7-9)**. Our findings showed that MoMab could recognize HBsAg of HBV genotypes A, B, C, D, E, and G, and of the serotypes adw2, adrq, and ayw. Its binding activity was higher for adw than for ayw. The most plausible explanation is that MoMab was derived from the peripheral blood lymphocytes of a vaccinated individual, as the vaccine employs adw HBsAg[237]. MoMab can specifically bind HBsAg expressed in yeast and CHO cells, and derived from human serum, but does not recognize HBsAg from Aldevron. TEM-imaging of Aldevron HBsAg revealed that the morphology of the Aldevron HBsAg was unusual (performed by Julia Sacherl), which offers a possible reason why MoMab

failed to bind the Aldevron HBsAg. This observation would indicate that the C8 fragment of MoMab recognizes HBsAg in a conformation-specific manner.

Anti-HBsAg antibodies can be applied to map neutralizing epitopes[270]. There are two main approaches to map anti-HBs antibody epitopes. To determine epitopes targeted by conformation-dependent antibodies, it is usual to assess the effect of single amino acid substitution in HBV-subviral particles on the interaction with an antibody[271]. Assessing the binding of a given antibody to biotinylated antigen peptides is commonly applied for the characterization of linear epitopes[263]. Previous studies have reported that the majority (90 %) of antibodies that recognize HBsAg are directed against conformational epitopes[272]. We assumed that also MoMab is confirmation specific as it did not recognize the denatured HBsAg in Western blots (data not shown). Hence, the former method was applied, to reveal that MoMab recognizes a conformational epitope within the 'a' determinant of SHBs. This observation is in the line with our finding that MoMab can neutralize hepatitis B virus particles **(Fig. 2.1.8-9)**. Additionally, the interaction of MoMab with HBsAg depends on cysteine residues (C121, C124, C137, C138, C139, C149, and C147) and/or the near-by residues **(Fig. 2.1.10)**. These cysteine residues contribute to the formation of three loops; mini-loop aa 121–124[273], the first-loop aa 124–137[274], and the second loop aa 139–147[275]. The cysteine residues form disulfide bonds that are essential for HBsAg conformation and antigenicity. Also substitution of residues C107, P108, and I110, the charged residues K141 and D144, and non-charged polar residue T148 diminished interaction between MoMab and S domain of HBsAg, presumably because they affect the HBsAg confirmation. One of the most common HBsAg escape mutations is the substitution of glycine to arginine at position 145 (G145R). Notably, MoMab binds G145A mutants with only a weak efficiency rate of less than 30 %. Furthermore, the alanine substitution of 123T, which is crucial for the antigenicity of HBsAg[276], had no influence on the reactivity of the HBsAg with MoMab. The R122K substitution is characteristic for the ay- serotypes[277]. The R122A substitution reduced MoMab binding activity,

which is consistent with the reduced affinity of MoMab for the ay- serotypes as compared to the ad- subtypes as depicted in **Fig. 2.1.9B**. Interestingly, Y225[278], which is conserved in all HBV-genotypes except for genotype F, was an important determinant of MoMab epitopes.

3.1.2. Generation and characterization of MoMab-conjugated SPIONs

In recent years, nanoparticles have increasingly been recognized as a useful tool for diagnosis, imaging, and treatment purposes of liver diseases[164, 279]. To develop nanoparticle-based detection approaches, SPIONs, conjugated with biological components such as antibodies, oligonucleotides, and aptamers, have been designed as specific and sensitive tools for imaging viral infections[155, 164, 280].

We show that the interaction between MoMab coated SPIONs and membrane-associated HBV envelope proteins can be visualized by transmission electron microscopy (TEM). SPIONs are well-established as T2-negative MR contrast-enhancing agents. In order to assess the feasibility of applying MoMab-SPION to detect HBsAg in solution, we measured the MoMab-SPION T2 values in the presence of different concentrations of HBsAg by NMR relaxometry **(Fig. 2.1.11)**. We could detect a change in the MoMab-SPION T2 values at the relatively low HBsAg concentration of 50 ng/ml. This indicates that MoMab-coated SPIONS can indeed be used for quantitative detection of HBsAg in biological fluids by NMR.

3.2. Surface localization of HBV envelope proteins

3.2.1. Membrane-associated HBV envelope proteins originates from intracellularly produced HBV envelope proteins

In this study, we applied confocal microscopy to show that HBV envelope proteins co-localize with the plasma membrane. So far, the immunohistochemical analysis of liver tissue required fixation,

by which cells are permealized[230-231]. IHC staining before fixation allowed the detection of membrane associated proteins by keeping the cell membrane intact. Using this approach, we could detect HBV envelope proteins on the membrane of HepG2.2.15 cells (constitutively replicate HBV), but not on HepG2 cells. Next, we tested if the detected membranous HBV envelope proteins on non-permeabilized HepG2.2.15 cells could stem from the attachment of circulating HBV-virions. We did not detect HBV envelope proteins on the membrane of HepG2 cells that were pre-incubated with supernatant containing HBV-virions, indicating that the HBV envelope proteins associated with the membrane of HepG2.2.15 cells stem from intracellular production **(Fig. 2.2.1-3)**. The localization of HBV envelope proteins within the plasma membrane was confirmed using different HBs-specific antibodies such as HB01 and 5F9 **(Fig. 2.2.1-3)**, which recognize a linear epitope within the 'a' determinant of the S domain[235, 269, 281]. Also staining with MoMab (conformational epitopes) and HBVax (rabbit polyclonal anti-HBs) confirmed the membrane-localization of HBsAg on HBV-replicating cells (Fig. 2.2.2-3).

Next, we investigated the distribution of HBV envelope proteins in the HBV-infected HepG2-NTCPcells which can stably express NTCP[282]. Our findings revealed that HBV envelope proteins on the cells' membrane of HBV infected HepG2-NTCP cells with punctate manner, and the staining intensity somewhat correlated with the extent of HBV replication **(Fig. 2.2.9)**. Co-staining of intracellular HBcAg confirmed that HBV envelope proteins was present only on HBV infected cells, although no correlation between speckled membrane-localization and intracellular HBcAg-expression could be affirmed by the results **(Fig. 2.2.10)**. These results indicate that HBV envelope proteins are present in the membrane of HBV-infected cells.

3.2.2. Localization of HBV envelope proteins on the plasma membrane does not require production and release of subviral particles

Beside infectious virions, HBV-replicating cells release subviral particles (SVPs) that consist of HBV envelope proteins only and do not contain viral DNA[283]. There are two types of SVP's, spheres and filaments, and SVPs are secreted in about 1,000-100,000-fold excess over HBV virions[65, 284]. Recently, it has been demonstrated that the endosomal sorting pathway via the formation of multivesicular bodies (MVBs) drives the release of infectious virions and filaments[118, 120-121, 227-228], whereas spherical SVPs are released by the constitutive secretion pathway[112]. It has been reported that LHB, similar to Gag of HIV, interacts with the ESCRT-I component TSG101 via alpha-taxilin for recruiting the ESCRT-machinery[227]. Moreover, mutations of Alix/AIP1, CHMP, and Vps4A/B significantly diminished the production and release of SVPs in cells co-expressing SHBS and LHBS[228]. Interestingly, the assembly and release of SVPs containing SHB alone occurs independent of the ESCRT-MVB[120]. To delineate which secretory pathways are required for HBV envelope proteins to end up in the membrane, we used HuH7-cells and transiently transfected them with plasmids expressing either the small (S, SHBs) or large (L, LHBs) surface antigens, or all HBsAg isoforms combined (SML).

Interestingly, surface localization of LHBs was detected, although LHBs expression in the absence of SHBs did not result in SVBs or HBsAg-secretion **(Fig. 2.2.6)**. LHBs acts as a regulatory protein and plays an essential role in the different specific secretion pathways of HBV-virions and subviral particles, and contains specific retention motifs that prevent secretion of filamentous particles containing LHBS only[119, 122, 228, 285].Thus, the detection of HBsAg on LHBs only expressing cells **(Fig. 2.2.7)**indicate that HBV envelope proteins alone can be transported via MVBs and consequently is embedded in the plasma membrane.

3.2.3. Ultrastructural analysis of the localization of HBV envelope proteins in HBV-replicating cells

Conventional electron microscopy has been applied to determine the intracellular distribution of HBV-virions and subviral particles in the hepatocytes[122, 286-287]. Expanding the conventional electron microscopy, Dr. *Kojima* was the first to carry out immune electron microscopy and reported that the membranous localization of HBsAg correlated with HBeAg in the serum[246]. Although the resolution and specificity of transmission electron microscopy (TEM) -imaging have been recently increased by using HBsAg-specific antibodies and gold-conjugated secondary antibodies compared to the conventional electron microscopy, cells or tissues must be fixed before immunostaining

In this study, TEM analysis was carried out on non-permeabilized HBV-replicating cells and HBV-infected hepatocytes for the visualization of HBV envelope proteins on the cell surface. Membranous HBV envelope proteins was detectable after staining with an anti-HBs monoclonal antibody (5F9) or polyclonal antibody (HBVax) and labeling with secondary antibodies conjugated with gold particles, although very few gold nanoparticles were detected **(Fig. 2.2.12-13)**. We speculated that the low intensity may be due to the dissociation of the primary antibodies and the secondary antibody coated gold nanoparticles during washing. To avoid a signal loss, we explored one-step staining of membrane-associated HBsAg using primary antibody conjugated nanoparticles for TEM-imaging.

Recently, nanoparticles conjugated with antibodies have been designed to particularly target proteins on the cell membrane and have been detected by TEM[288-289]. Some studies have reported that SPIONs were internalized and accumulated in the cells after antibody-antigen interaction, but further research suggested that this uptake of SPIONs was hardly observed at low temperatures[290]. Therefore, short incubation time and low temperature were paramount in our staining process. A TEM-analysis of HepG2-NTCP cells, pretreated with SPIONs, has

demonstrated that the SPIONs were not internalized in the cells. This indicated the method's ability to evaluate the membrane localization of HBsAg without the interference of SPIONs-internalization. Compared to HepG2-NTCP cells, MoMab-functionalized SPIONs were localized on the plasma membrane of the HBV-replicating cells (HepAD 38, HepG2.2.15) as well as HBV-infected cells (**Fig. 2.2.14**). These findings indicate that HBsAg is localized on the membrane of hepatocytes and that this membrane-associated HBsAg is recognized by MoMab-SPIONs.

We could also detect MoMab-SPIONs on the membrane of HepG2-NTCP cells preincubated with HBV viral particles for one hour, while this did not occur on HepG2 cells (**Fig. 2.2.3**). This indicates that MoMab-SPIONs can detect viral particles that associate with the hepatocyte membrane because of interaction with the NTCP. .This result is consistent with the findings from *Ko et al.* that NTCP is a necessary receptor for cell-cell HBV-transmission, mediated by extracellular virions[282].

3.2.4. **The membranous HBV envelope proteins as target for immunotherapeutic approaches**

Our studies verified that HBV envelope proteins are localized on the plasma membrane of HBV-replicating cells. Thus, these membranous proteins could be considered as a target antigen for killing HBV-infected hepatocytes or HCC cells expressing HBsAg from integrated HBV DNA. One common issue, for Chronic hepatitis B patients, is that they are lack of functional T-cells or have exhausted HBV-specific T-cells. Redirecting T-cells to HBV-infected cells would be an interesting approach to treat, and potentially cure, chronic hepatitis B[291-292].

Recently, chimeric antigen receptors (CAR), consisting of single-chain variable fragments binders specifically targeting the viral envelope proteins (S and L), have been developed for an immune-therapeutic approach for chronic HBV-infection[260]. Previous results from our laboratory indicated that S-CAR T-cells can infiltrate the liver of HBV transgenic mice and directly kill HBV-replicating

hepatocytes, even with vast amounts of subviral particles present in the serum of these mice[236]. We demonstrate that transiently transfected HuH7 cells expressing S- or SML proteins were efficiently targeted and killed by S-CAR T-cells, while the complete elimination of these cells is the consequence of strong antiviral cytokines **(Fig. 2.2.15A-B)**. The efficient killing of L-expressing cells indicated that S-CAR T-cells can be activated by membrane-associated viral envelope proteins in the absence of subviral particles in the medium.

Another immunotherapeutic strategy we investigated is the application of bi-specific antibodies (BiMab -SxCD3 and Bi-Mab SxCD28). MoMab and BiMab contain the same scFv fragment (C8), that is capable of specifically recognizing HBsAg **(Fig. 2.1.7)**. BiMabs interact with HBV envelope proteins on the hepatocyte, and recruit and activate T-cells by providing co-stimulation by interacting with the T cell CD3 and CD28 receptors. Our data showed that BiMabs activated T-cells and redirected this immune effector to eliminate the HBsAg-transfected HuH7 cells **(Fig. 2.2.15C-D).** These findings indicate that HBsAg is present on the cell membrane and can be used to redirect T cells to target these cells using bi-specific antibodies.

3.3. Visualization of HBV envelope proteins on HBV replicating cells *in vivo*

It has previously been demonstrated that HBV envelope proteins co-localizes with the cell membrane of hepatocytes in HBV infected patients with or without hepatocellular carcinoma[229-230]. We confirm the membrane-localization of HBsAg *in vivo* by staining hepatocytes from liver specimens of HBV-transgenic mice, HBV-infected chimpanzees, and chronically infected patients **(Fig. 2.3.1-2)**. Moreover, it was shown that all patients were tested positive for intrahepatic HBsAg, regardless of their HBeAg-status or the HBV DNA levels[229-230]. Interestingly, based on the appearance of HBeAg, HBsAg distribution displayed different localization patterns. The majority of the HBeAg-negative cases had a ‘patchy’ or membranous HBsAg-distribution, compared to 50 %

among HBeAg-positive cases[229-230]. In addition, patients with chronic hepatitis B (CHB), including inactive carriers and cirrhosis patients, showed highly accumulated HBsAg within the membrane of hepatocytes. This especially applied to those patients without seroconversion from HBsAg to antibodies[293-294].

So far, the membranous distribution of HBV envelope proteins was demonstrated by IHC staining where the cells or tissues needed to be fixed. We demonstrate that anti-HBsAg antibodies can target HBsAg on the membrane of non-permeabilized hepatocytes **(Fig. 2.2.1-4,7**). HBV-transgenic mice Alb-PSX express LHBS only, are therefore characterized by low or absent HBsAg levels in the serum[246]. We show that intravenously injected MoMab could infiltrate the liver of Alb-PSX mice and specifically target HBsAg-positive cells, even in mice with detectable HBsAg-levels in the serum **(Fig. 2.3.3)**.

3.4. Visualization of HBV replicating cells *in vivo* by MoMab-SPIONs

As we demonstrated above, the constructed anti-HBs MoMab has verified the membrane-localization of HBsAg **(Fig. 2.2.2)**. Intravenous administration of MoMab in Alb-PSX mice led to specific surface targeting **(Fig. 2.3.3)**. Subsequently, the TEM-analysis has proven that the incubation of MoMab-SPIONs with HBV-replicating cells resulted in a high accumulation of SPIONs on the cell membranes **(Fig. 2.2.14)**. In addition, co-incubation of MoMab-SPIONs at 37°C with S-mcherry-HuH7 cells demonstrated the incorporation of the particles by endocytosis (no data shown). Therefore, we investigated the potential of MoMab-SPIONs to visualize HBV envelope proteins expressing hepatoma cells *in vivo* by the SPIONs property as MR-negative contrast agent. HBV-infected patients exhibit high levels of HBsAg present in their blood, even after antiviral treatment[295]. In order to mimic the HBV-infected patients' situation, HBV-transgenic mice with similar circulating HBsAg levels have been used for the intravenous (IV) administration of MoMab-SPIONs. We evaluated the SPIONs accumulation through an MRI-scanner 4 hours

and 24 hours after the IV injection. As expected, a distinct reduction in the T2 signal was observed in MRI images of the liver of the mouse injected with MoMab-SPIONs, starting from 4 hours after IV injection. This signal loss increased even further after 24 hours. After 24 hours, the T2-values of the mouse injected with MoMab-SPIONs decreased 30-fold compared to the PBS injected mouse, and 20-fold compared to the mouse injected with unmodified SPIONs. The retention of MoMab-SPIONs could be observed in the liver but not in brain, heart, and lungs, although some uptake happened in the spleen **(Fig. 2.3.5)**. This indicates that MoMab-SPIONs can infiltrate the liver and specifically target the HBsAg-expressing hepatocytes, despite the high levels of sub-viral particles or HBsAgs present in the serum. Unfortunately, our attempts to confirm the distribution of MoMab and SPIONs in the liver by immunohistochemical (IHC) staining failed.

3.5. Visualization of HBV-replicating hepatoma cells in vivo by MoMab-SPIONs

We evaluated if MoMab-SPIONs can be applied to visualize subcutaneous and orthotopic xenografts of the HBV replicating human hepatoma cell line HepG2.2.15 in immunodeficient Rag2-/-mice. Subcutaneous tumors composed of HepG2.2.15 were induced on the right limb, and control tumors not expressing HBV antigens, consisting of HepG2 cells, were induced on the left limb. Simultaneously, intrahepatic xenografts of HepG2.2.15 cells were induced. Tumors were allowed to establish for three weeks preceding the visualization experiments **(Fig. 2.3.9A-B)**. Compared to the cells' injection to the spleen, the intrahepatic injection was supposed to increase the probability of achieving engraftment of human tumor tissue in the mouse liver[296]. Additionally, the orthotopic xenograft model is superior to the subcutaneous xenograft model due to its tumor microenvironment. After the administration of cells suspension, the secretion of HBsAg and HBeAg were monitored to confirm HepG2.2.15 cell engraftment. The subcutaneous tumors were monitored by eye **(Fig. 2.3.9C-D)**. *Zhao et al.* found that the subcutaneous tumor formation of

HepG2.2.15 cells demonstrated a lower proliferation and invasion ability than that of HepG2 cells[297]. In contrast, we did not observe major differences between the proliferation of HepG2- and HepG2.2.15 cells. IHC confirmed that HBsAg and HBcAg were only expressed in the HepG2.2.15 cells' xenografts (right limb and intrahepatic) **Fig. 2.3.10**, Thus, the model containing both HBV-positive and -negative hepatoma in one mouse body was successfully established.

Recently, SPIONs, functionalized with antibodies, have been used for MRI contrast enhancement and therapeutic targeting of brain glioma[298-299], central nervous system lymphoma[300], and Breast Cancer[301]. In this study, the intravenous administration of MoMab-SPIONs resulted in significant contrast enhancement of HepG2.2.15 cells in right-side subcutaneous tumors and orthotopic liver tumors **(Fig. 2.3.11)**. Unlike the HBV-transgenic mice, the number of intrahepatic HBsAg expressing cells is relatively low in this mouse model and therefore is a better correlate of relevant clinical situations, in which the number of cells replicating HBV or expressing HBV antigens would typically be low[294]. MRI data showed that the SPIONs significantly accumulated in the HBV-positive tumors. In the liver with orthotopic tumor transplantations, the accumulation of MoMab-SPIONs closely correlated with HBsAg- and HBcAg-expression. Taken together, our results suggested the possibility to apply MoMab-SPIONs for imaging and therapeutic targeting of HBV replicating cells in chronic hepatitis B patients, and in HBV related HCC.

4. Summary and Outlook

In this thesis, we firstly verified that HBV envelope proteins are localized to and can be targeted in the membrane of HBV replicating hepatocytes or HBsAg-expressing tumor cells. Hereby, we demonstrated:

i) A membrane-localization of HBV envelope proteins in liver specimens of HBV-transgenic mice, HBV-infected chimpanzees, and HBV related HCC patients;

ii) The speckled pattern of membrane-associated HBV envelop proteins in non-permeabilized HBV-positive cells is neither caused by SVP-production nor by secretion of virions;

iii) The localization of HBV envelope proteins in the membrane of HBV replicating cells was confirmed by TEM using MoMab-labeled SPIONs; The accumulation at distinct membrane sites correlated with the punctuate staining pattern by confocal microscopy;

iv) The S-specific MoMab antibody can be delivered to S- and L-expressing hepatocytes in the liver of mice;

v) Membranous HBV S protein can be targeted by bispecific T-cell engager antibodies or by S-CAR grafted T-cells; T cells become specifically activated and eliminate S-, L-, and SML-expressing transfected HuH7 cells.

Considering all results, targeting membrane-associated HBV envelope proteins represents a new and promising approach to detect and monitor HBV-infection.

Secondly, we showed that MoMab-SPIONs can be applied for targeting and imaging HBV-infection *in vivo*. We further provided the feasibility of the intravenously administered

MoMab-SPIONs to target HBsAg-expressing hepatocytes in HBV-transgenic mice, regardless of the high amount of HBsAg in the blood. The standard T2-weighted MRI revealed that MoMab-SPIONs conjugates specifically accumulated in the liver of HBV-transgenic mice. Additionally, the treatment of the hepatoma (HBV-positive and -negative) bearing animals with MoMab-SPIONs results in a predominant accumulation of SPIONs in HBV-positive tumors, as evidenced by MRI imaging. These data indicate that the MoMab-SPION conjugates are able to provide targeted delivery and efficient resonance contrast enhancement of HBsAg-expressing hepatomas. Our approach has the potential to be further developed for HBsAg-targeted theragnostic, i.e. simultaneous or subsequent diagnostics and therapeutic approaches targeting HBV-infected cells and HBV-associated tumors in the future.

5. Materials and methods

5.1 Materials

5.1.1 Laboratory equipment

Equipment	Manufacturer
Light Cycler 480 II	Roche Diagnostics
Centrifuge Rotanta 400R Micro 200R	Heraeus, Hanau, Germany
FACS CantoII	Beckton Dickinson
Freezer -20°C	Liebherr, Biberach, Germany
Freezer -80°C	Sanyo, Pfaffenhofen, Germany
Fridge 4°C	Liebherr, Biberach, Germany
CO2 Incubator	Tuttlingen, Germany
Fluoview FV101	Olympus, Hamburg, Germany
Vortexer	Lab Dancer IKA, Staufen, Germany
Pipettes Pipetman, P10-1000	Gilson, Middleton, USA
Multi-channel pipette, Pipetman Ultra	Gilson, Middleton, USA
Gel chambers	BIO-RAD Laboratories, Hercules, USA
ALT Reader	Reflotron® Roche Diagnostics, Mannheim, Germany
Photometer Nanodrop	Implen, München, Germany
Architect	Abbott
Infinite F200	Tecan
Light nicroscopy Axiovert 40C	Zeiss
PH meter	Mettler Toledo
Water bath	GLF

5.1.2 Software

Software name	Company
FlowJo v8.5.3	Treestar, Ashland, USA
ImageJ	NIH, USA
Graphpad Prism 5 Graph Pad Software	San Diego, USA
LightCycler 480 Software	Roche Diagnostics
Serial Cloner	Serial basics
FACSDiva	Becton Dickinson

5.1.3 Chemicals and Reagents

Name	Manufacturer
RPMI 1640 medium	Cambrex, Taufkirchen, Germany
Agarose	PeqLab
Dulbecco's Modified Eagle Medium	Gibco, Invitrogen, USA
FCS, heat-inactivated	Biochrom AG, Berlin, Germany
Trypan blue	Gibco, Invitrogen, USA
PBS	Gibco, Invitrogen, USA
Collagenase Type IV Worthington	Lakewood, USA

Human interferon alpha standard	PBL Biomedical Laboratories, USA
SYBR Green I Master Mix	Roche Diagnostics, Mannheim, Germany
Trizol reagent	Invitrogen, Carlsbad, USA
Bradford Reagent	SIGMA, USA
Complete Protease Inhibitor cocktail (25x)	Roth
Blasticidine	Gibco
Pageruler plus Protein ladder Fermentas	Karlsruhe, Germany
Ammonium persulfate (APS) 30%	Sigma
Ethanol	Roth
Paraffin oil	Roth
Rotifix 4% paraformaldehyde (PFA)	Roth
Sodium chloride (NaCl)	B. Braun
Sucrose	Sigma-Aldrich
Tris	Roth
Ampicillin	Roth
Amersham ECL Prime Western Bloting Detection Reagent	GE Healthcare, Sweden
DMSO	Sigma-Aldrich
EDTA	Roth
Glycerol	Roth
Gentamicin	Ratiopharm
Glucose	Roth
Glutamin	Gibco
Goat Serum	Life Technologies
Insulin	Sanofi Aventis
Isofurane	Abbott Laboratories
Hydrocortison	Pfizer
Isopropanol	Roth
Methanol	Roth
Milk powder	Roth
Penicillin/Streptomycin	Biochrom AG
Polyethylene Glycol (PEG) 6000	Promega
Sodium pyruvate	Gibco
Saponin	Roth
Sodium dodecyl sulfate (SDS)	Roth
Tissue-Tek O.C.T.	Sakura
Versene	Life Technologies
β-Mercaptoethanol 50mM	Gibco
Tetramethylethylenediamine (TEMED)	Roth
Triton X 100	Roth

5.1.4 Oligonucleotides for PCR and Plasmid

Name of Primers	Sequence 5'-3'
rcDNA1745 fw	GGAGGGATACATAGAGGTTCCTTGA
rcDNA1844 rev	GTTGCCCGTTTGTCCTCTAATTC
pgRNA 383 fw	CTCCTCCAGCTTATAGACC
pgRNA 705 rev	GTGAGTGGGCCTACAAA
cccDNA 92 fw	GCCTATTGATTGGAAAGTATGT

cccDNA 2251 rev	AGCTGAGGCGGTATCTA
18sRNA fw	AAACGGCTACCACATCCAAG
18sRNA rev	CCTCCAATGGATCCTCGTTA
GAPDH fw	AACGGATTTGGTCGTATTG
GAPDH rev	AAAGGTGGAGGAGTGGGT
Name of Plasmid	Source
pSVL	Prof. Volker Bruss, Virology, Helmholtz-Zentrum
pSVB45H	Prof. Volker Bruss, Virology, Helmholtz-Zentrum
pSVBX 24H	Prof. Volker Bruss, Virology, Helmholtz-Zentrum
pSVBX 24H-M-cherry	Prof. Volker Bruss, Virology, Helmholtz-Zentrum

5.1.5 Kits

Products	Supplier/Company
SuperScript® III First-Strand Synthesis SuperMix for qRT-PCR	Invitrogen, Karlsruhe, Germany
SYBR Green I Master Mix	Roch
NucleoSpin® RNAII kit	Macherey & Nagel
NucleoSpin® Tissue Kit	Macherey & Nagel
RNase-Free DNase Set	QIAGEN
GeneJET Plasmid Miniprep Kit	Thermo, USA
ECL Western Blotting Detection	Pierce
ELISA MAXTM Standard Set Human IFNγ	BioLegend

5.1.6 Enzymes

Product	Supplier
T7 polymerase	Promega
RNase H	Life Technologies
ThermoScript™Reverse Transcriptase	Life Technologies
RQ1 DNase	Promega
Proteinase K	Roth
Trypsin-EDTA (0.5%)	Gibco

5.1.7 Antibodies

Specificity	Clones	Purpose and Concentration	Source
Primary antibodies			
Anti-HBc	Polyclonal	IF (1:1000)	B0586,Dako, Denmark

HBsAg (HB1)		IF(1:200) WB (1:1000)	Dieter Gliber
PDI		IF (1:300)	
Secondary antibodies			
Human IgG	Alexa Fluor® 647	IF(1:500)	Life technologies
Mouse IgG	Alexa Fluor® 647	IF(1:500)	Life technologies
Rabbit IgG	Alexa Fluor® 594	IF(1:1000)	Life technologies
Mouse IgG	HRP	WB(1:10000)	Sigma-Aldrich
Human IgG	HRP	WB(1:10000)	Sigma-Aldrich

5.1.8 Mediums

DMEM complete medium	
DMEM	500 ml
FCS	50 ml
Pen/Strep (5000 I.U. / ml)	5.6 ml
L-Glutamine (200 mM)	5.6 ml
NEAA (100x)	5 ml
Sodium Pyruvate (100 mM)	5 ml
William's E basic medium	
William's E Medium	500 ml
FCS	50 ml
Pen/Strep (5000 I.U. / ml)	5.6 ml
L-Glutamine (200 mM)	5.6 ml
NEAA (100x)	5 ml
Sodium Pyruvate (100 mM)	5 ml
Hepatocytic differentiation medium	
William's E Medium	500 ml
FCS	50 ml
Pen/Strep (5000 I.U. / ml)	5.6 ml
L-Glutamine (200 mM)	5.6 ml
NEAA (100x)	5 ml
Sodium Pyruvate (100 mM)	5 ml
DMSO	10 ml
Freezing medium	
DMSO	1 ml (10%)
FCS	9 ml

5.1.9 Buffer

Buffer	Composition
PBS	0.14 M NaCl, 2.7 mM KCl, 3.2 mM Na2HPO4, 1.5 mM KH2PO4
IF blocking buffer	5% BSA PBS
FAC buffer	0.5% FCS PBS
TAE buffer	Tris 2 M, Acetic acide 2M, EDTA 50 mM at PH 8.0

TBST	0.01 M Tris-HCl (pH 8.0), 0.15 M NaCl, 0.05% Tween
WB blocking buffer	5% Skim Milk TBST

5.1.10 Cell lines

Cell line	Description
HepG2	Human hepatocellular carcinoma cell line
HepG2-NTCP	Human hepatocellular carcinoma cell line, high expression of NTCP
Huh 7	Human hepatocellular carcinoma cell line
HepG 2.2.15	HBV replicating human hepatocellular carcinoma cell line
Hep AD 38	HBV replicating human hepatocellular carcinoma cell line
HEK 293 T cells	Human embryonic kidney cells
CHO cells	Chinese Hammster Overy cells

5.2 Methods

5.2.1 Cell culture

Huh 7 and HEK 293T cells were cultured in T75 culture flask with DMEM complete medium and incubated at 37 °C and 5 % carbon dioxide (CO2). Cells were washed with PBS once and incubated with 2 ml Typsin until cells detached from the flask. Cells were resuspended with DMEM medium for the next step passage or seeding in the desired concentration. HepG2, HepG2-NTCP, HepG2.2.15 and HepAD 38 were seeded on the collagen coated culture Flasks or dishes. Collagen solution were diluted 1:10 in sterile dd H_2O water for 30 mins at 37°C. After incubation, flasks and dishes were washed three times in PBS. These cells were maintained in the DMEM medium at 37 °C and 5 % CO2 condition. Cells were split in a 1:10 dilution when they were 90% confluent.

Cells were frozen at early passage. Cells in confluent flasks were split and resuspended in medium. The cell suspension was further centrifuge for 5 mins at 1200 rpm, then resuspended in Freezing medium. The aliquots were quickly placed in the freezing container and stores at -80 37 °C fridge or changed to nitrogen for long time store. Thawing cells were immediately transferred into 50 ml Falcon tube and diluted into 1:10 with DMEM medium. After centrifugation at 1200 rpm

for 5 mins, pallets were resuspended in DMEM complete medium and transferred into T75 cell culture flask in a CO2 incubator at 37 °C.

5.2.2 Transfection of cells

HuH7 cells were seeded $1.2x10^6$ cells per well in 6 well- plate. FuGENE® HD Transfection Reagent was uses for transfection according to protocol and advises of the manufacturer. 4 µg plasmid and 12 µl FuGENE® HD Transfection Reagent mixed into 300 ml OPI medium and incubated at room temperature for 15 mins. Cells were changed freshed medium without any antibiotics. After the mixture, all mixed medium were added into cells medium. The supernatant and cell lysate were accumulated and measured after post-infection 24h, 48h and 72h.

5.2.3 Infection of HepG2-NTCP cells

HepG2-NTCP cells were seeded $5x10^4$ per well for 24-well plate, and cultivated overnight to get 90% confluency, then differentiated with differentiation medium (DMEM culture medium +1.8%DMSO) for two days. Different amount HBV virus were pre-mixed with differentiation medium including 4%PEG in total volume of 250 µl and added different MOI (, 200, 500 and 1000) to infect HepG2-NTCP cells. After 24h infection, infection medium was discarded before washing twice with PBS, then differentiation medium was added and changed every three days until 9 days dpi. HBsAg and HBeAg secretion from the corresponding supernatant were measured by Achtect Kit for HBV antigen (ELISA). Infection efficiency was evaluated by the expression level of cccDNA, rcDNA and pgRNA from the cell lysate at 9 dpi.

5.2.4 Immunofluorescent staining

Surface staining

Cells were blocked into 5% BSA blocking buffer for 1hour on the ice. After once washing with 1% BSA washing buffer, cells were centrifuged for 5 mins at 1200 rpm. Then the pellet was resuspended by antibody solutions at a curtained concentration (HBVax, HB01, 5F9 and Mo-mab, respectively). Following step is to detect with a corresponding Alexa-Fluor® 647 labeled goat anti-

rabbit, anti-mouse and anti-human IgG (1:500) and counterstained with Alexa-Fluor 488 coupled with the plasma membrane marker, wheat germ agglutinin (WGA), for 30 mins on ice. Subsequently, cells were washed 3 times with 1% BSA in PBS and fixed cells in 4% paraformaldehyde for 10 mins at room temperature. After washing 2 times with 1% BSA, then cells were resuspended in mounting medium containing DAPI for nuclei staining.

Double staining

Surface staining was performed firstly. Cells were re-stained by Mo-mab as additional primary antibody after extra blocking. Followed by incubation with Alexa-Fluor® 647 labelled goat anti-human IgG. Subsequently, intracellular PDI protein was stained with anti-PDI antibody (1:200) for 30 mins at RT after fixation (10 mins at RT with 4%PFA), and permeabilization (20 mins at RT with 0.1% Triton), blocking (overnight at 4°C with 10 % goat serum in PBS), then another counterstaining with Alexa-Fluor® 488 labeled goat anti-mouse IgG (1:1000) as secondary antibody medium for 20 mins at RT. Lastly, nuclei were stained in DAPI mounting medium.

In order to investigate the HBV infection efficiency in HepG2-NTCP cells, intracellular HBcAg was detected as well, it was prior to HBsAg surface staining. After fixation, permeabilization and blocking, cells were incubated with rabbit anti-HBcAg (1:400) overnight 4°C, then detected by Alexa-Fluor® 594 labeled goat anti-rabbit IgG (1:1000) for 2h at RT or overnight 4°C. Finally, cells were washed three times and resuspended in mounting DAPI solution. Fluorescent images were evaluated by a FluoView confocal microscopy (Olympus). For the image presentation the size and the contrast were adjusted using ImageJ and Photoshope 7.0 (Adobe Software Palo Alto CA).

5.2.5 Intrahepatic Immunohistochemical Analysis (IHC)

Liver specimens from HBV transgenic mice, infected chimpanzee and chronic hepatitis patients were fixed in 4% paraformaldehyde overnight at room temperature, then 2 µm paraffin-embedded tissue sections were stained by IHC staining. HBsAg were determined in the liver sections with

mouse anti-HBsAg or human antibody MoMab. The negative staining contrasts were stained with PBS. Histological analysis was performed with the Bond Polymer Refine Detection Kit (Leica) on the BondMax system (Leica). The distribution and patterns of HBsAg were described after the whole slides were scanned using an SCN-400 slide canner (Leica) and analyzed using Tissue IA image analysis software (Leitca) with optimized quantification algorithms.

5.2.6 Synthesis and physico-chemical characterization of MoMab-SPIONs conjugates

Superparamagnetic iron oxide nanoparticles (SPIONs) were prepared from iron salt solutions by co-precipitation as described earlier [2]. Briefly, FeSO4 and FeCl3 at a Fe2+/Fe3+ ratio of 1:2 was dissolved in water with the addition of CsCl. The magnetite suspension in water was treated by ultrasound at 22 kHz for 15 minutes. Low molecular weight dextran (MW 10 kD, Sigma) was added to the dispersion of nanoparticles to prevent sedimenation during the application of the ultrasound. The surface of the obtained particles was functionalized with monoclonal antibody MoMab. For conjugation with MoMab the dextran-coated nanoparticles were cross-linked with epichlorohydrin and aminated. Activated by water-soluble carbodiimide, dextran was coupled to the carboxyl groups of MoMab, producing superparamagnetic nanoparticles MoMab-SPIONs. The size distribution and nanoparticle size of SPIONs and MoMab-SPIONs were assessed by transmission electron microscopy (TEM) using a JEOL-2000 microscope (Jeol, Japan) and dynamic light scattering (DLS) using a Malvern instrument. The hydrodynamic size and electrophoretic properties were measured on Zetasizer Nano (Malvern Instruments, UK). The NMR relativity studies for assessment of the R2*, R2 and R1 coefficients was performed with the help of CXP-300 a NMR-spectrometry (Bruker, Germany) with a magnetic field 7.1 T.

For assessment of MoMab-SPIONs specific interaction with HBsAg the obtained conjugates or SPIONs (0, 02 mM Fe) were co-incubated with antigen for 24 hours. The estimation of specific ability of MoMab conjugates to bind HBsAg was performed by temporal measurement of T2 relaxation times in the ‘switch assay’ suggested by Tassa [210]et al.).

5.2.7 Electron microscopy

HepG 2.2.15, HepAD38 cells and infected (9dpi and at MOI 100) HepG2-NTCP cells were trypsined and seeded (1×10^5 cells/ml) in the 48-well plate. Overnight refreshed the medium with differentiation medium for 2 days. Following incubation with SPIONs or MoMab-SPIONs conjugates for 3 hours were washed by PBS 3 times, fixed in 2.5% electron microscopy grade glutaraldehyde in 0.1 M sodium cacodylate buffer pH 7.4 (Science Services, Munich, Germany), postfixed in 2% aqueous osmium tetraoxide (Dalton, 1952), dehydrated in gradual ethanol (30–100%) and propylene oxide, embedded in Epon (Merck, Darmstadt, Germany) and cured for 24 hours at 60°C. Semithin sections were cut and stained with toluidine blue. Ultrathin sections of 50 nm were collected onto 200 mesh copper grids, stained with uranyl acetate and lead citrate before examination by transmission electron microscopy (Zeiss Libra 120 Plus, Carl Zeiss NTS GmbH, Oberkochen, Germany). Pictures were acquired using a Slow Scan CCD camera and iTEM software (Olympus Soft Imaging Solutions, Münster, Germany).

5.2.8 Targeting membranous associated HBsAg

S-CAR T cells killing activity

Transduced Hepatitis B virus-specific chimeric antigen receptor (S-CAR) into the T cells first. The method is described before (Karins paper). On day later, HuH7 cells were transfected with the plasmids PSVB45H (SML), PSVL (L) and PSVBX24H for 24 hours. Cells were trypsined and seeded (3500 cells per well) into 96 well plates overnight, then co-cultured with S-CAR T cells and the decoy CAR-T cells (1x106 cells). The left refreshed HBsAg expressing cells were seeded into the 24 well plates for immunofluorescent staining. The xCELLigence RTCA SP system was used for real-time analysis these cells viability. Cells index was measured continuously for the following 4 days. Data analysis was performed using RTCA software v1.2.1. To further characterize T cell activation, the corresponding supernatant was collected after co-culture, IFN-ϒ, TNF-α and IL-2 level in the supernatant was measured via cytokine ELISA (BioLegend).

Redirecting T cells in PBMC at the presence of BiMab

Like 5.2.2 and 5.2.8, HuH7 cells transfected HBsAg variants for 24 hours. Then these cells were typsined and coated into the 96 well plates for overnight. The old medium was discarded, and the new fresh medium contained BiMabs (BiMab-SxCD3 and BiMab-SxCD28 at 0.25 µg /ml concentration, respectively) or cultural medium as negative control, followed by addition of ($1x10^5$ cells /well) fresh isolated or frozen PBMCs which rested overnight in RPMI culture medium. To visualize changes in target cell viability over time, the xCELLigence RTCA SP system was performed. The corresponding supernatant was collected at 90 hours for the testing of cytokines secretion.

5.2.9 DNA and RNA extraction

Intracellular DNA was extracted by the the “NucleoSpin® Tis¬sue”-kit (Macherey-Nagel, Düren, Germany). Following the standard protocol for cultured cells, cells should be lysed by lysis buffer for 10 mins at room temperature, in the meaning while, Proteinase K should be added, and then cells lysate incubated at 56°C on a heated shaking device at least 3 hours until the sample appeared visually lysed. Before the elution, the silica membrane was dried for two mins. Elution volume was 100 µl, at least incubated 2 mins.

For RNA isolation, the NucleoSpin® RNAII kit was used. Cells was lysed by 350 µl RNA lysis buffer and 3.5 µl β-merchaptoethanol prior to PBS washing first. The mixture was applied into the Collection Tube. After centrifugation, 350 µl 70% ethanol was performed to bind RNA. Cell lysate was loaded to the silica membrane, after desalting silica membrane with Membrane Desalting Buffer, DNA in samples was digested by rDNase at room temperature for 15 mins. Following the three steps of washing, silica membrane was incubated with 40 µl elution buffer for 2 mins. Finally, the extracted RNA was stored in the -80 °C fridge.

5.2.10 RT-PCR and qPCR

The first strand of cDNA was synthesized by SuperScript® III First-Strand Synthesis SuperMix for qRT-PCR" kit. The mix reaction was that: 5 µl of 2x RT reaction mix were combined with 1 µl of RT enzyme mix and 4 µl of extracted RNA. The following temperature profile was cDNA transcription: 25° C for 5 min, 50° C for 30 min, 85° C for 5 min, 4° C. Then 0.5 µl of RNaseH (5 000 U/ml) were added to each well. After centrifugation, samples were incubated at 37° C for 20 min. Products were diluted 1:3 with PCR grade water.

qPCR is applied to amplify and quantify a defined level of one DNA template by the measuring of emission of SYBR Geen dye. The q PCR procedure is that: 4 µl of cDNA sample were mixed with 0.5 µl of reverse primer (20 µM), 0.5 µl of forward primer (20 µM) and 5 µl SYBR® Green Mix (Invitrogen, Karlsruhe, Germany). qPCR runs were performed using Prp, GAPDH and 18s as reference gene. The following is the procedure of qPCR.

qPCR conditions of cccDNA

	T [°C]	t [sec]	Ramp [°C/sec]	Acquisition mode	Cycles
Denaturation	95	600	4.4		1
Amplification	95	15	4.4		50
	60	5	2.2		
	72	45	4.4		
	88	2	4.4	single	
Melting	95	1	4.4		1
	65	15	2.2		
	95		0.11	continouus: 5/°C	
Cooling	40	30	2.2		1

qPCR conditions of rcDNA and PrP

	T [°C]	t [sec]	Ramp [°C/sec]	Acquisition mode	Cycles
Denaturation	95	300	4.4		1
Amplification	95	25	4.4		40
	60	10	2.2		
	72	30	4.4	single	
Melting	95	1	4.4		1
	65	60	2.2		
	95		0.11	continouus: 5/°C	

Cooling	40	30	2.2		1

5.2.11 Animal experiments

MoMab injection in Alb-PSX mice

HBV transgenic mice Alb-PSX mice and C57BL/6 mice were bred in specific pathogen–free animal facilities. The study was conducted according to the German Law for the Protection of Animals. To further evaluate whether MoMab specifically target HBsAg expressed hepatocytes, two different doses of MoMab (50µg and 100µg/mouse, diluted in PBS) were intravenously injected into Alb-PSX mice or C57BL/6 mice (as a control) (200µl/mouse for injection). 4 hour after injection, mice were sacrificed. Blood and liver were taken. Binding of MoMab to the liver hepatocytes were examined by immunohistochemistry.

MoMab-SPIONs injection in Alb-PSX mice, transgenic mice

For assessment of the accumulation of the synthesized superparamagnetic nanoparticles the HBVtg 1.3xfs mice (HBVQ9 genotype D, serotype ayw13) and Alb-PSX mice were randomly divided into three groups (3 animals each): (1) i.v. injection of the phosphate-buffer solution (PBS) (control group); (2) i.v. injection of the SPIONs (2.5 mg/kg) for 24 hours; (3) i.v. injection of MoMab-SPIONs (2.5 mg/kg) for 24 hours. Assessment of nanoparticles targeting was performed using high-field 7.0 T MRI scanner (Bruker, Germany) with the following sequences: T1-Flash, anatomical high resolution T_2-weighted scans. For estimation of the accumulation of the nanoparticles in the tumor we utilized multi-slice multi-echo (MSME) sequences which were used to generate the T_2 maps. For calculation of the contrast enhancement on the T_2 maps we applied software

package Paravision 3.1 (Bruker BioSpin GmbH, Rheinstetten, Germany). Blood and liver were collected. Organs were detected by immunohistochemistry.

MoMab-SPIONs injection in Rag2/IL2Ynull mice

Each Rag2/IL2Ynull mice was injected HepG2.2.15 cells in liver ($2x10^6$) and the right leg subcutaneously. The left leg was subcutaneously injected the same amount of HepG2 cells. Mice were bred in specific pathogen–free animal facilities for 3 weeks until the tumor generated. Like 5.2.12.2, mice divided into three groups: (1) i.v. injection of the phosphate-buffer solution (PBS) (control group); (2) i.v. injection of the SPIONs (2.5 mg/kg) for 24 hours; i.v. injection of MoMab-SPIONs (2.5 mg/kg) for 24 hours. Finally, mice were measured by MRI. The organs were collected and stained by immunohistochemistry.

5.2.12 Statistical analysis and Image Analysis

Data are shown as means±SD. The significance of results was analyzed by two-tailed t test using GraphPad, p values less than 0.5 were considered significant. Image J was used for all data analysis.

6. Reference

1. Gust, I. D.; Burrell, C. J.; Coulepis, A. G.; Robinson, W. S.; Zuckerman, A. J., Taxonomic classification of human hepatitis B virus. *Intervirology* **1986,** *25* (1), 14-29.
2. Kidd-Ljunggren, K.; Miyakawa, Y.; Kidd, A. H., Genetic variability in hepatitis B viruses. *J Gen Virol* **2002,** *83* (Pt 6), 1267-80.
3. Seeger, C.; Jianming, H., Why are hepadnaviruses DNA and not RNA viruses? *Trends in Microbiology* **1997,** *5* (11), 447-450.
4. Yu, H.; Yuan, Q.; Ge, S. X.; Wang, H. Y.; Zhang, Y. L.; Chen, Q. R.; Zhang, J.; Chen, P. J.; Xia, N. S., Molecular and phylogenetic analyses suggest an additional hepatitis B virus genotype "I". *PLoS One* **2010,** *5* (2), e9297.
5. Kramvis, A., Genotypes and genetic variability of hepatitis B virus. *Intervirology* **2014,** *57* (3-4), 141-50.
6. Yousif, M.; Kramvis, A., Genotype D of hepatitis B virus and its subgenotypes: An update. *Hepatol Res* **2013,** *43* (4), 355-64.
7. Okamoto, H.; Imai, M.; Tsuda, F.; Tanaka, T.; Miyakawa, Y.; Mayumi, M., Point mutation in the S gene of hepatitis B virus for a d/y or w/r subtypic change in two blood donors carrying a surface antigen of compound subtype adyr or adwr. *J Virol* **1987,** *61* (10), 3030-4.
8. Sartorius, K.; Sartorius, B.; Aldous, C.; Govender, P. S.; Madiba, T. E., Global and country underestimation of hepatocellular carcinoma (HCC) in 2012 and its implications. *Cancer epidemiology* **2015,** *39* (3), 284-90.
9. Hepatitis B: fact sheet. *World Heal Organ 2017* **2017**.
10. Takano, T.; Tajiri, H.; Hosono, S.; Inui, A.; Murakami, J.; Ushijima, K.; Miyoshi, Y.; Etani, Y.; Abukawa, D.; Suzuki, M.; Brooks, S., Natural history of chronic hepatitis B virus infection in children in Japan: a comparison of mother-to-child transmission with horizontal transmission. *J Gastroenterol* **2017**.
11. Ganem, D., Persistent infection of humans with hepatitis B virus: mechanisms and consequences. *Rev Infect Dis* **1982,** *4* (5), 1026-47.
12. Hoofnagle, J. H.; Di Bisceglie, A. M., Serologic diagnosis of acute and chronic viral hepatitis. *Seminars in liver disease* **1991,** *11* (2), 73-83.
13. Shiffman, M. L., Management of acute hepatitis B. *Clin Liver Dis* **2010,** *14* (1), 75-91; viii-ix.
14. McMahon, B. J.; Alward, W. L.; Hall, D. B.; Heyward, W. L.; Bender, T. R.; Francis, D. P.; Maynard, J. E., Acute hepatitis B virus infection: relation of age to the clinical expression of disease and subsequent development of the carrier state. *J Infect Dis* **1985,** *151* (4), 599-603.
15. Peeridogaheh, H.; Meshkat, Z.; Habibzadeh, S.; Arzanlou, M.; Shahi, J. M.; Rostami, S.; Gerayli, S.; Teimourpour, R., Current concepts on immunopathogenesis of hepatitis B virus infection. *Virus Res* **2018,** *245*, 29-43.
16. MacLachlan, J. H.; Cowie, B. C., Hepatitis B Virus Epidemiology. *Cold Spring Harb Perspect Med* **2015,** *5* (5).
17. Jefferies, M.; Rauff, B.; Rashid, H.; Lam, T.; Rafiq, S., Update on global epidemiology of viral hepatitis and preventive strategies. *World journal of clinical cases* **2018,** *6* (13), 589-599.
18. Chen, C. L.; Yang, J. Y.; Lin, S. F.; Sun, C. A.; Bai, C. H.; You, S. L.; Chen, C. J.; Kao, J. H.; Chen, P. J.; Chen, D. S., Slow decline of hepatitis B burden in general population: Results from a population-based survey and longitudinal follow-up study in Taiwan. *J Hepatol* **2015,** *63* (2), 354-63.
19. Coppola, N.; Alessio, L.; Gualdieri, L.; Pisaturo, M.; Sagnelli, C.; Caprio, N.; Maffei, R.; Starace, M.; Angelillo, I. F.; Pasquale, G.; Sagnelli, E., Hepatitis B virus, hepatitis C virus and human immunodeficiency virus infection in undocumented migrants and refugees in southern Italy, January 2012 to June 2013. *Euro Surveill* **2015,** *20* (35), 30009.

20. Hampel, A.; Solbach, P.; Cornberg, M.; Schmidt, R. E.; Behrens, G. M.; Jablonka, A., [Current seroprevalence, vaccination and predictive value of liver enzymes for hepatitis B among refugees in Germany]. *Bundesgesundheitsblatt Gesundheitsforschung Gesundheitsschutz* **2016,** *59* (5), 578-83.
21. Nassal, M., Hepatitis B viruses: reverse transcription a different way. *Virus Res* **2008,** *134* (1-2), 235-49.
22. Tong, S.; Revill, P., Overview of hepatitis B viral replication and genetic variability. *J Hepatol* **2016,** *64* (1 Suppl), S4-S16.
23. Heermann, K. H.; Goldmann, U.; Schwartz, W.; Seyffarth, T.; Baumgarten, H.; Gerlich, W. H., Large surface proteins of hepatitis B virus containing the pre-s sequence. *J Virol* **1984,** *52* (2), 396-402.
24. Julithe, R.; Abou-Jaoude, G.; Sureau, C., Modification of the hepatitis B virus envelope protein glycosylation pattern interferes with secretion of viral particles, infectivity, and susceptibility to neutralizing antibodies. *J Virol* **2014,** *88* (16), 9049-59.
25. Wounderlich, G.; Bruss, V., Characterization of early hepatitis B virus surface protein oligomers. *Arch Virol* **1996,** *141* (7), 1191-205.
26. Ni, Y.; Sonnabend, J.; Seitz, S.; Urban, S., The pre-s2 domain of the hepatitis B virus is dispensable for infectivity but serves a spacer function for L-protein-connected virus assembly. *J Virol* **2010,** *84* (8), 3879-88.
27. Eble, B. E.; MacRae, D. R.; Lingappa, V. R.; Ganem, D., Multiple topogenic sequences determine the transmembrane orientation of the hepatitis B surface antigen. *Mol Cell Biol* **1987,** *7* (10), 3591-601.
28. Siegler, V. D.; Bruss, V., Role of transmembrane domains of hepatitis B virus small surface proteins in subviral-particle biogenesis. *J Virol* **2013,** *87* (3), 1491-6.
29. Stirk, H. J.; Thornton, J. M.; Howard, C. R., A topological model for hepatitis B surface antigen. *Intervirology* **1992,** *33* (3), 148-58.
30. Berting, A.; Hahnen, J.; Kröger, M.; Gerlich, W. H., Computer-Aided Studies on the Spatial Structure of the Small Hepatitis B Surface Protein. *Intervirology* **1995,** *38* (1-2), 8-15.
31. Poisson, F.; Severac, A.; Hourioux, C.; Goudeau, A.; Roingeard, P., Both pre-S1 and S domains of hepatitis B virus envelope proteins interact with the core particle. *Virology* **1997,** *228* (1), 115-20.
32. Eble, B. E.; Lingappa, V. R.; Ganem, D., The N-terminal (pre-S2) domain of a hepatitis B virus surface glycoprotein is translocated across membranes by downstream signal sequences. *J Virol* **1990,** *64* (3), 1414-9.
33. Schmitt, S., Structure of pre-S2 N- and O-linked glycans in surface proteins from different genotypes of hepatitis B virus. *Journal of General Virology* **2004,** *85* (7), 2045-2053.
34. Schmitt, S.; Glebe, D.; Alving, K.; Tolle, T. K.; Linder, M.; Geyer, H.; Linder, D.; Peter-Katalinic, J.; Gerlich, W. H.; Geyer, R., Analysis of the pre-S2 N- and O-linked glycans of the M surface protein from human hepatitis B virus. *J Biol Chem* **1999,** *274* (17), 11945-57.
35. Mehta, A.; Lu, X.; Block, T. M.; Blumberg, B. S.; Dwek, R. A., Hepatitis B virus (HBV) envelope glycoproteins vary drastically in their sensitivity to glycan processing: Evidence that alteration of a single N-linked glycosylation site can regulate HBV secretion. *Proceedings of the National Academy of Sciences* **1997,** *94* (5), 1822-1827.
36. Fernholz, D.; Galle, P. R.; Stemler, M.; Brunetto, M.; Bonino, F.; Will, H., Infectious Hepatitis B Virus Variant Defective in Pre-S2 Protein Expression in a Chronic Carrier. *Virology* **1993,** *194* (1), 137-148.
37. Bruss, V.; Ganem, D., The role of envelope proteins in hepatitis B virus assembly. *Proceedings of the National Academy of Sciences* **1991,** *88* (3), 1059-1063.
38. Gavilanes, F.; Gonzalez-Ros, J. M.; Peterson, D. L., Structure of hepatitis B surface antigen. Characterization of the lipid components and their association with the viral proteins. *J Biol Chem* **1982,** *257* (13), 7770-7.

39. Lambert, C.; Prange, R., Chaperone action in the posttranslational topological reorientation of the hepatitis B virus large envelope protein: Implications for translocational regulation. *Proceedings of the National Academy of Sciences* **2003,** *100* (9), 5199-5204.
40. Wang, Y. P.; Liu, F.; He, H. W.; Han, Y. X.; Peng, Z. G.; Li, B. W.; You, X. F.; Song, D. Q.; Li, Z. R.; Yu, L. Y.; Cen, S.; Hong, B.; Sun, C. H.; Zhao, L. X.; Kreiswirth, B.; Perlin, D.; Shao, R. G.; Jiang, J. D., Heat Stress Cognate 70 Host Protein as a Potential Drug Target against Drug Resistance in Hepatitis B Virus. *Antimicrobial Agents and Chemotherapy* **2010,** *54* (5), 2070-2077.
41. Lambert, C.; Mann, S.; Prange, R., Assessment of determinants affecting the dual topology of hepadnaviral large envelope proteins. *J Gen Virol* **2004,** *85* (Pt 5), 1221-5.
42. Ostapchuk, P.; Hearing, P.; Ganem, D., A dramatic shift in the transmembrane topology of a viral envelope glycoprotein accompanies hepatitis B viral morphogenesis. *Embo j* **1994,** *13* (5), 1048-57.
43. Bruss, V.; Lu, X.; Thomssen, R.; Gerlich, W. H., Post-translational alterations in transmembrane topology of the hepatitis B virus large envelope protein. *Embo j* **1994,** *13* (10), 2273-9.
44. Lambert, C.; Prange, R., Dual topology of the hepatitis B virus large envelope protein: determinants influencing post-translational pre-S translocation. *J Biol Chem* **2001,** *276* (25), 22265-72.
45. Prange, R.; Streeck, R. E., Novel transmembrane topology of the hepatitis B virus envelope proteins. *Embo j* **1995,** *14* (2), 247-56.
46. Glebe, D.; Urban, S., Viral and cellular determinants involved in hepadnaviral entry. *World J Gastroenterol* **2007,** *13* (1), 22-38.
47. Blank, A.; Markert, C.; Hohmann, N.; Carls, A.; Mikus, G.; Lehr, T.; Alexandrov, A.; Haag, M.; Schwab, M.; Urban, S.; Haefeli, W. E., First-in-human application of the novel hepatitis B and hepatitis D virus entry inhibitor myrcludex B. *J Hepatol* **2016,** *65* (3), 483-9.
48. Bremer, C. M.; Sominskaya, I.; Skrastina, D.; Pumpens, P.; El Wahed, A. A.; Beutling, U.; Frank, R.; Fritz, H. J.; Hunsmann, G.; Gerlich, W. H.; Glebe, D., N-terminal myristoylation-dependent masking of neutralizing epitopes in the preS1 attachment site of hepatitis B virus. *J Hepatol* **2011,** *55* (1), 29-37.
49. Bruss, V., A short linear sequence in the pre-S domain of the large hepatitis B virus envelope protein required for virion formation. *J Virol* **1997,** *71* (12), 9350-7.
50. Diab, A.; Foca, A.; Zoulim, F.; Durantel, D.; Andrisani, O., The diverse functions of the hepatitis B core/capsid protein (HBc) in the viral life cycle: Implications for the development of HBc-targeting antivirals. *Antiviral Res* **2018,** *149*, 211-220.
51. Kann, M.; Sodeik, B.; Vlachou, A.; Gerlich, W. H.; Helenius, A., Phosphorylation-dependent binding of hepatitis B virus core particles to the nuclear pore complex. *J Cell Biol* **1999,** *145* (1), 45-55.
52. Li, H. C.; Huang, E. Y.; Su, P. Y.; Wu, S. Y.; Yang, C. C.; Lin, Y. S.; Chang, W. C.; Shih, C., Nuclear export and import of human hepatitis B virus capsid protein and particles. *PLoS Pathog* **2010,** *6* (10), e1001162.
53. Schmitz, A.; Schwarz, A.; Foss, M.; Zhou, L.; Rabe, B.; Hoellenriegel, J.; Stoeber, M.; Pante, N.; Kann, M., Nucleoporin 153 arrests the nuclear import of hepatitis B virus capsids in the nuclear basket. *PLoS Pathog* **2010,** *6* (1), e1000741.
54. Zlotnick, A.; Cheng, N.; Stahl, S. J.; Conway, J. F.; Steven, A. C.; Wingfield, P. T., Localization of the C terminus of the assembly domain of hepatitis B virus capsid protein: implications for morphogenesis and organization of encapsidated RNA. *Proc Natl Acad Sci U S A* **1997,** *94* (18), 9556-61.
55. Jones, S. A.; Hu, J., Hepatitis B virus reverse transcriptase: diverse functions as classical and emerging targets for antiviral intervention. *Emerg Microbes Infect* **2013,** *2* (9), e56.
56. Jones, S. A.; Hu, J., Protein-primed terminal transferase activity of hepatitis B virus polymerase. *J Virol* **2013,** *87* (5), 2563-76.
57. Jones, S. A.; Boregowda, R.; Spratt, T. E.; Hu, J., In vitro epsilon RNA-dependent protein priming activity of human hepatitis B virus polymerase. *J Virol* **2012,** *86* (9), 5134-50.

58. Kimura, T.; Rokuhara, A.; Sakamoto, Y.; Yagi, S.; Tanaka, E.; Kiyosawa, K.; Maki, N., Sensitive enzyme immunoassay for hepatitis B virus core-related antigens and their correlation to virus load. *J Clin Microbiol* **2002,** *40* (2), 439-45.
59. Lin, C. L.; Kao, J. H., New perspectives of biomarkers for the management of chronic hepatitis B. *Clin Mol Hepatol* **2016,** *22* (4), 423-431.
60. Lee, H. R.; Cho, Y. Y.; Lee, G. Y.; You, D. G.; Yoo, Y. D.; Kim, Y. J., A direct role for hepatitis B virus X protein in inducing mitochondrial membrane permeabilization. *J Viral Hepat* **2017**.
61. Ma, J.; Sun, T.; Park, S.; Shen, G.; Liu, J., The role of hepatitis B virus X protein is related to its differential intracellular localization. *Acta Biochim Biophys Sin (Shanghai)* **2011,** *43* (8), 583-8.
62. Tang, H.; Oishi, N.; Kaneko, S.; Murakami, S., Molecular functions and biological roles of hepatitis B virus x protein. *Cancer Sci* **2006,** *97* (10), 977-83.
63. Crowther, R. A.; Kiselev, N. A.; Bottcher, B.; Berriman, J. A.; Borisova, G. P.; Ose, V.; Pumpens, P., Three-dimensional structure of hepatitis B virus core particles determined by electron cryomicroscopy. *Cell* **1994,** *77* (6), 943-50.
64. Dryden, K. A.; Wieland, S. F.; Whitten-Bauer, C.; Gerin, J. L.; Chisari, F. V.; Yeager, M., Native hepatitis B virions and capsids visualized by electron cryomicroscopy. *Mol Cell* **2006,** *22* (6), 843-50.
65. Blumberg, B. S., Australia antigen and the biology of hepatitis B. *Science* **1977,** *197* (4298), 17-25.
66. Cao, J.; Zhang, J.; Lu, Y.; Luo, S.; Zhang, J.; Zhu, P., Cryo-EM structure of native spherical subviral particles isolated from HBV carriers. *Virus Res* **2019,** *259*, 90-96.
67. Ko, C.; Michler, T.; Protzer, U., Novel viral and host targets to cure hepatitis B. *Curr Opin Virol* **2017,** *24*, 38-45.
68. Leistner, C. M.; Gruen-Bernhard, S.; Glebe, D., Role of glycosaminoglycans for binding and infection of hepatitis B virus. *Cell Microbiol* **2008,** *10* (1), 122-33.
69. Hagenbuch, B.; Meier, P. J., Molecular cloning, chromosomal localization, and functional characterization of a human liver Na+/bile acid cotransporter. *J Clin Invest* **1994,** *93* (3), 1326-31.
70. Dawson, P. A.; Lan, T.; Rao, A., Bile acid transporters. *J Lipid Res* **2009,** *50* (12), 2340-57.
71. Burwitz, B. J.; Wettengel, J. M.; Muck-Hausl, M. A.; Ringelhan, M.; Ko, C.; Festag, M. M.; Hammond, K. B.; Northrup, M.; Bimber, B. N.; Jacob, T.; Reed, J. S.; Norris, R.; Park, B.; Moller-Tank, S.; Esser, K.; Greene, J. M.; Wu, H. L.; Abdulhaqq, S.; Webb, G.; Sutton, W. F.; Klug, A.; Swanson, T.; Legasse, A. W.; Vu, T. Q.; Asokan, A.; Haigwood, N. L.; Protzer, U.; Sacha, J. B., Hepatocytic expression of human sodium-taurocholate cotransporting polypeptide enables hepatitis B virus infection of macaques. *Nat Commun* **2017,** *8* (1), 2146.
72. Yan, H.; Zhong, G.; Xu, G.; He, W.; Jing, Z.; Gao, Z.; Huang, Y.; Qi, Y.; Peng, B.; Wang, H.; Fu, L.; Song, M.; Chen, P.; Gao, W.; Ren, B.; Sun, Y.; Cai, T.; Feng, X.; Sui, J.; Li, W., Sodium taurocholate cotransporting polypeptide is a functional receptor for human hepatitis B and D virus. *Elife* **2012,** *1*, e00049.
73. Bogomolov, P.; Alexandrov, A.; Voronkova, N.; Macievich, M.; Kokina, K.; Petrachenkova, M.; Lehr, T.; Lempp, F. A.; Wedemeyer, H.; Haag, M.; Schwab, M.; Haefeli, W. E.; Blank, A.; Urban, S., Treatment of chronic hepatitis D with the entry inhibitor myrcludex B: First results of a phase Ib/IIa study. *J Hepatol* **2016,** *65* (3), 490-8.
74. Macovei, A.; Radulescu, C.; Lazar, C.; Petrescu, S.; Durantel, D.; Dwek, R. A.; Zitzmann, N.; Nichita, N. B., Hepatitis B virus requires intact caveolin-1 function for productive infection in HepaRG cells. *J Virol* **2010,** *84* (1), 243-53.
75. Huang, H. C.; Chen, C. C.; Chang, W. C.; Tao, M. H.; Huang, C., Entry of hepatitis B virus into immortalized human primary hepatocytes by clathrin-dependent endocytosis. *J Virol* **2012,** *86* (17), 9443-53.
76. Cooper, A.; Shaul, Y., Clathrin-mediated endocytosis and lysosomal cleavage of hepatitis B virus capsid-like core particles. *J Biol Chem* **2006,** *281* (24), 16563-9.

77. Oess, S.; Hildt, E., Novel cell permeable motif derived from the PreS2-domain of hepatitis-B virus surface antigens. *Gene Ther* **2000,** *7* (9), 750-8.
78. Rodriguez-Crespo, I.; Gomez-Gutierrez, J.; Nieto, M.; Peterson, D. L.; Gavilanes, F., Prediction of a putative fusion peptide in the S protein of hepatitis B virus. *J Gen Virol* **1994,** *75 (Pt 3)*, 637-9.
79. Delgado, C. L.; Nunez, E.; Yelamos, B.; Gomez-Gutierrez, J.; Peterson, D. L.; Gavilanes, F., Study of the putative fusion regions of the preS domain of hepatitis B virus. *Biochim Biophys Acta* **2015,** *1848* (4), 895-906.
80. Sun, S.; Yan, J.; Xia, C.; Lin, Y.; Jiang, X.; Liu, H.; Ren, H.; Yan, J.; Lin, J.; He, X., Visualizing hepatitis B virus with biarsenical labelling in living cells. *Liver Int* **2014,** *34* (10), 1532-42.
81. Rabe, B.; Glebe, D.; Kann, M., Lipid-mediated introduction of hepatitis B virus capsids into nonsusceptible cells allows highly efficient replication and facilitates the study of early infection events. *J Virol* **2006,** *80* (11), 5465-73.
82. Rabe, B.; Vlachou, A.; Pante, N.; Helenius, A.; Kann, M., Nuclear import of hepatitis B virus capsids and release of the viral genome. *Proc Natl Acad Sci U S A* **2003,** *100* (17), 9849-54.
83. Gallucci, L.; Kann, M., Nuclear Import of Hepatitis B Virus Capsids and Genome. *Viruses* **2017,** *9* (1).
84. Lupberger, J.; Schaedler, S.; Peiran, A.; Hildt, E., Identification and characterization of a novel bipartite nuclear localization signal in the hepatitis B virus polymerase. *World J Gastroenterol* **2013,** *19* (44), 8000-10.
85. Cao, F.; Tavis, J. E., Detection and characterization of cytoplasmic hepatitis B virus reverse transcriptase. *J Gen Virol* **2004,** *85* (Pt 11), 3353-60.
86. Yao, E.; Gong, Y.; Chen, N.; Tavis, J. E., The majority of duck hepatitis B virus reverse transcriptase in cells is nonencapsidated and is bound to a cytoplasmic structure. *J Virol* **2000,** *74* (18), 8648-57.
87. Guo, H.; Jiang, D.; Zhou, T.; Cuconati, A.; Block, T. M.; Guo, J. T., Characterization of the intracellular deproteinized relaxed circular DNA of hepatitis B virus: an intermediate of covalently closed circular DNA formation. *J Virol* **2007,** *81* (22), 12472-84.
88. Guo, H.; Mao, R.; Block, T. M.; Guo, J. T., Production and function of the cytoplasmic deproteinized relaxed circular DNA of hepadnaviruses. *J Virol* **2010,** *84* (1), 387-96.
89. Lien, J. M.; Aldrich, C. E.; Mason, W. S., Evidence that a capped oligoribonucleotide is the primer for duck hepatitis B virus plus-strand DNA synthesis. *J Virol* **1986,** *57* (1), 229-36.
90. Sohn, J. A.; Litwin, S.; Seeger, C., Mechanism for CCC DNA synthesis in hepadnaviruses. *PLoS One* **2009,** *4* (11), e8093.
91. Yang, W.; Summers, J., Illegitimate replication of linear hepadnavirus DNA through nonhomologous recombination. *J Virol* **1995,** *69* (7), 4029-36.
92. Guo, J. T.; Guo, H., Metabolism and function of hepatitis B virus cccDNA: Implications for the development of cccDNA-targeting antiviral therapeutics. *Antiviral Res* **2015,** *122*, 91-100.
93. Long, Q.; Yan, R.; Hu, J.; Cai, D.; Mitra, B.; Kim, E. S.; Marchetti, A.; Zhang, H.; Wang, S.; Liu, Y.; Huang, A.; Guo, H., The role of host DNA ligases in hepadnavirus covalently closed circular DNA formation. *PLoS Pathog* **2017,** *13* (12), e1006784.
94. Bock, C. T.; Schranz, P.; Schroder, C. H.; Zentgraf, H., Hepatitis B virus genome is organized into nucleosomes in the nucleus of the infected cell. *Virus Genes* **1994,** *8* (3), 215-29.
95. Newbold, J. E.; Xin, H.; Tencza, M.; Sherman, G.; Dean, J.; Bowden, S.; Locarnini, S., The covalently closed duplex form of the hepadnavirus genome exists in situ as a heterogeneous population of viral minichromosomes. *J Virol* **1995,** *69* (6), 3350-7.
96. Cho, E. Y.; Kim, H. J.; Park, C.; So, H. S.; Park, R. K.; Kim, H. C., Impact of Nucleotide Mutations at the HNF3- and HNF4-Binding Sites in Enhancer 1 on Viral Replication in Patients with Chronic Hepatitis B Virus Infection. *Gut and liver* **2013,** *7* (5), 569-75.

97. Shi, L.; Li, S.; Shen, F.; Li, H.; Qian, S.; Lee, D. H.; Wu, J. Z.; Yang, W., Characterization of nucleosome positioning in hepadnaviral covalently closed circular DNA minichromosomes. *J Virol* **2012,** *86* (18), 10059-69.
98. Pollicino, T.; Belloni, L.; Raffa, G.; Pediconi, N.; Squadrito, G.; Raimondo, G.; Levrero, M., Hepatitis B virus replication is regulated by the acetylation status of hepatitis B virus cccDNA-bound H3 and H4 histones. *Gastroenterology* **2006,** *130* (3), 823-37.
99. Belloni, L.; Pollicino, T.; De Nicola, F.; Guerrieri, F.; Raffa, G.; Fanciulli, M.; Raimondo, G.; Levrero, M., Nuclear HBx binds the HBV minichromosome and modifies the epigenetic regulation of cccDNA function. *Proc Natl Acad Sci U S A* **2009,** *106* (47), 19975-9.
100. Bock, C. T.; Schwinn, S.; Locarnini, S.; Fyfe, J.; Manns, M. P.; Trautwein, C.; Zentgraf, H., Structural organization of the hepatitis B virus minichromosome. *J Mol Biol* **2001,** *307* (1), 183-96.
101. Guo, Y. H.; Li, Y. N.; Zhao, J. R.; Zhang, J.; Yan, Z., HBc binds to the CpG islands of HBV cccDNA and promotes an epigenetic permissive state. *Epigenetics* **2011,** *6* (6), 720-6.
102. Lucifora, J.; Xia, Y.; Reisinger, F.; Zhang, K.; Stadler, D.; Cheng, X.; Sprinzl, M. F.; Koppensteiner, H.; Makowska, Z.; Volz, T.; Remouchamps, C.; Chou, W. M.; Thasler, W. E.; Huser, N.; Durantel, D.; Liang, T. J.; Munk, C.; Heim, M. H.; Browning, J. L.; Dejardin, E.; Dandri, M.; Schindler, M.; Heikenwalder, M.; Protzer, U., Specific and nonhepatotoxic degradation of nuclear hepatitis B virus cccDNA. *Science* **2014,** *343* (6176), 1221-8.
103. Bourne, C. R.; Katen, S. P.; Fulz, M. R.; Packianathan, C.; Zlotnick, A., A mutant hepatitis B virus core protein mimics inhibitors of icosahedral capsid self-assembly. *Biochemistry* **2009,** *48* (8), 1736-42.
104. Zlotnick, A.; Tan, Z.; Selzer, L., One protein, at least three structures, and many functions. *Structure (London, England : 1993)* **2013,** *21* (1), 6-8.
105. Melegari, M.; Wolf, S. K.; Schneider, R. J., Hepatitis B virus DNA replication is coordinated by core protein serine phosphorylation and HBx expression. *J Virol* **2005,** *79* (15), 9810-20.
106. Gazina, E. V.; Fielding, J. E.; Lin, B.; Anderson, D. A., Core Protein Phosphorylation Modulates Pregenomic RNA Encapsidation to Different Extents in Human and Duck Hepatitis B Viruses. *Journal of Virology* **2000,** *74* (10), 4721-4728.
107. Blondot, M. L.; Bruss, V.; Kann, M., Intracellular transport and egress of hepatitis B virus. *J Hepatol* **2016,** *64* (1 Suppl), S49-59.
108. Ning, X.; Nguyen, D.; Mentzer, L.; Adams, C.; Lee, H.; Ashley, R.; Hafenstein, S.; Hu, J., Secretion of genome-free hepatitis B virus--single strand blocking model for virion morphogenesis of para-retrovirus. *PLoS Pathog* **2011,** *7* (9), e1002255.
109. Ning, X.; Luckenbaugh, L.; Liu, K.; Bruss, V.; Sureau, C.; Hu, J., Common and Distinct Capsid and Surface Protein Requirements for Secretion of Complete and Genome-Free Hepatitis B Virions. *Journal of virology* **2018,** *92* (14), e00272-18.
110. Short, J. M.; Chen, S.; Roseman, A. M.; Butler, P. J.; Crowther, R. A., Structure of hepatitis B surface antigen from subviral tubes determined by electron cryomicroscopy. *J Mol Biol* **2009,** *390* (1), 135-41.
111. Hepatitis B surface antigen assembles in a post-ER, pre-Golgi compartment. *The Journal of Cell Biology* **1992,** *118* (6), 1305-1320.
112. Huovila, A. P.; Eder, A. M.; Fuller, S. D., Hepatitis B surface antigen assembles in a post-ER, pre-Golgi compartment. *J Cell Biol* **1992,** *118* (6), 1305-20.
113. Abdulkarim, A. S.; Cao, H.; Huang, B.; McNiven, M. A., The large GTPase dynamin is required for hepatitis B virus protein secretion from hepatocytes. *J Hepatol* **2003,** *38* (1), 76-83.
114. Lu, X.; Mehta, A.; Dwek, R.; Butters, T.; Block, T., Evidence That N-Linked Glycosylation Is Necessary for Hepatitis B Virus Secretion. *Virology* **1995,** *213* (2), 660-665.
115. Selzer, L.; Zlotnick, A., Assembly and Release of Hepatitis B Virus. *Cold Spring Harbor perspectives in medicine* **2015,** *5* (12), a021394.

116. Rost, M.; Mann, S.; Lambert, C.; Doring, T.; Thome, N.; Prange, R., Gamma-adaptin, a novel ubiquitin-interacting adaptor, and Nedd4 ubiquitin ligase control hepatitis B virus maturation. *J Biol Chem* **2006,** *281* (39), 29297-308.
117. Boehm, M.; Bonifacino, J. S., Adaptins: the final recount. *Mol Biol Cell* **2001,** *12* (10), 2907-20.
118. Stieler, J. T.; Prange, R., Involvement of ESCRT-II in hepatitis B virus morphogenesis. *PLoS One* **2014,** *9* (3), e91279.
119. Prange, R., Host factors involved in hepatitis B virus maturation, assembly, and egress. *Medical Microbiology and Immunology* **2012,** *201* (4), 449-461.
120. Lambert, C.; Doring, T.; Prange, R., Hepatitis B virus maturation is sensitive to functional inhibition of ESCRT-III, Vps4, and gamma 2-adaptin. *J Virol* **2007,** *81* (17), 9050-60.
121. Watanabe, T.; Sorensen, E. M.; Naito, A.; Schott, M.; Kim, S.; Ahlquist, P., Involvement of host cellular multivesicular body functions in hepatitis B virus budding. *Proc Natl Acad Sci U S A* **2007,** *104* (24), 10205-10.
122. Roingeard, P.; Sureau, C., Ultrastructural analysis of hepatitis B virus in HepG2-transfected cells with special emphasis on subviral filament morphogenesis. *Hepatology* **1998,** *28* (4), 1128-33.
123. Li, J.; Liu, Y.; Wang, Z.; Liu, K.; Wang, Y.; Liu, J.; Ding, H.; Yuan, Z., Subversion of cellular autophagy machinery by hepatitis B virus for viral envelopment. *J Virol* **2011,** *85* (13), 6319-33.
124. Wieland, S. F., The chimpanzee model for hepatitis B virus infection. *Cold Spring Harb Perspect Med* **2015,** *5* (6).
125. Dunn, C.; Peppa, D.; Khanna, P.; Nebbia, G.; Jones, M.; Brendish, N.; Lascar, R. M.; Brown, D.; Gilson, R. J.; Tedder, R. J.; Dusheiko, G. M.; Jacobs, M.; Klenerman, P.; Maini, M. K., Temporal analysis of early immune responses in patients with acute hepatitis B virus infection. *Gastroenterology* **2009,** *137* (4), 1289-300.
126. Wooddell, C. I.; Yuen, M. F.; Chan, H. L.; Gish, R. G.; Locarnini, S. A.; Chavez, D.; Ferrari, C.; Given, B. D.; Hamilton, J.; Kanner, S. B.; Lai, C. L.; Lau, J. Y. N.; Schluep, T.; Xu, Z.; Lanford, R. E.; Lewis, D. L., RNAi-based treatment of chronically infected patients and chimpanzees reveals that integrated hepatitis B virus DNA is a source of HBsAg. *Science translational medicine* **2017,** *9* (409).
127. Petersen, J.; Thompson, A. J.; Levrero, M., Aiming for cure in HBV and HDV infection. *J Hepatol* **2016,** *65* (4), 835-848.
128. von Weizsacker, F.; Kock, J.; MacNelly, S.; Ren, S.; Blum, H. E.; Nassal, M., The tupaia model for the study of hepatitis B virus: direct infection and HBV genome transduction of primary tupaia hepatocytes. *Methods in molecular medicine* **2004,** *96*, 153-61.
129. Baumert, T. F.; Yang, C.; Schurmann, P.; Kock, J.; Ziegler, C.; Grullich, C.; Nassal, M.; Liang, T. J.; Blum, H. E.; von Weizsacker, F., Hepatitis B virus mutations associated with fulminant hepatitis induce apoptosis in primary Tupaia hepatocytes. *Hepatology* **2005,** *41* (2), 247-56.
130. Yan, R. Q.; Su, J. J.; Huang, D. R.; Gan, Y. C.; Yang, C.; Huang, G. H., Human hepatitis B virus and hepatocellular carcinoma. II. Experimental induction of hepatocellular carcinoma in tree shrews exposed to hepatitis B virus and aflatoxin B1. *Journal of cancer research and clinical oncology* **1996,** *122* (5), 289-95.
131. Chisari, F. V.; Pinkert, C. A.; Milich, D. R.; Filippi, P.; McLachlan, A.; Palmiter, R. D.; Brinster, R. L., A transgenic mouse model of the chronic hepatitis B surface antigen carrier state. *Science* **1985,** *230* (4730), 1157-60.
132. Kim, C. M.; Koike, K.; Saito, I.; Miyamura, T.; Jay, G., HBx gene of hepatitis B virus induces liver cancer in transgenic mice. *Nature* **1991,** *351* (6324), 317-20.
133. Milich, D. R.; Jones, J. E.; Hughes, J. L.; Price, J.; Raney, A. K.; McLachlan, A., Is a function of the secreted hepatitis B e antigen to induce immunologic tolerance in utero? *Proc Natl Acad Sci U S A* **1990,** *87* (17), 6599-603.

134. Guidotti, L. G.; Matzke, B.; Schaller, H.; Chisari, F. V., High-level hepatitis B virus replication in transgenic mice. *J Virol* **1995,** *69* (10), 6158-69.
135. Protzer, U., Viral hepatitis: The bumpy road to animal models for HBV infection. *Nature reviews. Gastroenterology & hepatology* **2017,** *14* (6), 327-328.
136. Allweiss, L.; Dandri, M., Experimental in vitro and in vivo models for the study of human hepatitis B virus infection. *J Hepatol* **2016,** *64* (1 Suppl), S17-s31.
137. Mingozzi, F.; Liu, Y. L.; Dobrzynski, E.; Kaufhold, A.; Liu, J. H.; Wang, Y.; Arruda, V. R.; High, K. A.; Herzog, R. W., Induction of immune tolerance to coagulation factor IX antigen by in vivo hepatic gene transfer. *J Clin Invest* **2003,** *111* (9), 1347-56.
138. Dion, S.; Bourgine, M.; Godon, O.; Levillayer, F.; Michel, M. L., Adeno-associated virus-mediated gene transfer leads to persistent hepatitis B virus replication in mice expressing HLA-A2 and HLA-DR1 molecules. *J Virol* **2013,** *87* (10), 5554-63.
139. Lutgehetmann, M.; Bornscheuer, T.; Volz, T.; Allweiss, L.; Bockmann, J. H.; Pollok, J. M.; Lohse, A. W.; Petersen, J.; Dandri, M., Hepatitis B virus limits response of human hepatocytes to interferon-alpha in chimeric mice. *Gastroenterology* **2011,** *140* (7), 2074-83, 2083.e1-2.
140. Azuma, H.; Paulk, N.; Ranade, A.; Dorrell, C.; Al-Dhalimy, M.; Ellis, E.; Strom, S.; Kay, M. A.; Finegold, M.; Grompe, M., Robust expansion of human hepatocytes in Fah-/-/Rag2-/-/Il2rg-/- mice. *Nat Biotechnol* **2007,** *25* (8), 903-10.
141. Sun, S.; Li, J., Humanized chimeric mouse models of hepatitis B virus infection. *International journal of infectious diseases : IJID : official publication of the International Society for Infectious Diseases* **2017,** *59*, 131-136.
142. Erhardt, A.; Blondin, D.; Hauck, K.; Sagir, A.; Kohnle, T.; Heintges, T.; Haussinger, D., Response to interferon alfa is hepatitis B virus genotype dependent: genotype A is more sensitive to interferon than genotype D. *Gut* **2005,** *54* (7), 1009-13.
143. Flink, H. J.; van Zonneveld, M.; Hansen, B. E.; de Man, R. A.; Schalm, S. W.; Janssen, H. L., Treatment with Peg-interferon alpha-2b for HBeAg-positive chronic hepatitis B: HBsAg loss is associated with HBV genotype. *The American journal of gastroenterology* **2006,** *101* (2), 297-303.
144. Wiegand, J.; Hasenclever, D.; Tillmann, H. L., Should treatment of hepatitis B depend on hepatitis B virus genotypes? A hypothesis generated from an explorative analysis of published evidence. *Antivir Ther* **2008,** *13* (2), 211-20.
145. Kim, S. S.; Cheong, J. Y.; Cho, S. W., Current Nucleos(t)ide Analogue Therapy for Chronic Hepatitis B. *Gut and liver* **2011,** *5* (3), 278-287.
146. Lee, J. M.; Park, J. Y.; Kim, D. Y.; Nguyen, T.; Hong, S. P.; Kim, S. O.; Chon, C. Y.; Han, K. H.; Ahn, S. H., Long-term adefovir dipivoxil monotherapy for up to 5 years in lamivudine-resistant chronic hepatitis B. *Antivir Ther* **2010,** *15* (2), 235-41.
147. Chang, T. T.; Gish, R. G.; Hadziyannis, S. J.; Cianciara, J.; Rizzetto, M.; Schiff, E. R.; Pastore, G.; Bacon, B. R.; Poynard, T.; Joshi, S.; Klesczewski, K. S.; Thiry, A.; Rose, R. E.; Colonno, R. J.; Hindes, R. G., A dose-ranging study of the efficacy and tolerability of entecavir in Lamivudine-refractory chronic hepatitis B patients. *Gastroenterology* **2005,** *129* (4), 1198-209.
148. Lai, C. L.; Gane, E.; Liaw, Y. F.; Hsu, C. W.; Thongsawat, S.; Wang, Y.; Chen, Y.; Heathcote, E. J.; Rasenack, J.; Bzowej, N.; Naoumov, N. V.; Di Bisceglie, A. M.; Zeuzem, S.; Moon, Y. M.; Goodman, Z.; Chao, G.; Constance, B. F.; Brown, N. A., Telbivudine versus lamivudine in patients with chronic hepatitis B. *N Engl J Med* **2007,** *357* (25), 2576-88.
149. Marcellin, P.; Heathcote, E. J.; Buti, M.; Gane, E.; de Man, R. A.; Krastev, Z.; Germanidis, G.; Lee, S. S.; Flisiak, R.; Kaita, K.; Manns, M.; Kotzev, I.; Tchernev, K.; Buggisch, P.; Weilert, F.; Kurdas, O. O.; Shiffman, M. L.; Trinh, H.; Washington, M. K.; Sorbel, J.; Anderson, J.; Snow-Lampart, A.; Mondou, E.; Quinn, J.; Rousseau, F., Tenofovir disoproxil fumarate versus adefovir dipivoxil for chronic hepatitis B. *N Engl J Med* **2008,** *359* (23), 2442-55.

150. Revill, P.; Locarnini, S., Antiviral strategies to eliminate hepatitis B virus covalently closed circular DNA (cccDNA). *Current opinion in pharmacology* **2016,** *30*, 144-150.
151. Tang, L.; Zhao, Q.; Wu, S.; Cheng, J.; Chang, J.; Guo, J. T., The current status and future directions of hepatitis B antiviral drug discovery. *Expert opinion on drug discovery* **2017,** *12* (1), 5-15.
152. Gehring, A. J.; Protzer, U., Targeting Innate and Adaptive Immune Responses to Cure Chronic HBV Infection. *Gastroenterology* **2019,** *156* (2), 325-337.
153. Soriano, V.; Barreiro, P.; Benitez, L.; Pena, J. M.; de Mendoza, C., New antivirals for the treatment of chronic hepatitis B. *Expert opinion on investigational drugs* **2017,** *26* (7), 843-851.
154. Revill, P.; Testoni, B.; Locarnini, S.; Zoulim, F., Global strategies are required to cure and eliminate HBV infection. *Nature reviews. Gastroenterology & hepatology* **2016,** *13* (4), 239-48.
155. Shevtsov, M.; Zhao, L.; Protzer, U.; Klundert, M., Applicability of Metal Nanoparticles in the Detection and Monitoring of Hepatitis B Virus Infection. *Viruses* **2017,** *9* (7), 193.
156. Lobaina, Y.; Michel, M. L., Chronic hepatitis B: Immunological profile and current therapeutic vaccines in clinical trials. *Vaccine* **2017,** *35* (18), 2308-2314.
157. Chen, G. F.; Wang, C.; Lau, G., Treatment of chronic hepatitis B infection-2017. *Liver Int* **2017,** *37 Suppl 1*, 59-66.
158. Debarry, J.; Cornberg, M.; Manns, M. P., Challenges in warranting access to prophylaxis and therapy for hepatitis B virus infection. *Liver Int* **2017,** *37 Suppl 1*, 67-72.
159. Krajden, M.; McNabb, G.; Petric, M., The laboratory diagnosis of hepatitis B virus. *Can J Infect Dis Med Microbiol* **2005,** *16* (2), 65-72.
160. Yu, W.; Goddard, C.; Clearfield, E.; Mills, C.; Xiao, T.; Guo, H.; Morrey, J. D.; Motter, N. E.; Zhao, K.; Block, T. M.; Cuconati, A.; Xu, X., Design, synthesis, and biological evaluation of triazolo-pyrimidine derivatives as novel inhibitors of hepatitis B virus surface antigen (HBsAg) secretion. *J Med Chem* **2011,** *54* (16), 5660-70.
161. Zhou, L.; Ding, L.; Yin, P.; Lu, X.; Wang, X.; Niu, J.; Gao, P.; Xu, G., Serum metabolic profiling study of hepatocellular carcinoma infected with hepatitis B or hepatitis C virus by using liquid chromatography-mass spectrometry. *J Proteome Res* **2012,** *11* (11), 5433-42.
162. Zhou, K.; Li, L.; Tan, Z.; Zlotnick, A.; Jacobson, S. C., Characterization of hepatitis B virus capsids by resistive-pulse sensing. *J Am Chem Soc* **2011,** *133* (6), 1618-21.
163. Abe, A.; Inoue, K.; Tanaka, T.; Kato, J.; Kajiyama, N.; Kawaguchi, R.; Tanaka, S.; Yoshiba, M.; Kohara, M., Quantitation of hepatitis B virus genomic DNA by real-time detection PCR. *J Clin Microbiol* **1999,** *37* (9), 2899-903.
164. Reddy, L. H.; Couvreur, P., Nanotechnology for therapy and imaging of liver diseases. *J Hepatol* **2011,** *55* (6), 1461-6.
165. Shingyoji, M.; Gerion, D.; Pinkel, D.; Gray, J. W.; Chen, F., Quantum dots-based reverse phase protein microarray. *Talanta* **2005,** *67* (3), 472-8.
166. Ghosh, S.; Sood, A. K.; Kumar, N., Carbon nanotube flow sensors. *Science* **2003,** *299* (5609), 1042-4.
167. Zheng, G.; Patolsky, F.; Cui, Y.; Wang, W. U.; Lieber, C. M., Multiplexed electrical detection of cancer markers with nanowire sensor arrays. *Nat Biotechnol* **2005,** *23* (10), 1294-301.
168. Baselt, D. R.; Lee, G. U.; Natesan, M.; Metzger, S. W.; Sheehan, P. E.; Colton, R. J., A biosensor based on magnetoresistance technology. *Biosens Bioelectron* **1998,** *13* (7-8), 731-9.
169. Li, G.; Sun, S.; Wilson, R. J.; White, R. L.; Pourmand, N.; Wang, S. X., Spin valve sensors for ultrasensitive detection of superparamagnetic nanoparticles for biological applications. *Sens Actuators A Phys* **2006,** *126* (1), 98-106.
170. Millen, R. L.; Kawaguchi, T.; Granger, M. C.; Porter, M. D.; Tondra, M., Giant magnetoresistive sensors and superparamagnetic nanoparticles: a chip-scale detection strategy for immunosorbent assays. *Anal Chem* **2005,** *77* (20), 6581-7.

171. Li, Y.; Schluesener, H. J.; Xu, S., Gold nanoparticle-based biosensors. *Gold Bulletin* **2010,** *43* (1), 29-41.
172. Saha, K.; Agasti, S. S.; Kim, C.; Li, X.; Rotello, V. M., Gold nanoparticles in chemical and biological sensing. *Chem Rev* **2012,** *112* (5), 2739-79.
173. Horisberger, M.; Rosset, J., Colloidal gold, a useful marker for transmission and scanning electron microscopy. *Journal of Histochemistry & Cytochemistry* **1977,** *25* (4), 295-305.
174. van den Berg, L. M.; Ribeiro, C. M. S.; Zijlstra-Willems, E. M.; de Witte, L.; Fluitsma, D.; Tigchelaar, W.; Everts, V.; Geijtenbeek, T. B. H., Caveolin-1 mediated uptake via langerin restricts HIV-1 infection in human Langerhans cells. *Retrovirology* **2014,** *11* (1), 123.
175. Cordeiro, M.; Ferreira Carlos, F.; Pedrosa, P.; Lopez, A.; Baptista, P., Gold Nanoparticles for Diagnostics: Advances towards Points of Care. *Diagnostics* **2016,** *6* (4), 43.
176. Wu, Y.; Guo, W.; Peng, W.; Zhao, Q.; Piao, J.; Zhang, B.; Wu, X.; Wang, H.; Gong, X.; Chang, J., Enhanced Fluorescence ELISA Based on HAT Triggering Fluorescence "Turn-on" with Enzyme-Antibody Dual Labeled AuNP Probes for Ultrasensitive Detection of AFP and HBsAg. *ACS Appl Mater Interfaces* **2017,** *9* (11), 9369-9377.
177. Kelly, K. L.; Coronado, E.; Zhao, L. L.; Schatz, G. C., The Optical Properties of Metal Nanoparticles: The Influence of Size, Shape, and Dielectric Environment. *The Journal of Physical Chemistry B* **2003,** *107* (3), 668-677.
178. Reynolds, R. A.; Mirkin, C. A.; Letsinger, R. L., Homogeneous, Nanoparticle-Based Quantitative Colorimetric Detection of Oligonucleotides. *Journal of the American Chemical Society* **2000,** *122* (15), 3795-3796.
179. Liu, J.; Lu, Y., Colorimetric Biosensors Based on DNAzyme-Assembled Gold Nanoparticles. *Journal of Fluorescence* **2004,** *14* (4), 343-354.
180. Xu, W.; Xue, X.; Li, T.; Zeng, H.; Liu, X., Ultrasensitive and Selective Colorimetric DNA Detection by Nicking Endonuclease Assisted Nanoparticle Amplification. *Angewandte Chemie* **2009,** *121* (37), 6981-6984.
181. Wang, X.; Li, Y.; Wang, H.; Fu, Q.; Peng, J.; Wang, Y.; Du, J.; Zhou, Y.; Zhan, L., Gold nanorod-based localized surface plasmon resonance biosensor for sensitive detection of hepatitis B virus in buffer, blood serum and plasma. *Biosensors and Bioelectronics* **2010,** *26* (2), 404-410.
182. Bernacka-Wojcik, I.; Senadeera, R.; Wojcik, P. J.; Silva, L. B.; Doria, G.; Baptista, P.; Aguas, H.; Fortunato, E.; Martins, R., Inkjet printed and “doctor blade” TiO2 photodetectors for DNA biosensors. *Biosensors and Bioelectronics* **2010,** *25* (5), 1229-1234.
183. Veigas, B.; Pedrosa, P.; Carlos, F. F.; Mancio-Silva, L.; Grosso, A. R.; Fortunato, E.; Mota, M. M.; Baptista, P. V., One nanoprobe, two pathogens: gold nanoprobes multiplexing for point-of-care. *Journal of Nanobiotechnology* **2015,** *13* (1), 48.
184. Duan, L.; Wang, Y.; Li, S. S.-c.; Wan, Z.; Zhai, J., Rapid and simultaneous detection of human hepatitis B virus and hepatitis C virus antibodies based on a protein chip assay using nano-gold immunological amplification and silver staining method. *BMC Infectious Diseases* **2005,** *5* (1), 53.
185. Jia-Wu Song, Z. X., Lan Yao, Xiao-Feng Li, Jian-Xi Tang, Xiao-Jun Zhou, Bo Wu, Development of clinical highly sensitive biosensor-based microarray system. *World chinese journal of digestology* **2008,** *15*, 1628-1633.
186. Jang, K.-J.; Lee, H.; Jin, H.-L.; Park, Y.; Nam, J.-M., Restriction-Enzyme-Coded Gold-Nanoparticle Probes for Multiplexed DNA Detection. *Small* **2009,** *5* (23), 2665-2668.
187. Pingarrón, J. M.; Yáñez-Sedeño, P.; González-Cortés, A., Gold nanoparticle-based electrochemical biosensors. *Electrochimica Acta* **2008,** *53* (19), 5848-5866.
188. Pänke, O.; Kirbs, A.; Lisdat, F., Voltammetric detection of single base-pair mismatches and quantification of label-free target ssDNA using a competitive binding assay. *Biosensors and Bioelectronics* **2007,** *22* (11), 2656-2662.

189. Li, F.; Feng, Y.; Dong, P.; Tang, B., Gold nanoparticles modified electrode via a mercapto-diazoaminobenzene monolayer and its development in DNA electrochemical biosensor. *Biosensors and Bioelectronics* **2010,** *25* (9), 2084-2088.
190. Chen, C.-C.; Lai, Z.-L.; Wang, G.-J.; Wu, C.-Y., Polymerase chain reaction-free detection of hepatitis B virus DNA using a nanostructured impedance biosensor. *Biosensors and Bioelectronics* **2016,** *77*, 603-608.
191. Shourian, M.; Ghourchian, H.; Boutorabi, M., Ultra-sensitive immunosensor for detection of hepatitis B surface antigen using multi-functionalized gold nanoparticles. *Analytica Chimica Acta* **2015,** *895*, 1-11.
192. Wang, J.; Li, J.; Baca, A. J.; Hu, J.; Zhou, F.; Yan, W.; Pang, D.-W., Amplified Voltammetric Detection of DNA Hybridization via Oxidation of Ferrocene Caps on Gold Nanoparticle/Streptavidin Conjugates. *Analytical Chemistry* **2003,** *75* (15), 3941-3945.
193. Tang, D.; Yuan, R.; Chai, Y.; Zhong, X.; Liu, Y.; Dai, J., Electrochemical detection of hepatitis B surface antigen using colloidal gold nanoparticles modified by a sol–gel network interface. *Clinical Biochemistry* **2006,** *39* (3), 309-314.
194. Tang, D.; Li, H.; Liao, J., Ionic liquid and nanogold-modified immunosensing interface for electrochemical immunoassay of hepatitis B surface antigen in human serum. *Microfluidics and Nanofluidics* **2008,** *6* (3), 403.
195. Fu, Y.-Z.; Yuan, R.; Chai, Y.-Q., Reagentless Immunosensing Assay via Electrochemical Impedance for Hepatitis B Surface Antigen Monitoring Based on Polypyrrole and Gold Nanoparticles as Matrices. *Chinese Journal of Chemistry* **2006,** *24* (1), 59-64.
196. Tang, D. P.; Yuan, R.; Chai, Y. Q.; Zhong, X.; Liu, Y.; Dai, J. Y.; Zhang, L. Y., Novel potentiometric immunosensor for hepatitis B surface antigen using a gold nanoparticle-based biomolecular immobilization method. *Analytical Biochemistry* **2004,** *333* (2), 345-350.
197. Zhuo, Y.; Yuan, R.; Chai, Y.; Zhang, Y.; Li, X. l.; Zhu, Q.; Wang, N., An amperometric immunosensor based on immobilization of hepatitis B surface antibody on gold electrode modified gold nanoparticles and horseradish peroxidase. *Analytica Chimica Acta* **2005,** *548* (1), 205-210.
198. Hu, J.; Wang, L.; Li, F.; Han, Y. L.; Lin, M.; Lu, T. J.; Xu, F., Oligonucleotide-linked gold nanoparticle aggregates for enhanced sensitivity in lateral flow assays. *Lab on a Chip* **2013,** *13* (22), 4352-4357.
199. Kim, D.; Kim, Y.; Hong, S.; Kim, J.; Heo, N.; Lee, M.-K.; Lee, S.; Kim, B.; Kim, I.; Huh, Y.; Choi, B., Development of Lateral Flow Assay Based on Size-Controlled Gold Nanoparticles for Detection of Hepatitis B Surface Antigen. *Sensors* **2016,** *16* (12), 2154.
200. Nie, S.; Emory, S. R., Probing Single Molecules and Single Nanoparticles by Surface-Enhanced Raman Scattering. *Science* **1997,** *275* (5303), 1102-1106.
201. Kamińska, A.; Witkowska, E.; Winkler, K.; Dzięcielewski, I.; Weyher, J. L.; Waluk, J., Detection of Hepatitis B virus antigen from human blood: SERS immunoassay in a microfluidic system. *Biosensors and Bioelectronics* **2015,** *66*, 461-467.
202. Tamanaha, C. R.; Mulvaney, S. P.; Rife, J. C.; Whitman, L. J., Magnetic labeling, detection, and system integration. *Biosensors and Bioelectronics* **2008,** *24* (1), 1-13.
203. Shevtsov, M.; Multhoff, G., Recent Developments of Magnetic Nanoparticles for Theranostics of Brain Tumor. *Curr Drug Metab* **2016,** *17* (8), 737-744.
204. Petri-Fink, A.; Hofmann, H., Superparamagnetic iron oxide nanoparticles (SPIONs): from synthesis to in vivo studies - A summary of the synthesis, characterization, in vitro and in vivo investigations of SPIONs with particular focus on surface and colloidal properties. *IEEE Transactions on Nanobioscience* **2007,** *6* (4), 289-953.
205. Rocha-Santos, T. A. P., Sensors and biosensors based on magnetic nanoparticles. *TrAC Trends in Analytical Chemistry* **2014,** *62*, 28-36.

206. Xu, Y.; Wang, E., Electrochemical biosensors based on magnetic micro/nano particles. *Electrochimica Acta* **2012,** *84*, 62-73.
207. Jaffrezic-Renault, N.; Martelet, C.; Chevolot, Y.; Cloarec, J.-P., Biosensors and Bio-Bar Code Assays Based on Biofunctionalized Magnetic Microbeads. *Sensors* **2007,** *7* (4), 589.
208. Hsing, I. M.; Xu, Y.; Zhao, W., Micro- and Nano- Magnetic Particles for Applications in Biosensing. *Electroanalysis* **2007,** *19* (7-8), 755-768.
209. Haun, J. B.; Yoon, T.-J.; Lee, H.; Weissleder, R., Magnetic nanoparticle biosensors. *Wiley Interdisciplinary Reviews: Nanomedicine and Nanobiotechnology* **2010,** *2* (3), 291-304.
210. Tassa, C.; Shaw, S. Y.; Weissleder, R., Dextran-Coated Iron Oxide Nanoparticles: A Versatile Platform for Targeted Molecular Imaging, Molecular Diagnostics, and Therapy. *Accounts of Chemical Research* **2011,** *44* (10), 842-852.
211. Faraji, M.; Yamini, Y.; Rezaee, M., ChemInform Abstract: Magnetic Nanoparticles: Synthesis, Stabilization, Functionalization, Characterization, and Applications. *ChemInform* **2010,** *41* (50), no-no.
212. Xi, Z.; Huang, R.; Li, Z.; He, N.; Wang, T.; Su, E.; Deng, Y., Selection of HBsAg-Specific DNA Aptamers Based on Carboxylated Magnetic Nanoparticles and Their Application in the Rapid and Simple Detection of Hepatitis B Virus Infection. *ACS Applied Materials & Interfaces* **2015,** *7* (21), 11215-11223.
213. Wang, W.; Ma, P.; Dong, H.; Krause, H.-J.; Zhang, Y.; Willbold, D.; Offenhaeusser, A.; Gu, Z., A magnetic nanoparticles relaxation sensor for protein–protein interaction detection at ultra-low magnetic field. *Biosensors and Bioelectronics* **2016,** *80*, 661-665.
214. Fatemi, K.; Ghourchian, H.; Ziaee, A.-A.; Samiei, S.; Hanaee, H., Paramagnetic nanoparticle-based detection of hepatitis B virus using cathodic stripping voltammetry. *Biotechnology and Applied Biochemistry* **2009,** *52* (3), 221-225.
215. Nourani, S.; Ghourchian, H.; Boutorabi, S. M., Magnetic nanoparticle-based immunosensor for electrochemical detection of hepatitis B surface antigen. *Analytical Biochemistry* **2013,** *441* (1), 1-7.
216. Vaculovicova, M.; Smerkova, K.; Sedlacek, J.; Vyslouzil, J.; Hubalek, J.; Kizek, R.; Adam, V., Integrated chip electrophoresis and magnetic particle isolation used for detection of hepatitis B virus oligonucleotides. *ELECTROPHORESIS* **2013,** *34* (11), 1548-1554.
217. Nägele, E.; Moritz, R., Structure elucidation of degradation products of the antibiotic amoxicillin with ion trap MSn and accurate mass determination by ESI TOF. *Journal of the American Society for Mass Spectrometry* **2005,** *16* (10), 1670-1676.
218. Hassen, W. M.; Chaix, C.; Abdelghani, A.; Bessueille, F.; Leonard, D.; Jaffrezic-Renault, N., An impedimetric DNA sensor based on functionalized magnetic nanoparticles for HIV and HBV detection. *Sensors and Actuators B: Chemical* **2008,** *134* (2), 755-760.
219. Zhang, X.; Jiang, L.; Zhang, C.; Li, D.; Wang, C.; Gao, F.; Cui, D., A Silicon Dioxide Modified Magnetic Nanoparticles–Labeled Lateral Flow Strips for HBs Antigen. *Journal of Biomedical Nanotechnology* **2011,** *7* (6), 776-781.
220. Eustis, S.; El-Sayed, M. A., Why gold nanoparticles are more precious than pretty gold: Noble metal surface plasmon resonance and its enhancement of the radiative and nonradiative properties of nanocrystals of different shapes. *Chemical Society Reviews* **2006,** *35* (3), 209-217.
221. Mashhadizadeh, M. H.; Talemi, R. P., Synergistic effect of magnetite and gold nanoparticles onto the response of a label-free impedimetric hepatitis B virus DNA biosensor. *Materials Science and Engineering: C* **2016,** *59*, 773-781.
222. Kato, D.; Oishi, M., Ultrasensitive Detection of DNA and RNA Based on Enzyme-Free Click Chemical Ligation Chain Reaction on Dispersed Gold Nanoparticles. *ACS Nano* **2014,** *8* (10), 9988-9997.
223. Alizadeh, N.; Hallaj, R.; Salimi, A., A highly sensitive electrochemical immunosensor for hepatitis B virus surface antigen detection based on Hemin/G-quadruplex horseradish peroxidase-mimicking DNAzyme-signal amplification. *Biosensors and Bioelectronics* **2017,** *94*, 184-192.

224. Shen, G.; Zhang, Y., Highly sensitive electrochemical stripping detection of hepatitis B surface antigen based on copper-enhanced gold nanoparticle tags and magnetic nanoparticles. *Analytica Chimica Acta* **2010,** *674* (1), 27-31.
225. Lok, A. S.; Zoulim, F.; Dusheiko, G.; Ghany, M. G., Hepatitis B cure: From discovery to regulatory approval. *Hepatology* **2017,** *66* (4), 1296-1313.
226. Nassal, M., HBV cccDNA: viral persistence reservoir and key obstacle for a cure of chronic hepatitis B. *Gut* **2015,** *64* (12), 1972-84.
227. Hoffmann, J.; Boehm, C.; Himmelsbach, K.; Donnerhak, C.; Roettger, H.; Weiss, T. S.; Ploen, D.; Hildt, E., Identification of alpha-taxilin as an essential factor for the life cycle of hepatitis B virus. *J Hepatol* **2013,** *59* (5), 934-41.
228. Jiang, B.; Himmelsbach, K.; Ren, H.; Boller, K.; Hildt, E., Subviral Hepatitis B Virus Filaments, like Infectious Viral Particles, Are Released via Multivesicular Bodies. *J Virol* **2015,** *90* (7), 3330-41.
229. Safaie, P.; Poongkunran, M.; Kuang, P. P.; Javaid, A.; Jacobs, C.; Pohlmann, R.; Nasser, I.; Lau, D. T., Intrahepatic distribution of hepatitis B virus antigens in patients with and without hepatocellular carcinoma. *World J Gastroenterol* **2016,** *22* (12), 3404-11.
230. Chu, C. M.; Liaw, Y. F., Membrane staining for hepatitis B surface antigen on hepatocytes: a sensitive and specific marker of active viral replication in hepatitis B. *J Clin Pathol* **1995,** *48* (5), 470-3.
231. Busachi, C. A.; Ray, M. B.; Desmet, V. J., An immunoperoxidase technique for demonstrating membrane localized HBsAg in paraffin sections of liver biopsies. *J Immunol Methods* **1978,** *19* (1), 95-9.
232. Safaie, P.; Poongkunran, M.; Kuang, P.-P.; Javaid, A.; Jacobs, C.; Pohlmann, R.; Nasser, I.; Lau, D. T. Y., Intrahepatic distribution of hepatitis B virus antigens in patients with and without hepatocellular carcinoma. *World Journal of Gastroenterology* **2016,** *22* (12), 3404-3411.
233. Shevtsov, M.; Zhao, L.; Protzer, U.; Klundert, M., Applicability of Metal Nanoparticles in the Detection and Monitoring of Hepatitis B Virus Infection. *Viruses* **2017,** *9* (7).
234. Golsaz Shirazi, F.; Mohammadi, H.; Amiri, M. M.; Singethan, K.; Xia, Y.; Bayat, A. A.; Bahadori, M.; Rabbani, H.; Jeddi-Tehrani, M.; Protzer, U.; Shokri, F., Monoclonal antibodies to various epitopes of hepatitis B surface antigen inhibit hepatitis B virus infection. *J Gastroenterol Hepatol* **2014,** *29* (5), 1083-91.
235. Golsaz-Shirazi, F.; Mohammadi, H.; Amiri, M. M.; Khoshnoodi, J.; Kardar, G. A.; Jeddi-Tehrani, M.; Shokri, F., Localization of immunodominant epitopes within the "a" determinant of hepatitis B surface antigen using monoclonal antibodies. *Arch Virol* **2016,** *161* (10), 2765-72.
236. Krebs, K.; Böttinger, N.; Huang, L. R.; Chmielewski, M.; Arzberger, S.; Gasteiger, G.; Jäger, C.; Schmitt, E.; Bohne, F.; Aichler, M.; Uckert, W.; Abken, H.; Heikenwalder, M.; Knolle, P.; Protzer, U., T Cells Expressing a Chimeric Antigen Receptor That Binds Hepatitis B Virus Envelope Proteins Control Virus Replication in Mice. *Gastroenterology* **2013,** *145* (2), 456-465.
237. Bohne, F.; Chmielewski, M.; Ebert, G.; Wiegmann, K.; Kürschner, T.; Schulze, A.; Urban, S.; Krönke, M.; Abken, H.; Protzer, U., T Cells Redirected Against Hepatitis B Virus Surface Proteins Eliminate Infected Hepatocytes. *Gastroenterology* **2008,** *134* (1), 239-247.
238. Norder, H.; Courouce, A. M.; Coursaget, P.; Echevarria, J. M.; Lee, S. D.; Mushahwar, I. K.; Robertson, B. H.; Locarnini, S.; Magnius, L. O., Genetic diversity of hepatitis B virus strains derived worldwide: genotypes, subgenotypes, and HBsAg subtypes. *Intervirology* **2004,** *47* (6), 289-309.
239. Zanetti, A. R.; Van Damme, P.; Shouval, D., The global impact of vaccination against hepatitis B: a historical overview. *Vaccine* **2008,** *26* (49), 6266-73.
240. Salisse, J.; Sureau, C., A function essential to viral entry underlies the hepatitis B virus "a" determinant. *J Virol* **2009,** *83* (18), 9321-8.
241. Abou-Jaoude, G.; Sureau, C., Entry of hepatitis delta virus requires the conserved cysteine residues of the hepatitis B virus envelope protein antigenic loop and is blocked by inhibitors of thiol-disulfide exchange. *J Virol* **2007,** *81* (23), 13057-66.

242. Shevtsov, M. A.; Nikolaev, B. P.; Yakovleva, L. Y.; Marchenko, Y. Y.; Dobrodumov, A. V.; Mikhrina, A. L.; Martynova, M. G.; Bystrova, O. A.; Yakovenko, I. V.; Ischenko, A. M., Superparamagnetic iron oxide nanoparticles conjugated with epidermal growth factor (SPION-EGF) for targeting brain tumors. *Int J Nanomedicine* **2014,** *9*, 273-87.
243. Shao, H.; Yoon, T.-J.; Liong, M.; Weissleder, R.; Lee, H., Magnetic nanoparticles for biomedical NMR-based diagnostics. *Beilstein Journal of Nanotechnology* **2010,** *1*, 142-154.
244. Patient, R.; Hourioux, C.; Roingeard, P., Morphogenesis of hepatitis B virus and its subviral envelope particles. *Cell Microbiol* **2009,** *11* (11), 1561-70.
245. Prange, R., Host factors involved in hepatitis B virus maturation, assembly, and egress. *Med Microbiol Immunol* **2012,** *201* (4), 449-61.
246. Kojima, T., Immune electron microscopic study of hepatitis B virus associated antigens in hepatocytes. *Gastroenterol Jpn* **1982,** *17* (6), 559-75.
247. Chu, C. M.; Liaw, Y. F., Intrahepatic distribution of hepatitis B surface and core antigens in chronic hepatitis B virus infection. Hepatocyte with cytoplasmic/membranous hepatitis B core antigen as a possible target for immune hepatocytolysis. *Gastroenterology* **1987,** *92* (1), 220-5.
248. Crawford, D. R.; Ostrowski, S.; Vakharia, D.; Ilic, Z.; Sell, S., Separate origins of hepatitis B virus surface antigen-negative foci and hepatocellular carcinomas in transgenic HBsAg (alb/psx) mice. *The American journal of pathology* **2006,** *169* (1), 223-232.
249. Allard-Vannier, E.; Cohen-Jonathan, S.; Gautier, J.; Herve-Aubert, K.; Munnier, E.; Souce, M.; Legras, P.; Passirani, C.; Chourpa, I., Pegylated magnetic nanocarriers for doxorubicin delivery: a quantitative determination of stealthiness in vitro and in vivo. *Eur J Pharm Biopharm* **2012,** *81* (3), 498-505.
250. Thomas, R.; Park, I. K.; Jeong, Y. Y., Magnetic iron oxide nanoparticles for multimodal imaging and therapy of cancer. *Int J Mol Sci* **2013,** *14* (8), 15910-30.
251. Kwon, H.; Lok, A. S., Hepatitis B therapy. *Nature reviews. Gastroenterology & hepatology* **2011,** *8* (5), 275-84.
252. Ganem, D.; Prince, A. M., Hepatitis B virus infection--natural history and clinical consequences. *N Engl J Med* **2004,** *350* (11), 1118-29.
253. Ferrari, C., HBV and the immune response. *Liver Int* **2015,** *35 Suppl 1*, 121-8.
254. Allweiss, L.; Volz, T.; Giersch, K.; Kah, J.; Raffa, G.; Petersen, J.; Lohse, A. W.; Beninati, C.; Pollicino, T.; Urban, S.; Lutgehetmann, M.; Dandri, M., Proliferation of primary human hepatocytes and prevention of hepatitis B virus reinfection efficiently deplete nuclear cccDNA in vivo. *Gut* **2018,** *67* (3), 542-552.
255. Saito, T.; Kamimura, T.; Ishibashi, M.; Shinzawa, H.; Takahashi, T., Electron microscopic study of hepatitis B virus-associated antigens on the infected liver cell membrane in relation to analysis of immune target antigens in chronic hepatitis B. *Gastroenterol Jpn* **1992,** *27* (6), 734-44.
256. Ahmed, I.; Akram, Z.; Iqbal, H. M. N.; Munn, A. L., The regulation of Endosomal Sorting Complex Required for Transport and accessory proteins in multivesicular body sorting and enveloped viral budding - An overview. *International journal of biological macromolecules* **2019,** *127*, 1-11.
257. Harty, R. N.; Brown, M. E.; Wang, G.; Huibregtse, J.; Hayes, F. P., A PPxY motif within the VP40 protein of Ebola virus interacts physically and functionally with a ubiquitin ligase: implications for filovirus budding. *Proc Natl Acad Sci U S A* **2000,** *97* (25), 13871-6.
258. Schmitt, A. P.; Leser, G. P.; Morita, E.; Sundquist, W. I.; Lamb, R. A., Evidence for a new viral late-domain core sequence, FPIV, necessary for budding of a paramyxovirus. *Journal of virology* **2005,** *79* (5), 2988-2997.
259. Sakaguchi, T.; Kato, A.; Sugahara, F.; Shimazu, Y.; Inoue, M.; Kiyotani, K.; Nagai, Y.; Yoshida, T., AIP1/Alix is a binding partner of Sendai virus C protein and facilitates virus budding. *J Virol* **2005,** *79* (14), 8933-41.

260. Bohne, F.; Chmielewski, M.; Ebert, G.; Wiegmann, K.; Kurschner, T.; Schulze, A.; Urban, S.; Kronke, M.; Abken, H.; Protzer, U., T cells redirected against hepatitis B virus surface proteins eliminate infected hepatocytes. *Gastroenterology* **2008,** *134* (1), 239-47.
261. Gerlich, W. H., Medical virology of hepatitis B: how it began and where we are now. *Virol J* **2013,** *10*, 239.
262. Keller, M. A.; Stiehm, E. R., Passive immunity in prevention and treatment of infectious diseases. *Clin Microbiol Rev* **2000,** *13* (4), 602-14.
263. Kucinskaite-Kodze, I.; Pleckaityte, M.; Bremer, C. M.; Seiz, P. L.; Zilnyte, M.; Bulavaite, A.; Mickiene, G.; Zvirblis, G.; Sasnauskas, K.; Glebe, D.; Zvirbliene, A., New broadly reactive neutralizing antibodies against hepatitis B virus surface antigen. *Virus Res* **2016,** *211*, 209-21.
264. Li, D.; He, W.; Liu, X.; Zheng, S.; Qi, Y.; Li, H.; Mao, F.; Liu, J.; Sun, Y.; Pan, L.; Du, K.; Ye, K.; Li, W.; Sui, J., A potent human neutralizing antibody Fc-dependently reduces established HBV infections. *Elife* **2017,** *6*.
265. Wang, W.; Sun, L.; Li, T.; Ma, Y.; Li, J.; Liu, Y.; Li, M.; Wang, L.; Li, C.; Xie, Y.; Wen, Y.; Liang, M.; Chen, L.; Tong, S., A human monoclonal antibody against small envelope protein of hepatitis B virus with potent neutralization effect. *Mabs-Austin* **2016,** *8* (3), 468-77.
266. Golsaz-Shirazi, F.; Amiri, M. M.; Farid, S.; Bahadori, M.; Bohne, F.; Altstetter, S.; Wolff, L.; Kazemi, T.; Khoshnoodi, J.; Hojjat-Farsangi, M.; Chudy, M.; Jeddi-Tehrani, M.; Protzer, U.; Shokri, F., Construction of a hepatitis B virus neutralizing chimeric monoclonal antibody recognizing escape mutants of the viral surface antigen (HBsAg). *Antiviral Res* **2017,** *144*, 153-163.
267. Tharinger, H.; Rebbapragada, I.; Samuel, D.; Novikov, N.; Nguyen, M. H.; Jordan, R.; Frey, C. R.; Pflanz, S., Antibody-dependent and antibody-independent uptake of HBsAg across human leucocyte subsets is similar between individuals with chronic hepatitis B virus infection and healthy donors. *J Viral Hepat* **2017,** *24* (6), 506-513.
268. Gao, Y.; Zhang, T. Y.; Yuan, Q.; Xia, N. S., Antibody-mediated immunotherapy against chronic hepatitis B virus infection. *Hum Vaccin Immunother* **2017,** *13* (8), 1768-1773.
269. Berkower, I.; Spadaccini, A.; Chen, H.; Al-Awadi, D.; Muller, J.; Gao, Y.; Feigelstock, D.; Virnik, K.; Ni, Y., Hepatitis B virus surface antigen assembly function persists when entire transmembrane domains 1 and 3 are replaced by a heterologous transmembrane sequence. *J Virol* **2011,** *85* (5), 2439-48.
270. Zhu, Y.; Zhang, T.; Zhao, J.; Weng, Z.; Yuan, Q.; Li, S.; Zhang, J.; Xia, N.; Zhao, Q., Toward the development of monoclonal antibody-based assays to probe virion-like epitopes in hepatitis B vaccine antigen. *Hum Vaccin Immunother* **2014,** *10* (4), 1013-23.
271. Sureau, C.; Salisse, J., A conformational heparan sulfate binding site essential to infectivity overlaps with the conserved hepatitis B virus a-determinant. *Hepatology* **2013,** *57* (3), 985-94.
272. Horsfall, A. C.; Hay, F. C.; Soltys, A. J.; Jones, M. G., Epitope mapping. *Immunology today* **1991,** *12* (7), 211-3.
273. Qiu, X.; Schroeder, P.; Bridon, D., Identification and characterization of a C(K/R)TC motif as a common epitope present in all subtypes of hepatitis B surface antigen. *J Immunol* **1996,** *156* (9), 3350-6.
274. Dreesman, G. R.; Sanchez, Y.; Ionescu-Matiu, I.; Sparrow, J. T.; Six, H. R.; Peterson, D. L.; Hollinger, F. B.; Melnick, J. L., Antibody to hepatitis B surface antigen after a single inoculation of uncoupled synthetic HBsAg peptides. *Nature* **1982,** *295* (5845), 158-60.
275. Brown, S. E.; Howard, C. R.; Steward, M. W.; Ajdukiewicz, A. B.; Whittle, H. C., Hepatitis B surface antigen containing immune complexes occur in seronegative hepatocellular carcinoma patients. *Clin Exp Immunol* **1984,** *55* (2), 355-9.
276. Tian, Y.; Xu, Y.; Zhang, Z.; Meng, Z.; Qin, L.; Lu, M.; Yang, D., The amino Acid residues at positions 120 to 123 are crucial for the antigenicity of hepatitis B surface antigen. *J Clin Microbiol* **2007,** *45* (9), 2971-8.

277. Norder, H.; Courouce, A. M.; Magnius, L. O., Molecular basis of hepatitis B virus serotype variations within the four major subtypes. *J Gen Virol* **1992,** *73 (Pt 12)*, 3141-5.
278. Hossain, M. G.; Ueda, K., Investigation of a Novel Hepatitis B Virus Surface Antigen (HBsAg) Escape Mutant Affecting Immunogenicity. *PloS one* **2017,** *12* (1), e0167871-e0167871.
279. Moghadam, F. F., Using Nanoparticles in Medicine for Liver Cancer Imaging. *Oman Med J* **2017,** *32* (4), 269-274.
280. Lee, C. M.; Jeong, H. J.; Kim, S. L.; Kim, E. M.; Kim, D. W.; Lim, S. T.; Jang, K. Y.; Jeong, Y. Y.; Nah, J. W.; Sohn, M. H., SPION-loaded chitosan-linoleic acid nanoparticles to target hepatocytes. *Int J Pharm* **2009,** *371* (1-2), 163-9.
281. Inoue, J.; Krueger, E. W.; Chen, J.; Cao, H.; Ninomiya, M.; McNiven, M. A., HBV secretion is regulated through the activation of endocytic and autophagic compartments mediated by Rab7 stimulation. *J Cell Sci* **2015,** *128* (9), 1696-706.
282. Ko, C.; Chakraborty, A.; Chou, W.-M.; Hasreiter, J.; Wettengel, J. M.; Stadler, D.; Bester, R.; Asen, T.; Zhang, K.; Wisskirchen, K.; McKeating, J. A.; Ryu, W.-S.; Protzer, U., Hepatitis B virus genome recycling and de novo secondary infection events maintain stable cccDNA levels. *Journal of Hepatology* **2018,** *69* (6), 1231-1241.
283. Hu, J.; Liu, K., Complete and Incomplete Hepatitis B Virus Particles: Formation, Function, and Application. *Viruses* **2017,** *9* (3).
284. Bruss, V., Hepatitis B virus morphogenesis. *World J Gastroenterol* **2007,** *13* (1), 65-73.
285. Xu, Z.; Bruss, V.; Yen, T. S., Formation of intracellular particles by hepatitis B virus large surface protein. *Journal of virology* **1997,** *71* (7), 5487-5494.
286. Kamimura, T.; Yoshikawa, A.; Ichida, F.; Sasaki, H., Electron microscopic studies of Dane particles in hepatocytes with special reference to intracellular development of Dane particles and their relation with HBeAg in serum. *Hepatology* **1981,** *1* (5), 392-7.
287. Xia, Y.; Carpentier, A.; Cheng, X.; Block, P. D.; Zhao, Y.; Zhang, Z.; Protzer, U.; Liang, T. J., Human stem cell-derived hepatocytes as a model for hepatitis B virus infection, spreading and virus-host interactions. *J Hepatol* **2017,** *66* (3), 494-503.
288. Wang, X.; Xing, X.; Zhang, B.; Liu, F.; Cheng, Y.; Shi, D., Surface engineered antifouling optomagnetic SPIONs for bimodal targeted imaging of pancreatic cancer cells. *Int J Nanomedicine* **2014,** *9*, 1601-15.
289. Alric, C.; Herve-Aubert, K.; Aubrey, N.; Melouk, S.; Lajoie, L.; Meme, W.; Meme, S.; Courbebaisse, Y.; Ignatova, A. A.; Feofanov, A. V.; Chourpa, I.; Allard-Vannier, E., Targeting HER2-breast tumors with scFv-decorated bimodal nanoprobes. *J Nanobiotechnology* **2018,** *16* (1), 18.
290. Gu, J.; Xu, H.; Han, Y.; Dai, W.; Hao, W.; Wang, C.; Gu, N.; Xu, H.; Cao, J., The internalization pathway, metabolic fate and biological effect of superparamagnetic iron oxide nanoparticles in the macrophage-like RAW264.7 cell. *Science China Life Sciences* **2011,** *54* (9), 793-805.
291. Bertoletti, A.; Le Bert, N., Immunotherapy for Chronic Hepatitis B Virus Infection. *Gut and liver* **2018,** *12* (5), 497-507.
292. Wisskirchen, K.; Kah, J.; Malo, A.; Asen, T.; Volz, T.; Allweiss, L.; Wettengel, J. M.; Lutgehetmann, M.; Urban, S.; Bauer, T.; Dandri, M.; Protzer, U., T cell receptor grafting allows virological control of Hepatitis B virus infection. *J Clin Invest* **2019,** *130*.
293. Sunami, Y.; Ringelhan, M.; Kokai, E.; Lu, M.; O'Connor, T.; Lorentzen, A.; Weber, A.; Rodewald, A. K.; Mullhaupt, B.; Terracciano, L.; Gul, S.; Wissel, S.; Leithauser, F.; Krappmann, D.; Riedl, P.; Hartmann, D.; Schirmbeck, R.; Strnad, P.; Huser, N.; Kleeff, J.; Friess, H.; Schmid, R. M.; Geisler, F.; Wirth, T.; Heikenwalder, M., Canonical NF-kappaB signaling in hepatocytes acts as a tumor-suppressor in hepatitis B virus surface antigen-driven hepatocellular carcinoma by controlling the unfolded protein response. *Hepatology* **2016,** *63* (5), 1592-607.
294. Wursthorn, K.; Lutgehetmann, M.; Dandri, M.; Volz, T.; Buggisch, P.; Zollner, B.; Longerich, T.; Schirmacher, P.; Metzler, F.; Zankel, M.; Fischer, C.; Currie, G.; Brosgart, C.; Petersen, J., Peginterferon

alpha-2b plus adefovir induce strong cccDNA decline and HBsAg reduction in patients with chronic hepatitis B. *Hepatology* **2006,** *44* (3), 675-84.
295. Jaroszewicz, J.; Calle Serrano, B.; Wursthorn, K.; Deterding, K.; Schlue, J.; Raupach, R.; Flisiak, R.; Bock, C. T.; Manns, M. P.; Wedemeyer, H.; Cornberg, M., Hepatitis B surface antigen (HBsAg) levels in the natural history of hepatitis B virus (HBV)-infection: a European perspective. *J Hepatol* **2010,** *52* (4), 514-22.
296. Ahmed, S. U.; Zair, M.; Chen, K.; Iu, M.; He, F.; Adeyi, O.; Cleary, S. P.; Ghanekar, A., Generation of subcutaneous and intrahepatic human hepatocellular carcinoma xenografts in immunodeficient mice. *Journal of visualized experiments : JoVE* **2013,** (79), e50544.
297. Zhao, R.; Wang, T. Z.; Kong, D.; Zhang, L.; Meng, H. X.; Jiang, Y.; Wu, Y. Q.; Yu, Z. X.; Jin, X. M., Hepatoma cell line HepG2.2.15 demonstrates distinct biological features compared with parental HepG2. *World J Gastroenterol* **2011,** *17* (9), 1152-9.
298. Mu, K.; Zhang, S.; Ai, T.; Jiang, J.; Yao, Y.; Jiang, L.; Zhou, Q.; Xiang, H.; Zhu, Y.; Yang, X.; Zhu, W., Monoclonal antibody-conjugated superparamagnetic iron oxide nanoparticles for imaging of epidermal growth factor receptor-targeted cells and gliomas. *Molecular imaging* **2015,** *14*.
299. Shevtsov, M.; Nikolaev, B.; Marchenko, Y.; Yakovleva, L.; Skvortsov, N.; Mazur, A.; Tolstoy, P.; Ryzhov, V.; Multhoff, G., Targeting experimental orthotopic glioblastoma with chitosan-based superparamagnetic iron oxide nanoparticles (CS-DX-SPIONs). *Int J Nanomedicine* **2018,** *13*, 1471-1482.
300. Saesoo, S.; Sathornsumetee, S.; Anekwiang, P.; Treetidnipa, C.; Thuwajit, P.; Bunthot, S.; Maneeprakorn, W.; Maurizi, L.; Hofmann, H.; Rungsardthong, R. U.; Saengkrit, N., Characterization of liposome-containing SPIONs conjugated with anti-CD20 developed as a novel theranostic agent for central nervous system lymphoma. *Colloids and surfaces. B, Biointerfaces* **2018,** *161*, 497-507.
301. Moradi Khaniabadi, P.; Shahbazi-Gahrouei, D.; Malik Shah Abdul Majid, A.; Suhaimi Jaafar, M.; Moradi Khaniabadi, B.; Shahbazi-Gahrouei, S., In vitro Study of SPIONs-C595 as Molecular Imaging Probe for Specific Breast Cancer (MCF-7) Cells Detection. *Iranian biomedical journal* **2017,** *21* (6), 360-8.

7. Acknowledgements

First and foremost, I would like to give my deepest appreciation to my supervisor Professor Dr. Ulrike Protzer. Thank you for offering me this precious opportunity to explore the imaging and targeting of HBV infection together with you in the past five years. Without your professional guidance and continuously support, I could not have completed this thesis. Your profound knowledge in HBV scientific research area enlightens me not only in this thesis but also in my future study. Thanks for the trust, inspiration and freedom you have granted to me in the daily research as well as during the thesis writing.

Next, I would like to express my heartfelt gratitude to Dr. Felix Bohne for your productive discussions and constant encouragement in the first two years of my Ph.D. study. I learned a lot from your valuable advice and then grew rapidly not only experimental techniques but also the way to work efficiently. In addition, my sincere thanks also go to Dr. Maxim A. Shevtsov. Your selfless assistance, insightful discussions and ceaseless support in experiments, data analysis and paper writing in the past two years. I would like to thank Dr. Maarten van de Klundert, Dr. Chunkyu Ko, and Dr. Britta Möhl for reviewing my thesis and my publication. It would not have been possible to finish the thesis writing without your help. I have improved so much on writing skills in scientific way.

Furthermore, I would like to thank my thesis committee members Prof. Dr. Volker Bruss and Prof. Dr. Franz Pfeiffer. They provided me a lot of valuable advises during my study. With your theoretical support, I ultimately achieved a more in-depth understanding of the medical physics and molecular biology in my study. In addition, I am utmost grateful to my research partners, Prof. Dr. Camille Sureau, Dr. Michaela Aichler, Dr. Marc Ringelhan, for their excellent instructions and experimental support. Also, I am indebted to Dr. Karin Wisskirchen for organizing animal experiment, sharing her up-to-date information and encouraging me how to balance the life and work as a mother.

I appreciate and enjoy the fruitful collaborations, the innumerable discussions with all of you. My doctoral study has been made much easier with your help. I also must express great thanks to my former and current colleagues. Dr. Thomas Michler, Dr. Hanaa Gaber, Dr. Eva Loffredo-Verde, Dr. Anna Kosinska, Dr. Katrin Singethan, Dr. ShanShan Luo, Dr. Martin Mück-Häusl, Antje Malo, Dr. Jochen Wettengel, Dr. Daniela Stadler, Christoph Blossey, Oliver Quitt, Dr. Julia Hasreiter, Dr. Marvin Freitag, Sebastian Altstetter, Sophia Schreiber, Cam-Tu Ho, Dr. Suliman Qadir Afridi, Anindita Chakraborty, Lisa Wolff, Martin Kächele, Florian Wilsch, Stoyan Velkov, Samuel Jeske, for helping me with my projects and created a friendly atmosphere in the lab.

I would like to thank Theresa Asen, Raindy Tedjokusumo, Natalie Röder, Romina Bester, Frank Thiele, Hortenzia Jacobi and Phillip Hagen for their technical supports.

I would like to specially thank all Chinese colleagues, Jipeng Su, Fuwang Chen, Xiaoming Cheng, Yuchen Xia, Liangjun Qin, Shanshan Luo, Wen-Min Chou, and Ke Zhang. We helped each other, confided our troubles as friends and tried hard to progress together.

Special thanks go to my friend, Man Yao, Bifeng Wang, Chengyang Wang, Linyu Mu, Qi He, Qian Sun, Wei Wu, Dapeng Yang, Chao Xia, Xi Chen, Mingqian Li, Peng Zhang, Bowen Xue, Yupeng Qin, Liang Wang, Yin Li, Jiaoyu Ai, for the joy and companion during my Ph.D time. With their consistently unconditional assistant, my life in Munich was wonderful and colorful. They always encouraged me to move on and keep positive attitude to all difficulties and challenges.

Last but not least, I am deeply indebted to my beloved family in China for their consistent love, understanding, encouragement and support throughout my Ph.D. study. I am so lucky to fall in love with my husband in Munich and have a cute daughter in Utrecht. Without the encouragement and support of my husband, I was wondering I could not finish my thesis.

8. Publications and Meetings

a) Publications

1. Shevtsov, Maxim, **Lili Zhao** *et al*. Applicability of Metal Nanoparticles in the Detection and Monitoring of Hepatitis B Virus Infection. Viruses 2017. 9: 193

2. **Lili Zhao** *et al*. Hepatitis B virus envelope proteins can serve as therapeutic targets embedded in the host cell plasma membrane. Under Revision. https://doi.org/10.1101/2020.12.21.423802

3. Oliver Quitt, Shanshan Luo, Marten Meyer, Zhe Xie, Forough Golsaz-Shirazi , Eva Loffredo-Verde, Julia Festag, Jan Hendrik Bockmann, **Lili Zhao** *et al*. T-cell engager antibodies enable T cells to control hepatitis B virus infection and to target HBsAg-positive hepatoma in mice. J Hepatol. 2021

4. **Lili Zhao** *et al*. Anti-HBs conjugated superparamagnetic iron oxide nanoparticles (SPION) to visualize and target HBV infection *in vitro* and *in vivo*. In preparation.

b) Meetings and Activities

1. Participation of to the Falk Workshop “Viral Hepatitis – From Bench to Bedside,” Munich, Germany, 2015.

2. Participation of the 31st Annual Meeting of the German Association of the Study of the Liver (GASL), Munich, Germany, 2015.

3. HBV INTERNATIONAL MEETING Molecular Biology of Hepatitis B Virus, Seoul, Korea, 2016. (Title: Surface localization of HBV envelope proteins, post presentation)

4. Lab exchange, Laboratorie de Virologie, Institut National de la Transfusion Sanguine (INTS), Paris, France, 2016.

5. Workshop ‘Essentials of widefield and confocal microscopy’, Deutsches Zentrum fuer Infektionsforschung (DZIF) University Hospital Heidelberg, Heidelberg, Germany, 2017.

6. Organizer, Süddeutschland Biologie und Medizin Gesellschaft, Max-Planck-Institute of Biochemistry, Martinsried, Germany, 2017.